POLITECNICO DI TORINO

Master's Degree in Aerospace Engineering

Master's Degree Thesis

Liner optimization for boundary layer ingestion-fan noise reduction

SUPERVISORS
Prof. Francesco AVALLONE
Ing. Mattia BARBARINO
Ing. Francesco PETROSINO

CANDIDATE
Giuseppe PELLICO

April 2025

Ringraziamenti

Un grazie sincero e doveroso va al mio relatore, professor Francesco Avallone, e agli ingegneri del CIRA, ingegner Mattia Barbarino e ingegner Francesco Petrosino, per avermi accompagnato in questo percorso di 6 mesi. Durante questa esperienza ho arricchito il mio bagaglio culturale imparando nozioni tecniche, ma anche a livello umano, che sicuramente mi permetteranno di affrontare al meglio le sfide che mi si presenteranno in futuro. Le loro approfondite conoscenze riguardo all'argomento trattato in questo studio hanno permesso il fluido svolgimento e completamento del lavoro.

Contents

List of Figures

List of Tables

Symbols

Symbol	Description	Unit
a	Orifice radius (end effect)	m
a	Dimensionless proportionality constant	–
$AverageSPL$	Average Sound Pressure Level	dB
c	speed of sound	m/s
C_D	In-orifice discharge coefficient	–
d	Orifice diameter	m
F	Friction factor for pipe flow	–
F_j	Local mean flow information vector	–
f	Frequency	Hz
f_n	Natural frequency	Hz
h	Cavity depth	m
k	Spring Constant (spring-mass system)	$\mathrm{kg/s^2}$
k	Wavenumber (acoustic)	$\mathrm{cm^{-1}}$
k_μ	Viscous Stokes wave wakenumber	$\mathrm{m^{-1}}$
k_a	Axial wave number	–
K_i	Dimensionless entrance loss	–
K_e	Dimensionless exit loss	–
k_r	Radial wave number	–
l^*	Thickness	m
l_0	Thickness	m
L	Buffer zone thickness	m
M	Mach number	–
m	Circumferential mode	–
N_α	Galerkin shape function	–
N_{Re}	Reynold's number	–
n	Radial mode	–
$OSPL$	Overall Sound Pressure Level	dB
p	Element order (CFL condition)	–
p	Pressure	Pa
p_F	Pressure fluctuation	Pa
P	Flow resistance per unit thickness of the material	$\mathrm{kg{\cdot}m^{-3}{\cdot}s^{-1}}$
q	Vector of unknown	–
r	Hole radius	m
r_e^*	Effective radius of the honeycomb cell	m
R	Acoustic resistance (impedance)	$\mathrm{kg{\cdot}m^{-2}{\cdot}s^{-1}}$

Symbol	Description	Unit
R	Radius of circular duct (wave propagation in duct)	m
SPL	Sound Pressure Level	dB
t	Thickness (liner)	m
t	Time (time dependence of the wave solution)	s
T	Oscillation period	s
T	Temperature (Navier-Stokes equation)	K
u	Acoustic velocity	m/s
v_e	Effective particle velocity	m/s
V_h	In-orifice velocity	m/s
V_i	Incident velocity	m/s
X	Acoustic reactance	$\mathrm{kg}{\cdot}m^{-2}{\cdot}\mathrm{s}^{-1}$
X_c	Acoustic cavity reactance	$\mathrm{kg}{\cdot}m^{-2}{\cdot}\mathrm{s}^{-1}$
X_m	Acoustic mass reactance	$\mathrm{kg}{\cdot}m^{-2}{\cdot}\mathrm{s}^{-1}$
Z_0	Acoustic impedance of the air	$\mathrm{kg}{\cdot}m^{-2}{\cdot}\mathrm{s}^{-1}$
α	Absorption coefficient	–
β	Damping order controller	–
γ	Specific heat ratio (adiabatic compression)	–
γ	Propagation coefficient (bulk absorber)	m^{-1}
δ	End correction (Helmholtz resonator)	m
δ^*	Boundary layer displacement thickness	m
ϵ	Dimensionless end correction	–
ζ	Normalized Impedance	–
θ	Normalized Resistance	–
λ	Wavelength	m
μ	Dynamic viscosity	$\mathrm{kg}{\cdot}m^{-1}{\cdot}\mathrm{s}^{-1}$
ν	Cavity fluid kinetic viscosity	m^2/s
ξ_B	Characteristic impedance ratio	–
ρ_0	Air density	kg/m^3
σ	Liner porosity (liners)	–
σ	Damping factor (ActranDGM buffer zone)	–
τ	Thickness	m
χ	Normalized Reactance	–
χ_m	Normalized mass reactance	–
χ_{me}	Normalized mass reactance due to end correction	–
ω	Circular frequency	s^{-1}

Abstract

In the present study the optimization of an acoustic liner will be discussed. The problem linked to the noise generated by an aircraft, especially when the take-off or landing site is near a populated area, is becoming more and more important. This increasing interest in this topic is due to the increase in the number of flights. An acoustic liner could be represented as a boundary condition thanks to its impedance value. There are different way to compute it and different impedance models will be discussed. A specific geometry for the nacelle is used and a particular set of frequency is studied. A first part is dedicated to the reduction of the noise generated with a single frequency. The second part will be dedicated to the optimization of a liner that could work well in a series of frequency. Different optimizer are used to find a minimum for specific noise functions and in particular for the Average Sound Pressure Level and the Overall Sound Pressure Level. The number of liners is also a subject of these analyses. The main tool used in this study is the Actran software. This is a powerful tool for the computation of the noise generation and propagation in a medium. Its integration with the python language will be important and a python script will be used for the optimization process. A final configuration that produces the best noise reduction will be found. A representation of its integration inside the nacelle could be found in the last part.

Chapter 1

Introduction

Aviation is playing an important role in todays transportation, and it is growing continuously. Up to now around 100.000 flight are made every day transporting millions of passengers and this numbers will increase in the next years. Among the different problematic related to this, the acoustic noise generated from the aircraft is an important topic that must be studied. To reduce this noise different aviation organizations are imposing more stringent regulations on the noise levels that can be reached in all the flight phases. These levels affect the nature and human beings. A long-term exposure to high levels could increase stress and anxiety in people and this could affect the psychomotor performances with a negative effect in tasks that require concentration, calculation etc. (14) This long exposure could also increase the rick of disease in human ears. The main source of this noise is the turbofan noise coming from the rotation of the blade (fan) and the combustion and by-pass flow (jet).

1.1 Acoustic liners

To reduce this noise some approaches can be used and there are 3 types: 1) active control, 2) geometric shape optimization, 3) passive control. This study will focus on a passive control system, perforated liners. With its structure made by a perforated plate, the noise is reduced due the transformation of the acoustic pressure fluctuations into a non-radiating vortical fluctuations. The mechanism is about the conversion of sound energy into turbulent kinetic energy with sound absorption that involves also the formation and shedding of the vortices at the orifice discharge (15). The position of liners can be different depending on the main noise that must be reduced. For what concern the jet noise, the interest is on two different part of the engine as shown in Figure 1.1. In particular, the interested zones are the front and back part of the motor.

Today's tendency on engines is to increase the Bypass Ratio to improve the efficiency with the consequence of a reduction in the jet noise but with a more dominant broadband fan noise component. As a consequence, the liners must absorb sound over a wide frequency range.(1). Acoustic modes propagating in the duct give the noise source characteristic and the panel design depends on it. SDoF (Single Degree

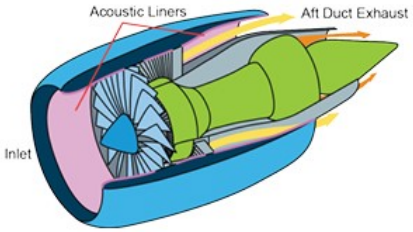

Figure 1.1: Engine nacelle with liners (1)

of Freedom) and DDoF (Double Degree of Freedom) liners are resonator panels. The damping that the resistance give, have an influence on their acoustic properties that can be linear or nonlinear. The damping resistance of a nonlinear liner face sheet (or septum face sheet) depends on the amplitude of the incident acoustic wave, whereas for linear liner face sheet (or septum face sheet) the behaviour is independent from the amplitude of the incident wave. Typically liners with a hole diameter between 0.6 and 0.8 mm(6) can present a nonlinear behavior. Motsinger and Kraft (6) describe three different type of liners depending on the range of frequencies in which the suppression is required.

1. The fist type of liners is the SDoF, Single Degree of Freedom depicted in Figure 1.2. This liner is composed by a sandwich where in the middle there is an honeycomb structure between a solid back-plate in the lower part and a porous face sheet in the upper part. This is effective in presence of the narrowest frequency range and, adjusting its main properties it can be tuned to the frequency band containing the single fan tone. The behavior is similar to an Helmholtz resonator with its absorption peak at the resonance frequency. The main parameters of the SDoF liner are the orifices diameter d, the honeycomb depth h, the thickness of the porous face-sheet t and the porosity σ defined as the number of orifices per unit surface. The key factor to reach a resonant response, and so maximum attenuation, is the cell dept (h). The honeycomb cell size will be sized to consider the liner as locally reacting. (16)

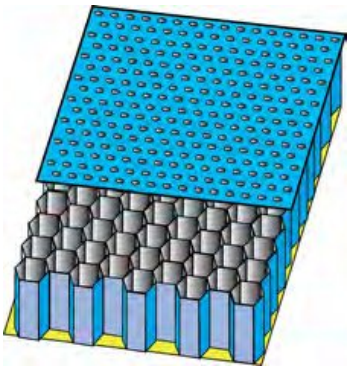

Figure 1.2: Single Degree of Freedom liners (1)

2. The second type of linear is the DDoF, Double Degree of Freedom. This is essentially the union of two SDoF liners. It is composed by a two porous sheet,

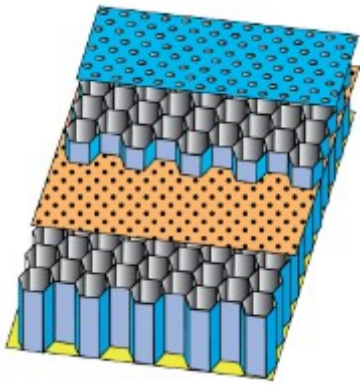

Figure 1.3: Double Degree of Freedom liners (1)

the face and mid sheets, two honeycomb structure and a rigid backplate. A first honeycomb is positioned between the porous face sheet and the septum while the second honeycomb is positioned between the septum and the rigid backplate. This type of acoustic treatment is shown in Figure 1.3. This liner has a wider bandwidth respect to the SDoF liners with two resonance frequencies in with the absorption is maximum. In this case the basic parameters are the same but doubled. Is possible to find the two cells height h_1 and h_2, the two orifice diameters d_1 and d_2 and so on.

3. The third acoustic treatment is the bulk absorber as shown in Figure 1.4. In this liner the honeycomb core is substituted with a porous material. The bulk absorber is effective for the widest bandwidth (2).

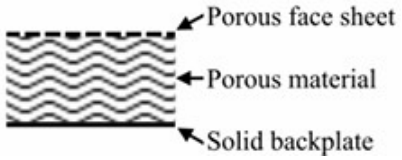

Figure 1.4: Bulk absorber (2)

Sugimoto et al. (3) present another type of acoustic treatment, the folded cavity. The concept of this liner is based on the assumption that the liner cavity is folded to lie parallel to the duct axis to do not intact excessively the liner depth but providing at the same time a large reactive volume. This can be applied for the reduction of noise at lower frequency. This type of liner can present different geometries as shown in Figure 1.5. The values of resistance and reactance depend on this.

Jones and Parrott (4) presented a honeycomb porous liner. This is composed by a structure similar to the SDoF liner but in this case there are rigid porous plates instead of a honeycomb structure as shown in Figure 1.6. Some studies demonstrate that the attenuation bandwidth is increased by 70% but with a peak attenuation reduction of 20%. A disadvantage can be found in more complex liner models to develop and produce.

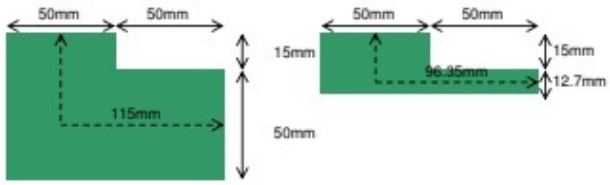

Figure 1.5: Different geometries for folded cavity (3)

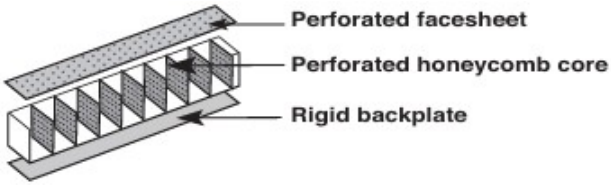

Figure 1.6: Porous honeycomb liner (4)

1.1.1 Extended and local reacting liners

Generally liners are subdivided into two big family: extended-reacting liners and locally-reacting (or point-reacting (6)) liners as shown in Figure 1.7. In the extended-reacting liner the core is filled with foam without internal rigid partition and can be covered on the top with a porous rigid plate or can be let free if the foam material is sufficiently robust. The majority of the acoustic resistance is given by the foam and the acoustic wave propagates in all directions in the liner. This type of liner has a bigger bandwidth but less resonant behavior compared to the other type (1).

The local-reacting liner presents in its core several rigid partitions that prevent the acoustic wave to move inside the liner. In the upper part is possible to find a porous face-sheet that enhance the fluid pumping with a spatially concentrated absorption. This can provide a strong absorption in a narrow bandwidth (1).

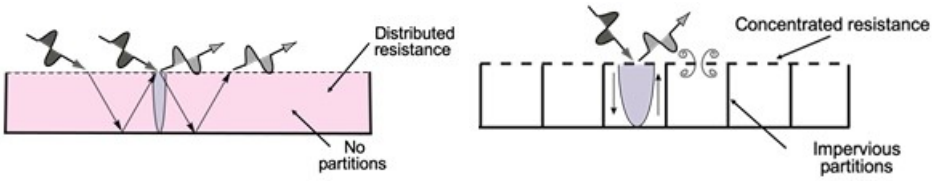

Figure 1.7: extended- and local-reacting liners (1)

1.1.2 Bias and Grazing flow

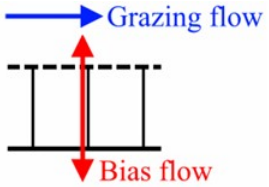

Figure 1.8: Bias and Grazing flow (2)

As shown in Figure 1.8 liners are subjected to two different flows. The grazing flow is characteristic of liners mounted in an engine inlet and is the flow that moves along the perforated face-sheet. Usually this is a turbulent boundary layer. The structure can be designed to have also ad in- or outflow over the liner face-sheet and can be used to have a boundary layer suction or blowing, to ensure a cooling of the liner and to tune the frequency response of the liner. The grazing flow has an important influence on the liner's performances. In fact, this flow can carry downstream a series of merged vortices created by the orifices upstream having an influence on the invested orifices (17).

1.2 Resonance

The SDoF liner can be seen as a panel of Helmholtz resonators (2). The ideal form of the Helmholtz resonator has a "cavernous space" with a thin wall that almost close the space and in which there is a small orifice that allow the communication between the internal and external gas. Helmholtz arrived to this theory with the supposition that the perforation is small and so the wavelength of the vibration is great (18).

1.2.1 Mechanical system

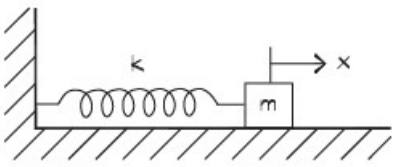

Figure 1.9: Spring-mass system(5)

The basis of the Helmholtz resonator can be found in the resonance concept. There are systems that, when moved from their equilibrium point, have forces that tend to restore the initial equilibrium position. This is the case for example of a spring-mass system, composed by a frictionless mass attached to a spring as shown in Figure 1.9. When the mass is moved from this point the elastic force tends to move back the mass into its equilibrium position, moving it through this point and beyond of it, only to return again and repeat the process. This movement repeats itself for a given period and so at a characteristic frequencies, called natural frequency or resonant frequency (5). The governing equation for the mass-spring system is the Hooke's law described in Equation 1.1

$$F = -k \cdot x \tag{1.1}$$

and k is the spring constant.

During the motion the spring force is counterbalanced by the inertial forces, given by the mass, according with the Newton's second law:

$$F = m \cdot a = m\frac{d^2x}{dt^2} \tag{1.2}$$

where F in the force applied to the mass m and a is the acceleration produced by the force. The two forces that play a role in the spring-mass system are the inertial force of the accelerating mass and the spring force. From Equation 1.1 and 1.2 it is possible to obtain the equation of motion

$$m\frac{d^2x}{dt^2} + k \cdot x = 0 \tag{1.3}$$

$$\frac{d^2x}{dt^2} + \omega_n^2 \cdot x = 0 \tag{1.4}$$

In Equation 1.4 it is possible to see the parameter ω_n that is linked to the natural frequency. Solving this equation it is possible to extract the period $T = 2\pi\sqrt{m/k}$ and so the natural frequency f_n (5).

$$f_n = \frac{1}{2\pi}\sqrt{\frac{k}{m}} \tag{1.5}$$

1.2.2 Helmholtz resonator

Helmholtz resonator is a special type of air spring oscillator (5) depicted in Figure 1.10. This oscillator is composed by a frictionless mass and a volume of air. Being compressed, the pressure of the air increases creating a force on the surface and the behavior is similar to a mass-spring system.

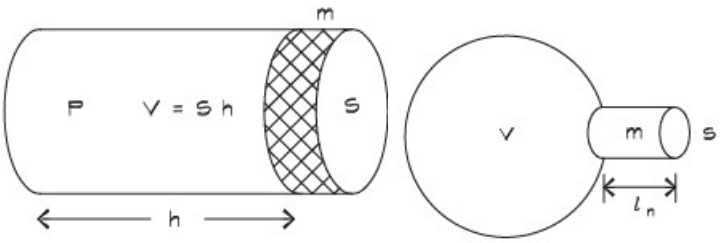

Figure 1.10: Air spring oscillator and Helmholtz resonator(5)

As in the mass-spring system, from the Newton's second law is possible to obtain the natural or resonant frequency. The pressure change is related the the change of volume in the neck as shown in Equation 1.6.

$$dP = -\gamma P\frac{dV}{V} \tag{1.6}$$

More similar to a liner is the neckless Helmholtz resonator (Figure 1.11), an enclosed volume with an opening area with a thickness τ (or l_0) that act like a small neck. The air compressed generates a pressure and so a force on the air surface of the neck S.

$$dF = S \cdot dP = -\gamma PS\frac{dV}{V} \tag{1.7}$$

Now the Newton's second law can be applied as shown in Equation 1.8. In this case the air mass $m = \rho_0 S\tau$ and the volume variation $dV = Sx$ in the neck must be considered.

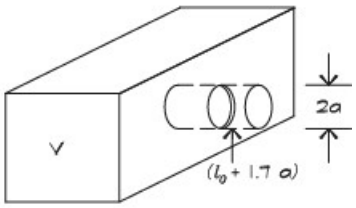

Figure 1.11: Neckless Helmholtz Resonator (5)

$$\begin{aligned} dF &= m\tfrac{d^2x}{dt^2} \\ -\gamma P S \tfrac{Sx}{V} &= \rho_0 S\tau \tfrac{d^2x}{dt^2} \\ \rho_0 S\tau \tfrac{d^2x}{dt^2} + \gamma P \tfrac{S^2}{V} x &= 0 \end{aligned} \tag{1.8}$$

Equation 1.8 is now similar to Equation 1.3 and so is possible to obtain the natural frequency. In the first left hand term is possible to see the mass $m = \rho_0 S\tau$ and in the second left hand term the spring stiffness $k = \gamma P S^2/V$. Considering also the relation $c_0^2 = \gamma P/\rho_0$ the natural frequency for a neckless Helmholtz resonator can be written as:

$$\begin{aligned} f_n &= \tfrac{1}{2\pi}\sqrt{\tfrac{\gamma P S^2}{V \rho_o S\tau}} \\ f_n &= \tfrac{c_0}{2\pi}\sqrt{\tfrac{S}{V\tau}} \end{aligned} \tag{1.9}$$

Long (5) refers to a "end effect" both in the top and bottom end of the orifice leading to the replacement of the real thickness with an effective length $l_0 + 2\cdot(0.85a)$ obtaining the final expression for the natural frequency of this resonator presented in Equation 1.10. The term $a{=}d/2$ represents the radius of the hole.

$$f_n = \frac{c_0}{2\pi}\sqrt{\frac{S}{V(\tau + 1.7a))}} \tag{1.10}$$

This equation find a confirmation in Ingard (19) that introduced the end correction $\delta{=}\ (16/3\pi)a \simeq 1.7a$. This is valid for a circular piston and to make it applicable to other aperture shapes, Ingard (19) defined the end correction as $\delta{=}\ 0.96\sqrt{S}$.

Usually SDoF and DDoF liners present multiple orifice in the face-sheet and this must be considered introducing a new parameter called porosity σ. The porosity represents the number of openings per unit area. Considering the volume as $V = S{\cdot}d$ where d is the depth of the airspace behind the orifices it is possible to obtain the natural frequency for multiple orifice resonator.

$$f_n = \frac{c_0}{2\pi}\sqrt{\frac{\sigma}{d(\tau + 1.7a))}} \tag{1.11}$$

1.3 Acoustic Impedance

In sound absorption the most important parameter is the impedance that characterize how well the liner can reduce the noise. In the case of a locally-reacting liner the

impedance can be defined as the ratio between the Fourier coefficient of the sound pressure and the normal component of the acoustic particle velocity in a given point. The impedance can be also normalized by using the characteristic impedance of the air $Z_0 = \rho_0 \cdot_0 c$ where ρ_0 is the air density and c in the speed of sound. This is shown in Equation 1.12 (1).

$$\zeta = \frac{p}{\rho c\,(\overrightarrow{u} \cdot \overrightarrow{n})} = \theta + i\chi \tag{1.12}$$

It is possible to notice two terms: θ is the resistance and χ is the reactance. The resistance is an indication of the force responsible to dissipate the acoustic energy and the reactance gives an indication about the frequency at which the absorption is maximum. In fact, when the reactance is zero, the resistance is maximum and so there is a peak in the absorption. These two parameters depend on frequency, aeroacoustic environment and liner geometry. In this work the study will be focus on the optimization of liner characteristics such as orifice diameter, cavity depths etc.

1.4 Optimization

The main goal of this thesis is to find the optimal value for the different liner's parameters. The objective functions to minimize are the Average Sound Pressure Level (ASPL) and the Overall Sound Pressure Level (OSPL). This is an iterative process and in each step the SPL is measured from a series of microphones located at a certain distance from the inlet. The sound pressure level comes from the computation of the field using aeroacoustic simulation software like ACTRAN that, among other equation types, solves the Linearized Euler Equation (LEE) to compute the required quantities in the space. The process can be automated using a Python script linked with ACTRAN. Initial parameter must be chosen in order to compute the impedance boundary condition in ACTRAN, using one of the models presented in the following. ACTRAN gives as output the sound pressure level on each microphone and then an average value can be obtained. The optimization algorithm chosen will now choose a new value for the parameters that must be optimized, and compute a new value of impedance. Then this value is changed in ACTRAN and as output it extract a new set of sound pressure level on the microphones. The process will stop when a minimum is reached and depending on the optimizer chosen, this can be a local or global minimum. In the optimization process very important are the physical constrains in order to obtain a more realistic acoustic liner.

Chapter 2

Impedance models

The main goal of noise research is to find a way to predict the acoustic performance of a new treatment (20). In this way, many problems described above can be solved finding the best set of liner's parameters that result in a better noise reduction. Depending on the situation, a different impedance model must be used and this plays an important role in the optimization loop.

2.1 Motsinger and Kraft

Motsinger and Kraft (6) present the Impedance in the classical way, as the ratio between the cause (pressure) and the effect (normal particle velocity) and this is reported in Equation 2.1.

$$Z = \frac{p}{v} = R + iX \tag{2.1}$$

Motsinger and Kraft (6) used the convention $e^{+i\omega t}$ for the wave solution of acoustic pressure and velocity and in which ω represent the circular frequency and t is the time. In this study they considered liner with internal rigid partitions to prevent the propagation of the wave in the liner and these are the so called point-reacting liners. The impedance is usually normalized with the characteristic impedance of the air ρc obtaining what was shown in Equation 1.12. Each wave are considered the superposition of a series of plane waves, where each of them hits the wall at different angles. The solution of the plane-wave is the same of an acoustic mode that propagates in a duct. In an idealized case it is possible to compute the fraction of incident energy absorbed by the acoustic treatment that depends on the angle of incidence with the convention shown in Figure 2.1, with the use of Equation 2.2.

$$\alpha = \frac{4\theta \cos\phi}{(1 + \theta\cos\phi)^2 + (\chi\cos\phi)^2} \tag{2.2}$$

In the case of a plane-wave mode with $\phi = 90°$ and with a duct of rectangular shape, the Cremer's analysis give the optimal impedance.

$$\frac{Z_{opt}}{\rho c} = (0.92 - 0.77i)\frac{H}{\lambda} \tag{2.3}$$

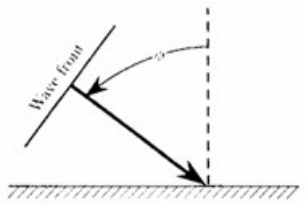

Figure 2.1: Wavefront on an acoustic treatment panel

In Equation 2.3 is possible to find the non-dimensional frequency parameter that is the ratio between the duct height H and the wavelength of sound λ.

Single Degree of Freedom liners

$$\frac{Z}{\rho c} = \frac{R}{\rho c} + i\left(\frac{X_m}{\rho c} + \frac{X_c}{\rho c}\right) \tag{2.4}$$

In Equation 2.4 there are the face sheet normalized resistance $R/(\rho c)$, the normalized face sheet mass reactance $X_m/(\rho c)$ and the normalized cavity reactance $X_c/(\rho c) = -\cot(kh)$ where k in cm^{-1} is the wavenumber and h in cm is the cavity depth.

Double Degree of Freedom liner

$$\frac{Z}{\rho c} = \frac{Z_1}{\rho c} + \frac{\frac{Z_2}{\rho c}\frac{\cot(kh_1)\sin(kh_2)}{\sin(kh)} - i\cot(kh)}{1 + i\frac{Z_2}{\rho c}\frac{\sin(kh_1)\sin(kh_2)}{\sin(kh)}} \tag{2.5}$$

In Equation 2.5 there is the contribution of two impedance Z_1 and Z_2 that can be written as follow.

$$\frac{Z_1}{\rho c} = \frac{R_1}{\rho c} + \frac{X_{m1}}{\rho c} \tag{2.6}$$

$$\frac{Z_2}{\rho c} = \frac{R_2}{\rho c} + \frac{X_{m2}}{\rho c} \tag{2.7}$$

In these equation the quantities with the subscript 1 and 2 indicate respectively the face-sheet and the septum impedance, resistance and reactance. The term h indicate the total depth of the liner.

Bulk absorber panels

$$\frac{Z}{\rho c} = \frac{Z_B}{\rho c} + \xi_B \coth(\gamma h) \tag{2.8}$$

where

$$\frac{Z_B}{\rho c} = \frac{R_B}{\rho c} + i\frac{X_B}{\rho c} \tag{2.9}$$

In Equation 2.8, ξ_B represent the characteristic impedance ratio between the impedance of the bulk absorber and the impedance of air, and γ is the propagation coefficient in the bulk absorber that represent the wavenumber.

Resistance and Reactance

In all the three cases above, is possible to find the same parameters like resistance, mass reactance etc. There are some formulation to compute these terms given by Motsinger and Kraft (6).

The general expression for the resistance is shown in 2.10.

$$\frac{R}{\rho c} = A + BV_i \tag{2.10}$$

where V_i is the incident velocity, computed experimentally or with the root-mean square of the fluctuating acoustic velocity, and A and B were determined experimentally. In Equation 2.10 A is the linear term of the resistance while B is the non linear term, being in the velocity-dependent component. This last term makes the resistance a function of the incident wave amplitude. A and B for a perforated plate

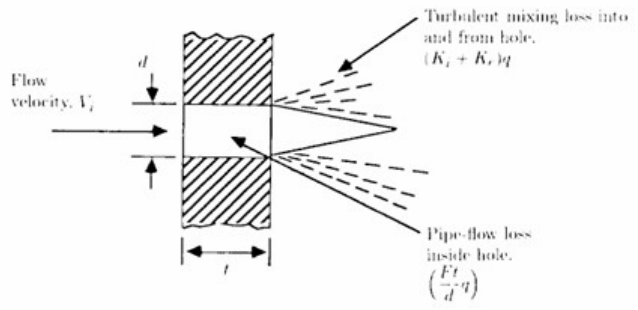

Figure 2.2: Flow mechanics for the resistance (6)

can be computed from fluid dynamics taking into account that the pressure differential across the sample generates an energy loss mechanism. Referring to Figure 2.2 the first term in Equation 2.10 is given by the pressure loss due to hole-flow friction and the second term is due to the turbulence given by the entrance and exit loss. Depending on the hole opening area the flow inside can be laminar or turbulent and, depending on this, one term is predominant on the other. If the flow is laminar the first term is more important while if the flow is turbulent, in most of perforated sheet of SDoF and DDof, the second nonlinear term is predominant. The general expression for the resistance is

$$\frac{R}{\rho c} = \frac{\Delta p}{\rho c V_i} \tag{2.11}$$

Is possible to compute the ratio between the pressure loss and the dynamic pressure within the hole as

$$\frac{\Delta p}{q} = \frac{F\tau}{d} + K_i + K_e \tag{2.12}$$

where τ is the face-sheet thickness, F is the friction factor for pipe flow, K_i and K_e are the dimensionless entrance and exit loss respectively ($K_i + k_e$ is approximately 1 (6)). The friction factor and the dynamic pressure can be written as follow

$$F = \frac{a}{N_{Re}} = \frac{a\mu}{\rho V_h d} \tag{2.13}$$

$$q = \frac{1}{2}\rho V_h^2 \tag{2.14}$$

In Equation 2.13 and Equation 2.14 appear the in orifice velocity $V_h = V_i/(C_D\sigma)$ where $C_D \simeq 0.76$ (6) is the orifice discharge coefficient and $\sigma = \pi n d^2/4$ is the porosity in a multi-hole plate. In Equation 2.13 $a = 64$ (6) is a dimensionless proportionality constant and N_{Re} is the Reynold's number. Now rewriting the Equation 2.11

$$\frac{R}{\rho c} = \frac{\Delta p}{\rho c V_i} = \frac{a\mu\tau}{2\rho c(\sigma C_D)d^2} + \frac{K_i + K_e}{2c(\sigma C_D)^2} V_i = A + BV_i \tag{2.15}$$

the term A and B can be computed

$$A = \frac{a\mu\tau}{2\rho c(\sigma C_D)d^2} \tag{2.16}$$

$$B = \frac{K_i + K_e}{2c(\sigma C_D)^2} \tag{2.17}$$

The mass reactance can be computed in the same way for the face-sheet and septum as

$$\frac{X_m}{\rho c} = \frac{k(\tau + \epsilon d)}{\sigma} \tag{2.18}$$

where the dimensionless end correction $\epsilon = 0.85$ (6) depends on the material of the face-sheet and the septum. Ingard (19) presented also a porosity effect that must be added to this end effect.

$$\epsilon = 0.85(1 - 0.7\sqrt{\sigma}) \tag{2.19}$$

It is possible to compute also the impedance for the bulk absorber of Equation 2.8 as

$$\frac{Z_B}{\rho c} = 1 + 0.05854\left(\frac{f\rho}{P}\right)^{-0.75} + i0.08777\left(\frac{f\rho}{P}\right)^{-0.73} \tag{2.20}$$

where P is the linear part of the flow resistance per unit thickness of the material. In is also possible to compute the value of γ in the second term of Equation 2.8 as

$$\gamma = \alpha_B + i\beta_B = 0.19478k\left(\frac{f\rho}{P}\right)^{-0.59} + ik\left[1 + 0.09476\left(\frac{f\rho}{P}\right)^{-0.7}\right] \tag{2.21}$$

The coefficients of Equation 2.21 were obtained experimentally by Delany and Bazley (21). Experiment were done on different fibrous commercial material in an impedance tube and the results were plotted leading to a simple power-law relation for α_B and β_B.

Effect of grazing flow and Sound Pressure Level

Grazing flow and Sound Pressure Level have an influence on the impedance model. Using Equation 2.10 and substituting the expression of V_i given by Motsinger and Kraft (6) the resistance became

$$\frac{R}{\rho c} = A + \frac{Bp}{\rho c\sqrt{(R/\rho c)^2 + (X/\rho c)^2}} \tag{2.22}$$

If A is negligible and the reactance is zero, the Resistance can be written as

$$\frac{R}{\rho c} = \sqrt{\frac{Bp}{\rho c}} \tag{2.23}$$

In the absence of grazing flow the magnitude of the pressure p can be computed as a function of the SPL of the incident wave.

$$|p| = p_{ref} 10^{SPL/20} \tag{2.24}$$

When a flow turbulence is present the effect of a flow turbulence pressure fluctuation must be added and to estimate these fluctuation experimental data were used with different Mach number. A good fit was shown between the measured and predicted resistance data when they used a value of the pressure fluctuation equal to $p_F = 90'000M^2$.

With all these information, the final expression of the resistance in the zero reactance case can be found.

$$\frac{R_{gf}}{\rho c} = \sqrt{\frac{(K_i + K_e)90'000}{2cC_D^2 \rho c}} \frac{M}{\sigma} \tag{2.25}$$

In this equation $K_i + K_e = 1$, $\rho c = 41.5\ rayls$, $c = 34'380\ cm/sec$ and $C_D = (1 - 2\delta^*/d)^2$ with the assumption of its typical value of $C_D = 0.76$ (6). With these data the term multiplying M/σ is 0.25, similar to the value indicated by Heidelberg and Rice (22) of 0.3. In a first approximation Heidelberg and Rice (22) ignored the influence of the boundary-layer. Later in the study was demonstrated that the boundary-layer was thicker than predicted and that it has an influence on the resistance of a perforated plate. The resistance in presence of a grazing flow becomes dependent on the boundary layer displacement thickness δ^* as shown in Equation 2.26.

$$\frac{R_{gf}}{\rho c} = \frac{M_0}{\sigma \left(2 + 1.256 \frac{\delta^*}{d}\right)} \tag{2.26}$$

The mass end correction term ϵ is also dependent on the mach number and follows the relation in Equation 2.27 given by Rice (23).

$$\epsilon = 0.85 \frac{(1 - 0.7\sqrt{\sigma})}{1 + 305M^3} \tag{2.27}$$

Now the mass reactance of equation 2.18 can be written as

$$\frac{X_m}{\rho c} = \frac{k\left(\tau + \frac{0.85(1-0.7\sqrt{\sigma})}{1+305M^3} d\right)}{\sigma} \tag{2.28}$$

2.2 Kooi and Sarin

Murray and Astley (24) presented an impedance model based on the equations given by Kooi and Sarin with the addition of a nonlinear term for the resistance while the

reactance follows what was presented by Rice (23). The general expression for the normalized resistance is

$$\frac{R}{\rho c} = \frac{R_{vis}}{\rho c} + \frac{R_{gf}}{\rho c} + \frac{R_{nl}}{\rho c} \tag{2.29}$$

where R_{vis} is the resistance given by the viscous hole losses, R_{gf} are the liner losses given by the grazing flow and R_{nl} are the nonlinear losses. These are presented in the following

$$\frac{R_{vis}}{\rho c} = \frac{k_1 \mu \tau}{\rho c \sigma C_D d^2} \tag{2.30}$$

$$\frac{R_{gf}}{\rho c} = \frac{k_2 M[5 - (\tau/d)]}{4\sigma} - \frac{k_3 df}{\sigma c} \tag{2.31}$$

$$\frac{R_{nl}}{\rho c} = \frac{k_4(1-\sigma^2)}{2cC_D^2\sigma^2} u = S \cdot u \tag{2.32}$$

The S in this last resistance term is similar to what will be presented by Dahl (25) in equation 2.47.

The normalized reactance follows what was elaborated by Rice (23) but with a small correction in the definition of the perforate face-sheet end correction ϵ. The general form is

$$\frac{X}{\rho c} = \frac{X_m}{\rho c} + \frac{X_c}{\rho c} \tag{2.33}$$

where

$$\frac{X_m}{\rho c} = \frac{k(\tau + \epsilon d)}{\sigma} \quad \text{with} \quad \epsilon = \frac{0.85(1 - 0.7\sigma^{0.5})}{1 + 200M^3} \tag{2.34}$$

$$\frac{X_c}{\rho c} = -\cot(kh) \tag{2.35}$$

The acoustic velocity is expressed by u that can be calculated using the formulation

$$u = \frac{P}{\{[(R_{vis} + R_{gf} + R_{nl})\rho c]^2 + [(X_m + X_c)\rho c]^2\}^{0.5}} \tag{2.36}$$

In the R_{nl}, the acoustic velocity u is present so an iterative process must be done.

In-situ measurement in the NLR Aerospace Acoustic Laboratory in Holland were done on a single degree of freedom liner with different Mach numbers. It was noticed that with a grazing flow the resistance increases particularly at low frequencies. This is in line with what was found by Zhang and Bodony in their grazing flow modeling study. They indicated that a stronger vortex shedding is produced when the incident wave is at lower frequencies. It was also noticed an increase in the resonant frequency. It was also shown a good agreement with predicted and measured impedance data.

2.3 Dahl

Dahl (25) presented different models for the normalized impedance $\zeta = Z/\rho c$. Two of them, Two-Parameter (TP) and Crandall Full-solution (CF) models, analyzed this impedance as follows

$$\zeta = \theta + i\xi = \theta_{lin} + \theta_{nonlin} + \theta_{gf} + i\left\{\chi_{fs} - \cot(kh)\right\} \tag{2.37}$$

In Equation 2.37, $\theta = R/(\rho c)$ represents the normalized resistance and the subscripts lin, $nonlin$ and gf represent the viscous, nonlinear and grazing flow contribution to the resistance. The mass reactance of the face-sheet and the cavity reactance are indicated by χ_{fs} and $-\cot(kh)$. Also in this case the convention used for the time is based on $e^{i\omega t}$. The acoustic oscillatory flow through the perforate is treated as be incompressible and quasi-steady thanks to the assumption of lumped element and that the cell depth is small compared to the wavelength, so it can be considered an Helmholtz resonator (25).

The Two-Parameters model was early presented in the Motsinger and Kraft section and is based on the parameters A and B.

Crandall Full-Solutin model (CF)
This model use, for the oscillatory flow, a pure analytical solution to give a Poiseuille-type and frequency dependent viscous losses. Bessel functions are used to describe the resistance and reactance component in the hole and so two function for resistance and reactance end correction must be calculated. This model give an impedance in a form similar to the Equation 2.37.

$$\zeta = \theta_0 + \theta_{0,\omega} + S_R v_{rms} + \theta_{gf} + i\left\{\chi_m + \chi_{me} + S_m v_{rms} - \cot(kh)\right\} \tag{2.38}$$

If the source has just a single tone an iterative process must be done to compute both ζ and v_{rms} defined as

$$v_{rms} = \frac{p_{ref} 10^{SPL/20}}{\rho c|\zeta|} \tag{2.39}$$

where $p_{ref} = 20\mu Pa$. If there is a broadband source, the frequency dependent components are combined to determine the value of $v_{rms}(f)$. From Equation 2.38 can be collect another impedance defined as

$$\zeta_{0,\omega} = (\theta_0 + \theta_{0,\omega}) + i(\chi_m + \chi_{me}) \tag{2.40}$$

where the subscript ω indicate a dependency on the frequency. χ_m and χ_{me} indicate the mass reactance and the mass reactance due to the end correction. The impedance terms can be computed as:

$$(\theta_0 + \theta_{0,\omega}) = Re\left\{\frac{i\omega(\tau + \epsilon_{Re} d)/(c\sigma)}{F(k_\mu r)}\right\} \tag{2.41}$$

$$(\chi_m + \chi_{me}) = Im\left\{\frac{i\omega(\tau + \epsilon_{Im} d)/(c\sigma)}{F(k_\mu r)}\right\} \tag{2.42}$$

In these expression r represents the hole radius and ϵ_{Re}, ϵ_{Im} and $F(k_\mu r)$ can be expressed as:

$$\epsilon_{Re} = \frac{1 - 0.7\sqrt{\sigma}}{1 + 305M^3} \tag{2.43}$$

$$\epsilon_{Im} = 0.85\epsilon_{Re} \tag{2.44}$$

$$F(k_\mu r) = 1 - \frac{2J_1(k_\mu r)}{k_\mu r J_0(k_\mu r)} \tag{2.45}$$

In Equation 2.45 J_0 and J_1 are the zero- and first-order Bessel functions. k_μ represents the viscous Stokes wave wavenumber

$$k_\mu^2 = -i\frac{\omega\rho}{\mu} \tag{2.46}$$

The resistance due to the grazing flow is that presented in Equation 2.26. Finally the last two term multiplying v_{rms} in Equation 2.38 are defined as

$$S_R = \frac{133.6541}{\rho c}\left(\frac{\rho(1-\sigma)^2}{2C_D^2\sigma^2}\right) \tag{2.47}$$

$$S_M = -0.00207\frac{k}{\sigma^2} \tag{2.48}$$

These indicate the nonlinear resistance slope and the nonlinear mass reactance slope respectively. In the S_R expression the definition of the discharge coefficient depend on the ratio between the thickness of the plate and the hole diameter.

$$\begin{cases} C_D = 0.80695\sqrt{\sigma^{0.1}/e^{-0.5072(\tau/d)}} & \text{if } \tau/d \leq 1 \\ C_D = 0.584854\sqrt{\sigma^{0.1}/e^{-1.151(d/\tau)}} & \text{if } \tau/d \geq 1 \end{cases} \tag{2.49}$$

2.4 Zorumski and Tester

Zorumski and Tester (20) present an impedance given by the contribution of linear and nonlinear terms. This can be seen as the ratio between the acoustic pressure and the acoustic particle velocity and depends on the frequency.

Linear impedance
As in the linear electrical circuit theory this is an useful parameter in acoustic because the dynamics of the liner is independent on the amplitudes of the variables and depend only on their ratio. For sheet material the impedance can be defined as expressed in Equation 2.50.

$$Z_\omega^* = \frac{p_\omega^*}{v_\omega^*} = R_\omega^* - iX_\omega^* \tag{2.50}$$

In this expression the terms p_ω^* and v_ω^* represent the amplitude of a complex harmonic motion in the time domain where the time factor is $e^{-i\omega t}$. R_ω^* and X_ω^* are respectively the resistance and the reactance of the liner.

Nonlinear impedance
Since the propagation process is described by linear equation the impedance can be considered independent of the amplitude of the acoustic motion. Studies demonstrate that in operational environment, like engine ducts, the behavior of the fluid motion near liners is nonlinear so the impedance of commercial liners depend on the amplitude of the incident wave. The steady flow or zero frequency case confirm the existence of nonlinear effect. Zorumski and Parrott (7) related experimentally the

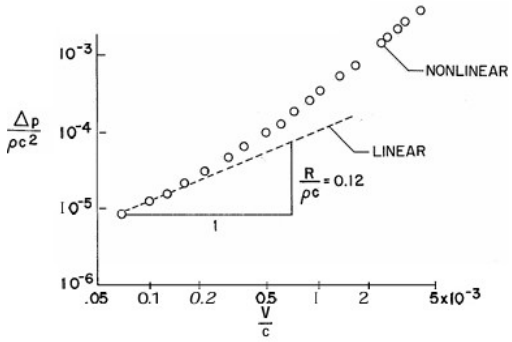

Figure 2.3: Pressure drop as a velocity function (7)

pressure drop in a thin sheet, with the instantaneous fluid velocity $v(t)$ as shown in Figure 2.3 and Equation 2.51.

$$\Delta p(t) = R_t[v(t)] + X(t)[v(t)]\frac{\partial v}{\partial t} \tag{2.51}$$

The term $R_t[v]$ has a dependency on time, as indicated by the subscript, and refers to the steady flow resistance at velocity v. For high Reynolds number it can be expressed as $R_t[v] = b|v|$ where b is a constant. Neglecting the $X_t[v(t)]$ term, so $\Delta p(t) = R_t[v(t)]$, and assuming that there is just one frequency ω_1 the velocity and the pressure drop are:

$$\begin{aligned} v(t) &= v_1 \sin(t) \\ \Delta p(t) &= b v_1^2 \sin(t)|\sin(t)| \end{aligned} \tag{2.52}$$

Considering the Fourier transform is possible to obtain the Fourier component of the fluctuating pressure differential in the given frequency ω_1

$$\Delta p_1 = \frac{8b}{3\pi} v_1^2 \tag{2.53}$$

Now is possible to compute the ratio between the pressure drop and the velocity that represent the impedance (20).

$$R_1 = \frac{\Delta p_1}{v_1} = \frac{8b|v_1|}{3\pi} \tag{2.54}$$

At low Reynold number, linear effect are present and $R[v]$ is independent to the velocity v obtaining $R_1 = a$. Usually in possible to find both linear and nonlinear effect so the final expression is

$$R_1 \simeq a + \frac{8b|v_1|}{3\pi} \tag{2.55}$$

For perforated plates an approximation is presented in equation 2.56.

$$\Delta Z_\omega = [a + b v_e] - i\,[g - h v_e] \tag{2.56}$$

In Equation 2.56 v_e is an estimation of the particle velocity normal to the surface and the coefficient b and h multiplying it depend on the properties and geometry of

the material. There are different expression for the value of b and one is presented in Equation 2.57.

$$b = 1.14\left(\frac{1-\sigma^2}{\sigma^{2.1}}\right) exp\left[-0.507\frac{l^*}{d^*} - 1.7\left(\frac{l^* f}{c}\right)\frac{\sigma}{v_e}\right] \tag{2.57}$$

Duct Liners

If the lined surfaces is independent of the local sound field properties, the liner is said to be point or locally reacting. In certain conditions the liner's impedance is a function of the liner parameters. The impedance of this local reacting liner can be expressed as

$$Z_\omega = \Delta Z_\omega + i\frac{k_a}{k^*}\cot\left(k^* d^*\right) \tag{2.58}$$

The second right hand term is the impedance of the air cavity. In this term is possible to see the wave number of the motion in the cavity k^* and the cavity depth d^* while the term $k_a = \omega/c_a$ in the case of plane wave is equal to k^*. Taking into account the viscous dissipative effect in the cavity the wave number must be modified adding a small imaginary part as shown in equation 2.59.

$$k^* = \frac{\omega}{c_a} + i\frac{1}{r_e^* c_a}\left(\frac{\omega\nu}{2}\right)^{1/2} \tag{2.59}$$

In this expression r_e^* is the effective radius of the honeycomb cell and ν is the cavity fluid kinetic viscosity. Zorumski and Tester (20) present also an impedance for an extended reaction liner presented in Equation 2.60

$$Z_c(f_j) = \left[-z^*(f_j)/\left\{\rho_a c_a k_{rm}^*\right\}\right]\cot\left\{k_{rm}^*(f_j) d^*\right\} \tag{2.60}$$

In the equation k_{rm}^* is the wavenumber in extended reacting liner.

Chapter 3

Actran

The main character of the present work is the acoustic software Actran. Actran is a software developed by Free Field Technologies SA software company, founded in 1998. The true revolution on this was the idea to use a finite element-based simulation tool in vibro-acoustic simulation in order to substitute the past used Boundary Element Method (BEM) with all its limitations. More complex noise sources can be simulated and multi-million degrees-of-freedom models can be managed. Python and C++ are the main languages in which Actran is written and it can be subdivided in different modules depending on which kind of study must be performed. Among others, the modules of our interest are Actran AeroAcoustics, Actran Turbo-machinery (TM) for the prediction of turbo-machinery noise and Actran DGM. Turbo-machinery noise is a very important noise source and it is present in aircraft engines and helicopter turbines. Actran TM is a part of a modeling strategy called Direct Frequency Response (DFR). There are different modeling strategy in Actran (26):

- Actran DGM uses Linearized Euler Equation (LEE), Pseudo Vortical Linearized Euler Equation (PVLEE) or Acoustic Perturbation Equation (APE) and can be used in presence of complex mean flow.
- Actran DFR is used to solve most common acoustic field and uses Mohring's equation in presence of a flow or Helmholtz's equation with no flow conditions.
- Actran Ffowcs-Williams Hawkings equation is used to compute the far field radiation.

3.1 Actran DGM

Actran DGM (Discontinuous Galerkin Method) is designed to predict the propagation of the noise in complex flow conditions, with high temperature gradient, non-homoentropic fluxes etc. This method is free from the finite element method and the mesh could be non-homogeneous due to the automatic adaptation of the element order. In this way is possible to find elements of different dimensions on the same mesh. (27) Actran DGM is a Discontinuous Galerkin implementation for solving, among other type of equations mentioned above, the Linearized Euler Equations (LEE) in the time domain (8).

3.1.1 Linearized Euler Equations (LEE)

The Linearized Euler Equations are obtained from a series of assumption made on the Navier-Stokes equation. These last equations fully describe the motion of viscous fluid substances. Navier-Stokes equation are balance equation that originate from the application of the Newton's second law to fluid motion assuming that the sum of a pressure term and a diffusing viscous term, related to the velocity gradient, represents the stress in the fluid (28). The balance equation concern the mass equation, momentum balance equation and energy balance equation. All the quantities described in these equation can be seen as composed by two different contribution: the mean component where its derivative respect to the time is zero, and the fluctuating component marked by the superscript $'$. These quantities can be seen as

- $\rho = \rho_0 + \rho'$
- $p = p_0 + p'$
- $\mathbf{v} = \mathbf{v}_0 + \mathbf{v}'$
- $s = s_0 + s'$

The orders above the 1th are neglected leading to a linear system without non-linear effects. This is valid until the sound level is not so high. The assumption made to pass from the Navier-Stokes equation to the Linearized Euler Equation can be summarized as follow:

- $\tau' = 0$, viscous forces fluctuation are neglected
- $q' = 0$, thermal conductivity fluctuation is neglected
- the fluid is considered as an ideal gas

The set of Linearized Euler Equation (LEE) is different if the acoustic process is Homentropic or Isentropic. The homentropic process is characterized by the fluctuating entropy constant in time and uniform in space.

$$\frac{\partial s'}{\partial t} = \nabla s' = 0 \tag{3.1}$$

The energy equation is satisfied and the pressure and density fluctuations are directly related with $p' = c^2\rho'$ where c is the speed of sound. The pressure fluctuation p' is not a primary unknown but it can be calculated with this relation in a post-processing phase. The set of Linearized Euler Equation for an Homentropic process is composed just by the mass and momentum balance equations and the energy equation is automatically satisfied as shown in the Equation system 3.2.

$$\begin{cases} \frac{\partial \rho'}{\partial t} + \nabla \cdot (\rho' \mathbf{v}_0 + \rho_0 \mathbf{v}') = 0 \\ \rho' \mathbf{v}_0 \cdot \nabla \mathbf{v}_0 + \rho_0 \left(\frac{\partial \mathbf{v}'}{\partial t} + \mathbf{v}' \cdot \nabla \mathbf{v}_0 + \mathbf{v}_0 \cdot \nabla \mathbf{v}' \right) = -\nabla (c^2 \rho') \end{cases} \tag{3.2}$$

The set or Linearized Euler Equation in presence of an isentropic process is composed by 5 partial differential equation: 1 for the mass balance, 1 momentum balance

equation for each of the three axes and 1 for the energy balance. This represent the most general set of LEE and the range of validity is wider. In this case the process for the acoustic propagation is isentropic and it can be described by the Equation system 3.3.

$$\frac{\partial s'}{\partial t} + \mathbf{v}_0 \cdot \nabla s' = 0 \tag{3.3}$$

The set of Isentropic Linearized Euler Equations is expressed in Equation 3.4.

$$\begin{cases} \frac{\partial \rho'}{\partial t} + \nabla \cdot (\rho' \mathbf{v}_0 + \rho_0 \mathbf{v}') = 0 \\ \rho' \mathbf{v}_0 \cdot \nabla \mathbf{v}_0 + \rho_0 \left(\frac{\partial \mathbf{v}'}{\partial t} + \mathbf{v}' \cdot \nabla \mathbf{v}_0 + \mathbf{v}_0 \cdot \nabla \mathbf{v}' \right) = -\nabla p' \\ \left(\frac{D_0 \rho'}{Dt} + \mathbf{v}' \cdot \nabla \rho_0 \right) c_0^2 = \frac{D_0 p}{Dt} + \mathbf{v}' \cdot \nabla p_0 \end{cases} \tag{3.4}$$

Since the general formulation of the material derivative is

$$\frac{DX}{Dt} = \frac{\partial X}{\partial t} + \mathbf{v} \cdot \nabla X \tag{3.5}$$

the energy equation can be expressed as:

$$\left(\frac{\partial \rho'}{\partial t} + \mathbf{v}_0 \cdot \nabla \rho' + \mathbf{v}' \cdot \nabla \rho_0 \right) c_0^2 = \frac{\partial p'}{\partial t} + \mathbf{v}_0 \cdot \nabla p' + \mathbf{v}' \cdot \nabla p_0 \tag{3.6}$$

3.1.2 Discretization

Spatial scheme

The specific feature of the Discontinuous Galerkin is that neighbor element don't share the same degrees of freedom. Non-structured tetrahedral are the main components of the acoustic domain and the accuracy depends on the imposition of a sufficient number of degrees of freedom. To design the mesh accurately the mode that must be chosen is the mode with the shortest length scale. The candidate that couples with this condition is the upstream propagating modes. The minimal wavelength can be computed as shown in Equation 3.7 (10).

$$\lambda_{min} = \frac{\sqrt{v_i^0 v_i^0} - c}{f} \tag{3.7}$$

Since the degree of freedoms are not shared by two consecutive elements, the solution may differ from one side of an element face to another. In this way the continuity of the solution inside the mesh is an indicator of the convergence of this solution on it.
The general form of the equations above described is shown in Equation 3.8.

$$\frac{\partial q}{\partial t} + \frac{\partial}{\partial x_j} (F_j \cdot q) = 0 \tag{3.8}$$

In Equation 3.8 the term q in the vector containing all the unknown, F_j in a vector containing all the local mean flow information. Now the spatial discretization of the problem can be expressed as (10):

$$\int_\Omega N_\alpha \frac{\partial q}{\partial t} dV = \int_\Omega \frac{\partial N_\alpha}{\partial x_j} F_j \cdot q dV - \oint_{\partial\Omega} N_\alpha F_j \cdot q n_j dS \tag{3.9}$$

In the right hand term of Equation 3.9 is possible to see a surface integral on the element border and this must be computed following the boundary conditions described above.
The Galerkin shape functions N_α are multiplied to the mass, momentum and energy equations and are high order Lagrange polynomial functions. These functions, with order ranging from 1 to 16, are used to the interpolation on the mesh as shown in Figure 3.1. As mentioned above ActranDGM adapts automatically the interpola-

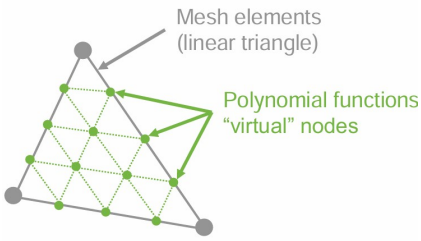

Figure 3.1: 4th order element (8)

tion order on each mesh elements and this depends on the frequency, the flow inside the element and the element size. This automatic definition of the orders allows to catch also the smallest acoustic wavelength. The ratio between this smallest wavelength and the maximum element length λ_{min}/L_{max} is the basis of this adaptation mechanism. Higher L_{max} leads to smaller values of this ratio and so Actran will chose higher orders to represent accurately the small length scales. In smaller elements with low L_{max} values (large λ_{min}/L_{max} ratio) the spatial fluctuations are large if compared to the element size and so a lower order can be used. This is well represented in Figure 3.2. The best order for efficiency reasons is 6 corresponding to a λ_{min}/L_{max} range equals to [0.667,1]. This means that the preferable maximum length of the element shall be between λ_{min} and $1.5\lambda_{min}$. To select appropriately the

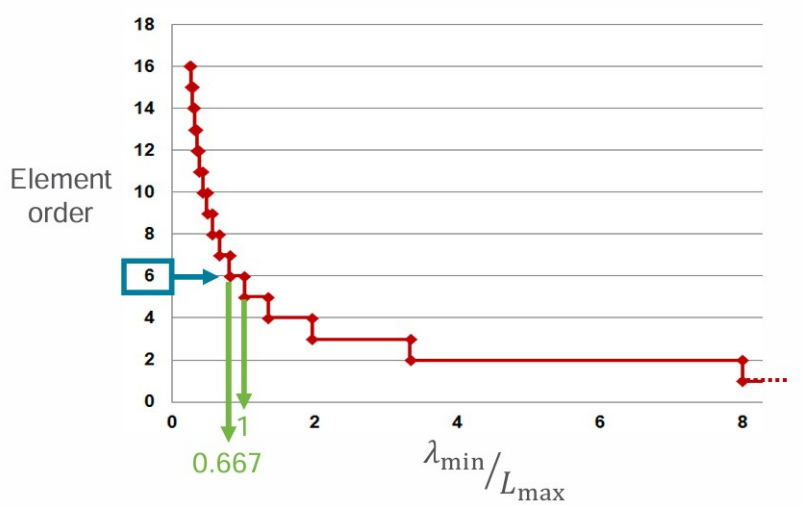

Figure 3.2: Element order as λ_{min}/L_{max} function (9)

order the regularity of the element shape is important. The efficiency is higher when there are equilateral elements with a proper element order in all directions. If there

are highly-distorted element in some direction there may be an over-estimation of the order. An example of good and bad shape of an element is shown in Figure 3.3

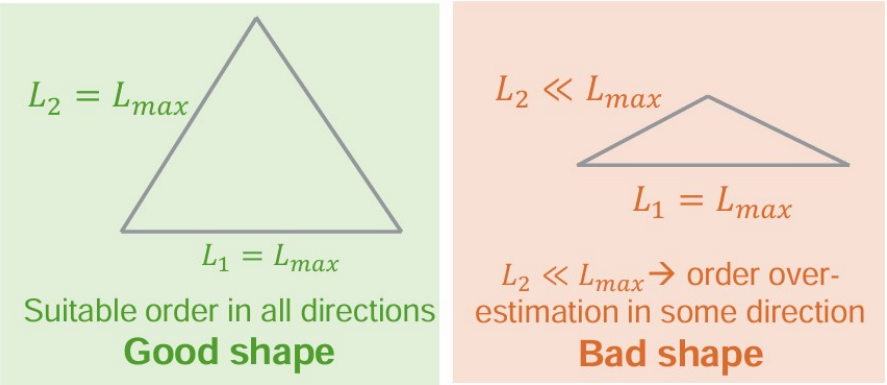

Figure 3.3: Example of good and bad element shape (9)

There are two indicators for the numerical quality of the simulation: dissipation and dispersion error. The dissipation error in an indication based on the acoustic propagation path and indicates the decrease in amplitude along it. The dispersion error is an indication of the change in the propagation speed and takes as reference the expected propagation speed. In these two errors an important role is played by the element order and, as presented above, this depends on the ratio between the minimal wavelength and the maximum element length. These errors have a value for each of the possible orders and so for each element can be computed the order that leads to a lower errors.

Time scheme

Once the spatial discretization was investigated a small introduction of time discretization is presented. ActranDGM uses by default a 4th order Runge-Kutta scheme (RK4) (10). The main properties of this numerical scheme is the low computational cost for high-order derivative to obtain both accuracy and speed. This technique is of common use for the solution of turbulent gas flow. The set of Navier-Stokes equation can be reduced, thanks to quadrature techniques, to a set of ordinary differential equation (ODE) solved by the RK4(**?**). In the differential quadrature method, the function and its derivative are calculated as an approximation given by the sum of the function in certain grid point weighted with some weighting coefficients A and B (first and second order coefficients). These coefficients depend on the particular quadrature scheme used such us Polynomial Differential Quadrature Method (PDQM), Discrete Singular Convolution Differential Quadrature Method (DSCDQM) etc (**?**). Once a set of ordinary differential equation is obtained the RK4 scheme can be used. The Runge-Kutta method is expressed numerically in Equation 3.10.

$$f(x, y, z, t_0 + \Delta t) = f(x, y, z, t_0) + \frac{1}{6}\left[E_1 + 2E_2 + 2E_3 + E_4\right] \tag{3.10}$$

where

$$E_1 = \Delta t \frac{df}{dt}\left(u, v, w, \rho, p, t_0\right) \tag{3.11}$$

$$E_2 = \Delta t \frac{df}{dt}\left(u + \frac{E_1}{2}, v + \frac{E_1}{2}, w + \frac{E_1}{2}, \rho + \frac{E_1}{2}, p + \frac{E_1}{2}, t_0 + \frac{\Delta t}{2}\right) \tag{3.12}$$

$$E_3 = \Delta t \frac{df}{dt}\left(u + \frac{E_2}{2}, v + \frac{E_2}{2}, w + \frac{E_2}{2}, \rho + \frac{E_2}{2}, p + \frac{E_2}{2}, t_0 + \frac{\Delta t}{2}\right) \tag{3.13}$$

$$E_4 = \Delta t \frac{df}{dt}\left(u + E_3, v + E_3, w + E_3, p + E_3, \rho + E_3, t_0 + \Delta t\right) \tag{3.14}$$

Some consideration must be done on the time step Δt. This is automatically computed by Actran using the Courant-Friedrichs-Lewy (CFL) condition. This is expressed in 3.15.

$$\Delta t \leq C(p)\frac{r}{c} \tag{3.15}$$

In the above equation the CFL number $C(p) \simeq \frac{1}{2p+1}$ is used in Actran and is expressed in function of the element order p. r represent the radius of the circle inscribed in the element and c is the speed of sound. The fourth order Runge-Kutta is an explicit scheme and its stability is ensured by the CFL condition. Since Actran chose the smallest time step, the good or bad shape of an element impact the performances. In Figure 3.3 a good shape in all the elements ensure a large time step because the radius of an inner circle is bigger. If one single element has a bad shape (smaller radius and consequently small Δt) the performances of the whole model are affected.
To well understand the link between the element size and the time step, it is necessary to refer to Figure 3.4.

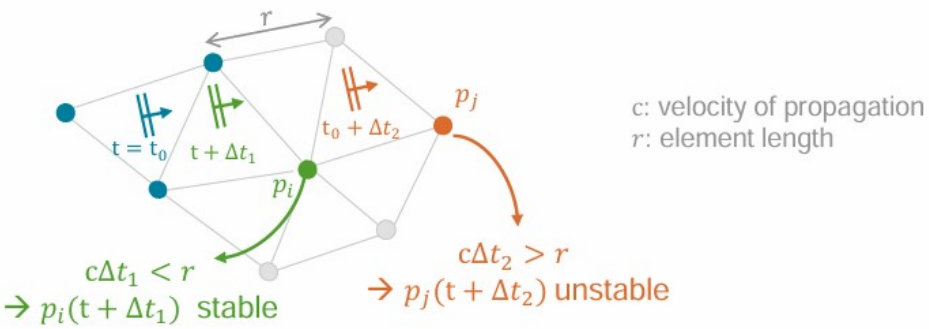

Figure 3.4: CFL condition (9)

These analyses refer to propagating acoustic waves so the condition is that during a time step the distance traveled by the acoustic wave must not exceed the element length.

3.1.3 Boundary condition

In Equation 3.9 in Section 3.1.2 the boundary integral must be computed considering the boundary conditions. This integral is computed taking in consideration the two solution in the nearby elements of the border. There are different type of boundary condition as presented in the following sections.

Non-reflecting boundary condition

This condition establishes that for the far field propagation the outgoing modes are free to leave the domain and the incoming modes are set to zero. This condition acts very well in presence of normal incidence waves but it can produce some reflection for the traverse propagating waves. Since the non-reflecting boundary condition generates some numerical reflection and this boundary is positioned as close as possible to the near field to reduce the computational cost, usually this is connected with a buffer zone in which there is a damp of the acoustic waves incoming. This allows a reduction in the reflecting mechanism enhancing the properties of a non reflecting boundary condition. Another way to ensure the proper functioning of the condition is to respect some rule in the choosing of the geometry. Sharp angles must be avoided and the shape of the boundary must be as close as possible to the shape of the propagating waves in order to reach the border as normal as possible avoiding the reflections mentioned above. This will be verified in the next section when a rectangular boundary was chosen for the first analyses. A scheme of the combination between all these characteristics is shown in Figure 3.5.

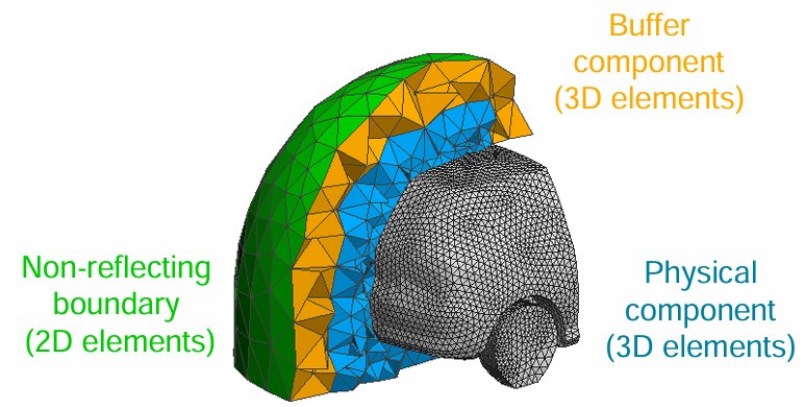

Figure 3.5: Non reflecting boundary condition and buffer zone (10)

Buffer Zones

This zone is always linked with the non reflecting boundary condition to avoid numerical reflections due to waves that are not perfectly normal to the boundary. This zone damps the waves to reduce the reflection with a progressive dumping while moving through this zone. The expression for the damping is expressed in Equation 3.16.

$$\sigma(x) = \sigma_{max}|1 + \frac{d(x) - L}{L}|\beta \tag{3.16}$$

The damping increase progressively until reach its maximum value σ_{max} near the non-reflecting boundary condition. In the above equation, L is the thickness of the zone, $d(x)$ is the distance from the bottom of the damping zone and β is a parameter that controls the damping increase. A representation of the damping ratio is shown in Figure 3.6. Referring to the vector q in equation 3.9 the damping ratio can be applied to every time step $\hat{q}'_{n+1} = (1 - \sigma(x))q_{n+1}$.

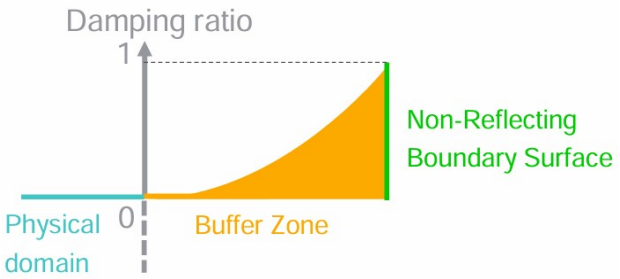

Figure 3.6: Damping ratio in the near field (10)

Wall condition

The hard wall condition imposes that the velocity normal to the wall is set to zero. In this way the acoustic waves will be completely reflected. This velocity is just one of the 3 (if 3D) component of the velocity that can be decomposed as:

$$v_i' = v_n n_i + v_t t_i + v_b b_i \tag{3.17}$$

where n_i, t_i and b_i are the three vectors of an orthogonal plane.

Admittance/Impedance

These boundary condition represent the acoustic treatment used in the study. This is the main boundary condition that will be studied in the present work. Using an admittance boundary condition means express the velocity as:

$$v_n = v_i' n_i = A(\omega) p' \tag{3.18}$$

In ActranDGM are available a series of boundary condition that can express the properties of an acoustic liner. The most used in the present work it will be the Impedance that is the inverse of the Admittance

$$I(\omega) = \frac{1}{A(\omega)} \tag{3.19}$$

The computation of this boundary condition could be done following one of the impedance model described in Section 2.

3.1.4 Acoustic sources

There are different simple models that could describe the generation of the acoustic field. The main acoustic source can be collected in spherical sources (point source), cylindrical source (line source) or plane wave source.

Harmonic spherical source (Point source)

The incident sound field is represented by the pressure p_i that could be defined as in Equation 3.20.

$$p_i = A \frac{e^{-ikr}}{r} \tag{3.20}$$

This acoustic source can be determined just by its amplitude A and its position in the point P. In the above equation is possible to notice the wavenumber k that could be easily computed knowing the frequency f and the speed of sound c

$$k = \frac{2\pi f}{c} \tag{3.21}$$

r represents the distance from the acoustic source. This kind of source could be computed also in the case it is immersed in a uniform mean flow.

Harmonic quadrupole source

This souce is related to the momentum equation and a source of this type can be seen as a stress source. In free field the solution can be written as expressed in Equation 3.22.

$$p_i = \frac{e^{-ikr}}{4\pi r^2}\left[\left(ik + \frac{1}{r}\right)^2 \frac{\vec{r}\otimes\vec{r}}{r} + \frac{\vec{r}\otimes\vec{r}}{r^3} - \left(ik + \frac{1}{r}\right)\left(\mathbf{I} + \frac{\vec{r}\otimes\vec{r}}{r^2}\right)\right] : \bar{\bar{\tau}} \tag{3.22}$$

In the above equation it is possible to see the following quantities:

- r: distance between the point of the computed incident pressure and the source
- $\vec{r}$: distance vector
- k: wave number
- $\mathbf{I}$: second order identity tensor
- $\bar{\bar{\tau}}$: amplitude tensor
- $\otimes$: dyadic product between two vectors
- : is the double tensor contraction

The be sure to obtain a quadrupole source it is possible to define the tensor $\bar{\bar{\tau}}$ as in Equation 3.23. This allows to compute the canonical quadrupole that can be depicted as in Figure 3.7.

$$\bar{\bar{\tau}} = a\left(A.C.A^T\right) \tag{3.23}$$

In the above equation is possible to see the transformation matrix A and canonical tensor C described below and a scalar amplitude a.

$$\begin{aligned} A &= \begin{pmatrix} d_1^x & d_2^x & d_3^x \\ d_1^y & d_2^y & d_3^y \\ d_1^z & d_2^z & d_3^z \end{pmatrix} \\ C &= \begin{pmatrix} 1 & 0 & 0 \\ 0 & -1 & 0 \\ 0 & 0 & 0 \end{pmatrix} \end{aligned} \tag{3.24}$$

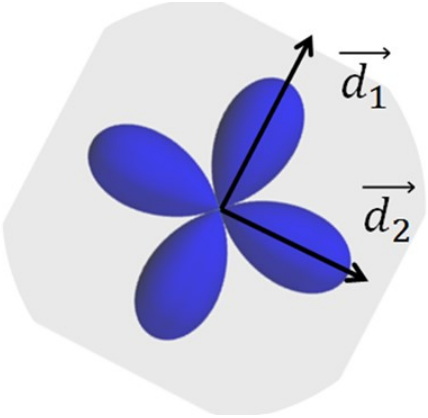

Figure 3.7: Canonical quadrupole with direction $\vec{d_1}$, $\vec{d_2}$ and $\vec{d_3} = \vec{d_1} \times \vec{d_2}$ (10)

Harmonic cylindrical source (Line source)

The incident sound field in the case of a line source can be expressed as

$$p_i = -iAH_0^2(kr) \tag{3.25}$$

Is possible to recognize what was preciously described in Equation 3.20. In this case there is an orientation of the source and this is along the vector $\vec{v}$. Differently from the point source, r represents the distance between the orientation line and the point in which it is being computed the field. This is well represented in Figure 3.8. H_0 could be computed as follow

$$H_0^2(kr) = J_0(kr) - iY_0(kr) \tag{3.26}$$

and represent the zero-th order Hankel function of second type (10). This function depends on the zero-th order Bessel function of first kind J_0 and the zero-th order Belles function of second kind.

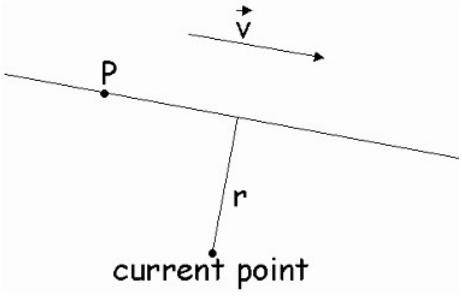

Figure 3.8: Cylindrical source scheme(10)

Harmonic plane wave source

As previously seen for the line source, also in this case there is a propagation along a specific vector $\vec{v}$. The incident sound field can be calculated as

$$p_i = Ae^{-ikr} \tag{3.27}$$

In this case, in the evaluation of the distance r, will be considered the plane perpendicular to the propagation direction along $\vec{v}$. This quantity is considered as the distance between the point in which the acoustic field is evaluated and this perpendicular plane. This acoustic field is generated in the plane containing the source point P so the field can be defined just in the half side containing the vector $\vec{v}$ as shown in Figure 3.9

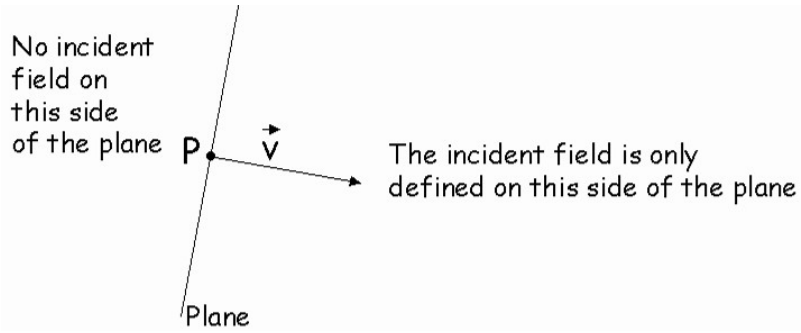

Figure 3.9: Plane wave scheme(10)

3.1.5 Aeroacoustic sources

Ligthill (29) was the first to present the concept of the noise generated arodinamically by an airflow . This, depending on its properties, can be the basis for different phenomena. The fluctuations contained in an airflow can produce an eddy pattern, responsible for the sound generated by a musical instrument, at low Reynolds number or they can produce a turbulent motion at high Reynolds number, responsible for the jet airplanes noise. An important properties of the sound generated aerodynamically, discovered with experiments, is that the frequency of the airflow is the same of the generated sound.
To have a better understanding of this phenomenon, Lighthill (29) used the following approach. This starts considering a large volume of fluid in with just a small part is occupied by a fluctuating fluid flow and the whole remaining part is at rest. Then the equations of the acoustic medium at rest and the equation describing the density fluctuations in the fluid are compared thanks to their difference. This difference could be interpreted as the effect of the fluctuating external force field. If the equation are written in the form used by Reynolds, the change of momentum is obtained thanks the combined action of the flow across the boundary of momentum-bearing fluid, represented symbolically with $\rho v_i v_j$ called "momentum flux tensor" or "fluctuating Reynolds stresses" and the stresses that are acting on the boundary. These fluctuating Reynolds stresses must be added to the real stresses expressed as p_{ij}. In a uniform acoustic medium at rest the only possible stress form that can be experienced is under the form of an hydrostatic pressure field.
The sound generated aerodynamically can be seen as the sound produced by a distribution of quadrupoles. These sources could be expressed thanks to the Lighthill's tensor $\frac{\partial^2 \mathbf{T}_{ij}}{\partial x_i \partial x_j}$ where

$$\mathbf{T}_{ij} = \rho v_i v_j + \delta_{ij}(p - c^2\rho) - \tau_{ij} \tag{3.28}$$

The d'Alembert's operator on the fluctuating density governs the wave propagation and, in the Reynold's form, one of the equation of motion of the fluid can be written as

$$\frac{\partial^2 \rho}{\partial t^2} - a_0^2 \nabla^2 \rho = \frac{\partial^2 \mathbf{T}_{ij}}{\partial x_i x_j} \tag{3.29}$$

Using this approach is equivalent to extract the noise source when the flow is computed and so the aerodynamic information are given as a input data. Once the aeroacoustic sources terms are computed from CFD data these are used in the right hand side of the Linearized Euler Equation seen above. Then is possible to use the above described Discontinuous Galerkin Method for the acoustic propagation in the field. It must be noticed that in the present work there will not be considered a CFD code but a brief introduction of these sources must be helpful to better understand the software.

Linearized Euler Equation with source terms

In Section 3.1.1 a general description of the Linearized Euler Equation were made. The non conservative form of the Linearized Euler Equation (LEE) with the aeroacoustic sources are presented in Equation 3.30.

$$\begin{array}{l} \frac{\partial \rho'}{\partial t} + \nabla \cdot (\rho' \mathbf{v}_0 + \rho_0 \mathbf{v}') = R_\rho \\ \rho' \mathbf{v}_0 \cdot \nabla \mathbf{v}_0 + \rho_0 \left(\frac{\partial \mathbf{v}'}{\partial t} + \mathbf{v}' \cdot \nabla \mathbf{v}_0 + \mathbf{v}_0 \cdot \nabla \mathbf{v}' \right) + \nabla p = R_m \\ \left(\frac{D_0 \rho}{Dt} + \mathbf{v}' \cdot \nabla \rho_0 \right) c_0^2 = \frac{D_0 p'}{Dt} + \mathbf{v}' \cdot \nabla p_0 = R_s \end{array} \tag{3.30}$$

In the above Equation 3.30 the terms with the superscript $'$ indicate the fluctuating component of the corresponding quantity while the terms marked with the subscript 0 indicate the quantity mean value. The three sources are respectively:

- R_ρ: mass source
- R_m: momentum source
- R_s is the energy source

To solve the set of equation 3.30 it is necessary to sole first the zero-th order form of the Euler Equations that give as output the mean values of the unknown: ρ_0, $\mathbf{v}_0$ and p_0. Then, using the above questions, is possible to compute the remaining unknown: ρ', $\mathbf{v}'$ and p'.

3.1.6 Far Field solution

Once the propagation of the acoustic perturbation is computed in the near field, to have an estimation of the far field acoustic fluctuation an ActranDGM utility is used. This utility solves the Ffowcs-Williams and Hawkings equation in the frequency domain. ActranDGM uses automatically a surface positioned between the buffer layer and the physical component (10). The solution for the pressure p' obtained

solving the FWH equations is presented in Equation 3.31:

$$4\pi p'(x) = \int_{S_t} \left(\frac{e^{\frac{-i\omega}{c_0} r_\beta}}{r_\beta (1+M_r)^2} \frac{(i\omega - c_0(M_r + ||\mathbf{M}||^2))}{r_\beta (1+M_r)} \left(U_n + \frac{L_r}{c_0} \right) + \frac{L_r + L_m}{r_\beta} \right) dS_t(\hat{x}) \tag{3.31}$$

In the above equation the following parameter were introduced:

- x: observer position
- $\hat{x}$: source position
- $\mathbf{R} = x - \hat{x}$, $n = \frac{\mathbf{R}}{||\mathbf{R}||}$: radiation direction vector, norm
- $\mathbf{M}_0 = \frac{\mathbf{v}_0}{c_0}$: vector of source local mach number
- $\beta^2 = 1 - M^2$
- $r_\beta = \left(\frac{\mathbf{R} \cdot \mathbf{v}_0}{c_0} + \sqrt{\frac{(\mathbf{R} \cdot \mathbf{v}_0)^2}{c_0^2} + \beta^2 ||R||} \right) / \beta^2$
- $\mathbf{r} = R - r_\beta \mathbf{M}_0$
- $v_{0n} = \mathbf{v}_0 \cdot \mathbf{n}$
- $\hat{v}'_n = \hat{\mathbf{v}}' \cdot \mathbf{n}$
- $U_n = \rho_0 \hat{v}'_n + \hat{\rho}' v_{0n}$
- $\mathbf{L} = \hat{p}' \mathbf{n} + \rho_0 v_{0n} \mathbf{v}'$
- $L_m = \mathbf{L} \cdot \mathbf{M}_0$
- $L_r = \frac{\mathbf{L} \cdot \mathbf{r}}{r_\beta}$
- $M_r = \frac{\mathbf{r} \cdot \mathbf{M}_0}{r_\beta}$

In the above list it is possible to notice the variable $\hat{p}'(\hat{x})$, $\hat{\mathbf{v}}'(\hat{x})$ and $\hat{\rho}'(\hat{x})$ are the corresponding quantities computed on the moving surface S_t at the source position $\hat{x}$.

3.1.7 Wave propagation in a duct

The well understanding of the propagation of an acoustic wave in a duct can be useful to study the noise generated by ducted fan engines. Inside an engine the noise can be generated by different sources like rotor wake-stator interaction etc. (30). The following formulation depends on the flow speed. In the present work the analyses will be done not considering the flow but this is the most general formulation that better suit with real engines working operation.
In this study will be considered a circular or annular cross section in which there is

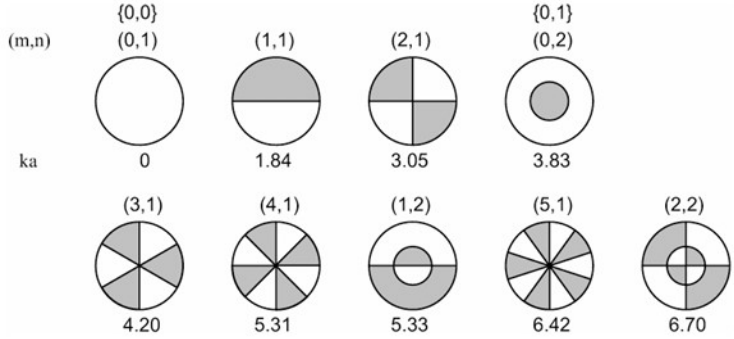

Figure 3.10: Representation of the combination between the radial and circumferential modes (11)

a flow with a contained Mach number ($M < 1$). The equation for the small pressure perturbation propagation is expressed in Equation 3.32.

$$\left(\frac{1}{c_0}\frac{\partial}{\partial t} + M\frac{\partial}{\partial x}\right)^2 \mathbf{p}' - \nabla^2 \mathbf{p}' = 0 \tag{3.32}$$

The boundary condition on the pressure on the wall is $\partial \mathbf{p}'/\partial \mathbf{r} = 0$. The above equation is expressed in axial coordinates but it can rewritten in cylindrical ones (r, θ, x). The complex solution for the pressure is in the form

$$p' = \mathbf{P}(r, \theta, x)e^{i\omega t} \tag{3.33}$$

In the above solution $\mathbf{P}$ represents the acoustic pressure amplitude and the expression for the acoustic propagation can be written based on this amplitude as

$$(1 - \mathbf{M}^2)\frac{\partial^2 \mathbf{P}}{\partial x^2} + \nabla_2^2 \mathbf{P} - 2ik\mathbf{M}\frac{\partial \mathbf{P}}{\partial x} + k^2 \mathbf{P} = 0 \tag{3.34}$$

In Equation 3.34 is possible to notice the two-dimensional Laplacian in polar coordinates ∇_2^2 and $k = \omega/c_0$. The expression for the pressure fluctuation can be written as:

$$\mathbf{p}' = A_{mn} J_m[k_r(m, n)r]e^{i[\omega t - m\theta - k_a(m,n)x]} \tag{3.35}$$

In the above equation k_a is the axial wave number and k_r is the radial wave number and depend on the circumferential order m and the radial order n. A representation of the circumferential and the radial modes is shown in Figure 3.10. The radial wave number can be extracted solving the equation

$$J'_m[k_r(m, n)R] = 0 \tag{3.36}$$

Where R is the radius of the circular duct. $J_m(\cdot)$ is the first kind Bessel function of m-th order. Once the radial wave number is computed, is possible to compute the axial wave number as

$$k_a(m, n) = \frac{k}{\beta^2}\left[-M \pm \sqrt{1 - \left[\beta\frac{k_r(m, n)}{k}\right]^2}\right] = \frac{k}{\beta^2}\left[-M \pm \sqrt{1 - \frac{1}{\beta_{mn}^2}}\right] \tag{3.37}$$

In the above equation m=0,1,2,... and $\beta^2 = 1 - M^2$ as defined above. Is also possible to define the cut-off ratio

$$\beta_{mn} = \frac{k}{\beta k_r(m,n)} \tag{3.38}$$

This cut-off ratio is an important parameter that gives an indication of the behavior of the wave. The mode, defined as the couple (m,n) propagates in the case of $\beta mn > 1$ but it will decay if the cut-off radio $\beta_{mn} < 1$ (30).

3.2 Actran Direct Frequency Response (DFR)

Actran DFR is used to solve easier acoustic configuration respect to ActranDGM. In this case the equation solved are the Möhring equation when no flow is present and the Helmholtz equation in presence of a flow. The equation can be extracted re-arranging the Navier Stokes equation. A scalar equation in time domain is obtained as expressed in Equation 3.39.

$$\frac{\partial}{\partial t}\left(\frac{\rho_o}{\rho_T^2 c_0^2}\frac{D_0 b}{Dt}\right) + \nabla \cdot \left(\frac{\rho_0 v_0}{\rho_T^2 c_0^2}\frac{D_0 b}{Dt} - \frac{\rho_0}{\rho_T^2}\nabla b\right) = R \tag{3.39}$$

In the above equation b is the scaled enthalpy and it can be computed starting from the stagnation enthalpy B as

$$\frac{Db}{Dt} = \rho_T \frac{DB}{Dt} \tag{3.40}$$

and where D/Dt is the material derivative.
In Equation 3.39 is possible to define the aeroacoustic source R as

$$R = -\nabla\left(\frac{\rho}{\rho_T}(v \times (\nabla \times v))\right) \tag{3.41}$$

Some assumption are made on the different equations. In the energy equation there are neglected the heat and power dissipation mechanism deriving from viscous forces. The acoustic velocity can be seen as $\mathbf{v} = \frac{\rho_0}{\rho_T}\nabla b$ and in this way there not will be considered vortical acoustic wave. In in the case of pure acoustic propagation the aeroacoustic source propagation can be seen equals to zero ($R = 0$).
To define the equations mentioned above in the frequency domain, a Fourier transform must be applied on the Equation 3.39. The most general equation is the one that takes in consideration the flow and so the Möhring equation can be written as

$$-\frac{\omega^2\rho_0}{\rho_T^2 c_0^2}b + \frac{\omega^2\rho_0}{\rho_T^2 c_0^2}v_0 \cdot \nabla b + \nabla \cdot \left(\frac{i\omega\rho_0 v_0}{\rho_T^2 c_0^2}b + \frac{i\omega\rho_0 v_0}{\rho_T^2 c_0^2}v_0 \cdot \nabla b - \frac{\rho_0}{\rho_T^2}\nabla b\right) = 0 \tag{3.42}$$

This equation is used in general cases but this could be reduced for particular cases. When the flow is at rest it is possible to obtain the above mentioned Helmholtz equation. In this case since the velocity of the flow is zero $v_0 = 0$ the total density is reduced just to the static component $\rho_T = \rho_0$. The Helmholtz equation can be defined as

$$-\frac{\omega^2}{\rho_0 c_0^2}b - \nabla \cdot \left(\frac{1}{\rho_0}\nabla b\right) = -\frac{\omega^2}{\rho_0 c_0^2}p - \nabla \cdot \left(\frac{1}{\rho_0}\nabla p\right) = 0 \tag{3.43}$$

The main advantages of this method is that it performs a stable resolution but it requires high RAM consumption when the model is complex (31).
The Helmholtz equation can be also computed from the d'Alembert wave equation. In the time domain the d'Alembert equation can be written as

$$\Delta p - \frac{1}{c^2}\frac{\partial^2 p}{\partial t^2} = 0 \tag{3.44}$$

This equation is expressed in the time domain but applying the Fourier transform

$$P(\omega) = \int_{-\infty}^{+\infty} p(t)e^{-\omega t}dt \tag{3.45}$$

is possible to obtain the following Helmholtz equation

$$\Delta P + \frac{\omega^2}{c^2}P = 0 \tag{3.46}$$

Chapter 4

Analysis

The main goal of this work is the optimization of the main parameters of a liner. A python script was written to automatize the optimization process. Optimize a variable means find the right value that minimize a certain noise parameter. Two main parameter were investigated: Overall Sound Pressure Level (OSPL) and Average Sound Pressure Level (AverageSPL). These parameters are function of the pressure perceived on some microphones positioned in the far-field. This pressure is computed after the equations in the near-field are solved and so an acoustic field is computed. As explained above, there are different method to solve this acoustic field and, at first, both were used to try to find out what was the best and fastest way to obtain this pressure field. The pressure, and consequently the Overall Sound Pressure Level and Average Sound Pressure Level, change depending on the acoustic treatment used. The acoustic treatment was simulated in Actran as an impedance boundary condition. As seen above, there are different models that could be used to compute this impedance starting from the liner parameters and the Motsinger and Kraft model was used 2.1. Two different kind of liners were investigated: Single Degree of Freedom (SDoF) liner and Double Degree of Freedom (DDoF) liner and so two different expression for the impedance were used.
The work can be divided in two macro-areas. The first concern the reduction of the noise generated by just one frequency and the second is about the reduction of more than one frequency. The main objective of the second section is to find out a liner, or a series of liners, that can reduce the noise for a series of frequencies.

4.1 Engine geometry

The analyses were performed on the engine from the DLR project ELTON SST. This project is about the Estimation of Landing and Take-Off Noise for supersonic transport (12). To ensure a low noise design for the engine, new and innovative solution for the acoustic treatment must be found. A picture of the rendered geometry of the supersonic aircraft on which the engin will be installed is shown in Figure 4.1. This aircraft is designed to transport up to 10 passenger and to flight a Mach 1.4. High-pressure compressors and turbines were recycled from an operating engine called CFM56-7B but new low-pressure compressors and turbines were designed.
Since this study concerns the noise reduction in the take-off and landing phases,

Figure 4.1: ELTON SST aircraft (12)

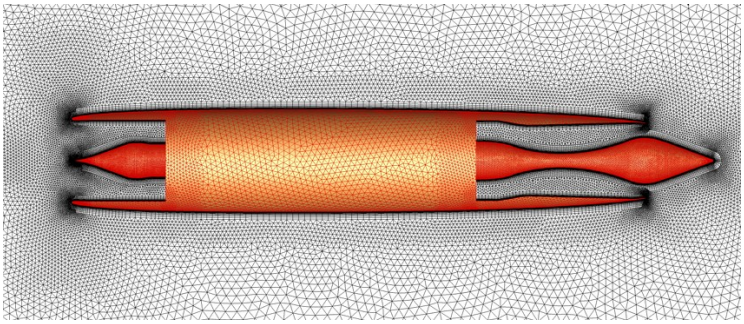

Figure 4.2: Representation of the engine subsonic configuration (12)

the subsonic configuration of the engine must be taken and this is shown in Figure 4.2. Starting from this configuration a proper mesh on Actran must be designed to compute the acoustic field.

4.2 Actran analysis

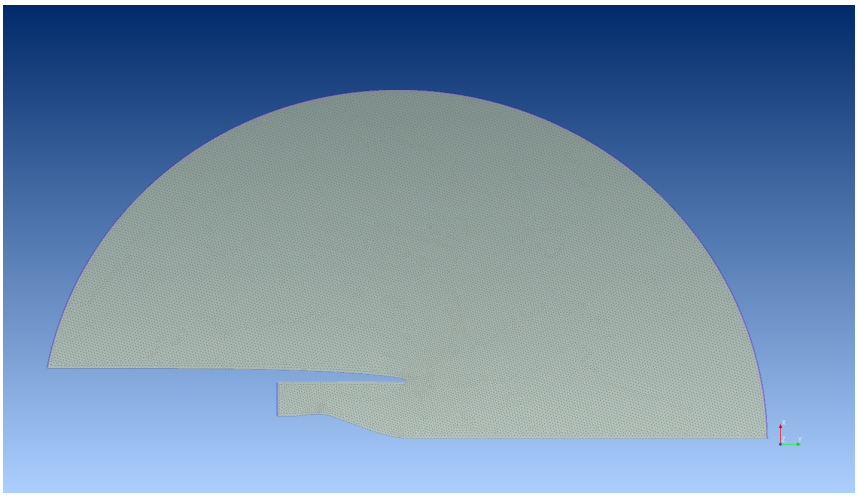

Figure 4.3: Infinite element (purple), acoustic element (yellow) and duct mode injection (blu)

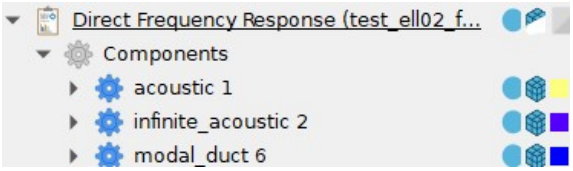

Figure 4.4: Direct frequency response components

An example of a general Actran analysis is presented in this section. The first step is to define the mesh and the domain. The Direct Frequency Response is the analysis used in most of the present work. In the definition of the DFR the frequency of the analysis and the axi-symmetric order are specified. Three main components are used for the DFR: the infinite element, the acoustic element, and the duct-mode injection. These are all represented in Figure 4.3 and 4.4. The medium in which the acoustic wave propagates is defined. In this case this medium is air so its principal characteristic are added like the speed of sound and the density. The component called "modal_duct 6" is one of the main section of the present work in which are defined the acoustic frequency, the radial mode and the amplitude in Pa. The python script will act on this section adding the right parameters for the selected frequency. The mesh can be modified defining the portion where the impedance boundary condition will be added. The red line in Figure 4.9 represents the mesh portion dedicated to this boundary condition (or conditions if several liners are used). In the present work the impedance boundary condition was used, allocating to the determined portion of space a specific value of impedance computed with the models described below. This is also an important part in the python optimization script. At each iteration the value of impedance is computed and changed in the Actran analysis. A study of the best configuration of liner (position, number, type etc.) is done and the results are discussed below.
It must be defined the post-processing output. These can be grouped in two main output files, the Function Frequency Response (FTF) text file and an .nff file containing the field maps. The first file is an useful tool to represent the noise directivity. The second will be mainly used to represent the pressure field map. Both are very useful tools to better understand how well a liner is working.

4.3 Mesh and Noise sources

Actran is the basis of the present work. Thanks to this software is possible to compute the acoustic field starting from a specific acoustic mode and frequency. The nacelle was recreated and a mesh around it must be constructed following the advice given in the Section 3.1.2. A zoom of the nacelle structure is presented in Figure 4.5.

Once the nacelle and the mesh are created, two type of Actran analyses were tried: Direct Frequency Response (DFR) and Discontinuous Galerkin Method (DGM) time analysis. This was done to try to find out what was the most accurate but at the same time the fasted method. Some oscillatory results, shown in the following, lead to the conclusion of also doing some analysis on the domain shape. In the pre-

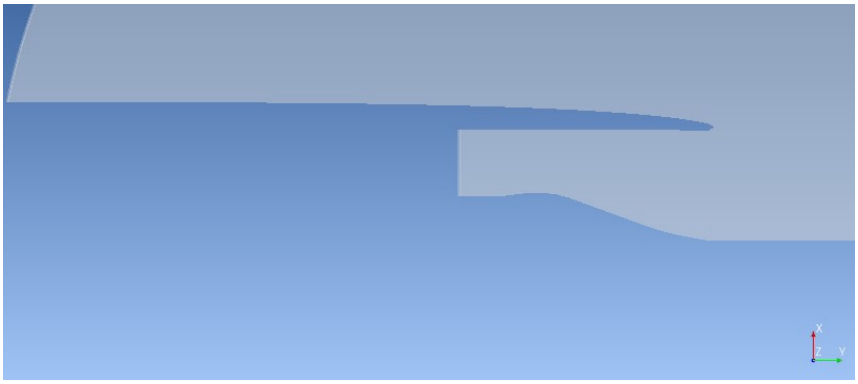

Figure 4.5: Nacelle construction

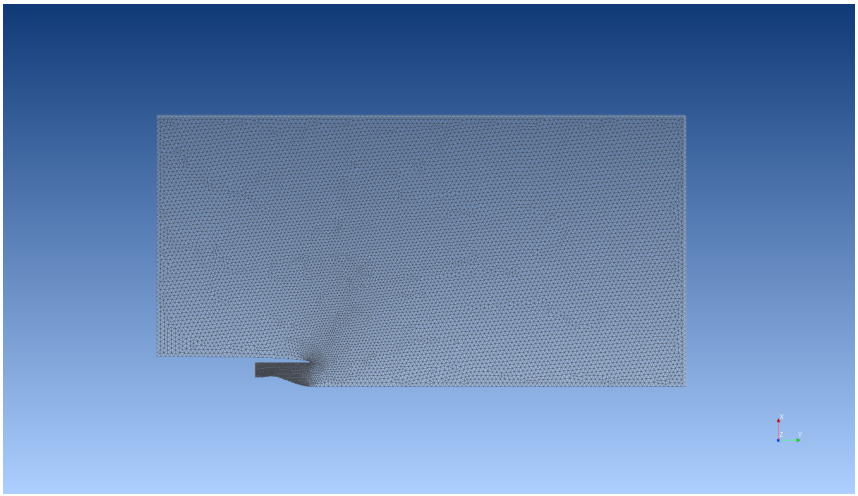

Figure 4.6: Rectangular domain

vious analyses were used a rectangular domain as shown in Figure 4.6 and the idea is to try a different shape. Following the assumption discussed above to create a domain as close as possible to the shape of the propagating wave, an elliptic domain was tried as shown in Figure 4.7.

The pressure is measured on a series of microphones positioned on an arch with 44.5 m of radius and spanning from 0° to 120° respect to the y-axis. During the analyses the span of the microphones is reduced to $[40°, 110°]$ to avoid the portion of domain that return instable values. This is done also to simulate more accurately the portion of space in which a ground observer can be during a take-off or landing phase. The distribution of microphones is shown in Figure 4.8. As mentioned above, this work can be divided in two macro-areas with two main objectives. The first is the reduction of the noise generated by a source with the following characteristic. The most onerous work is done on the finding the right configuration that work

Frequency [Hz]	**Amplitude [Pa]**	**m**	**n**
3200	30.45185	4	6

Table 4.1: One frequency scenario

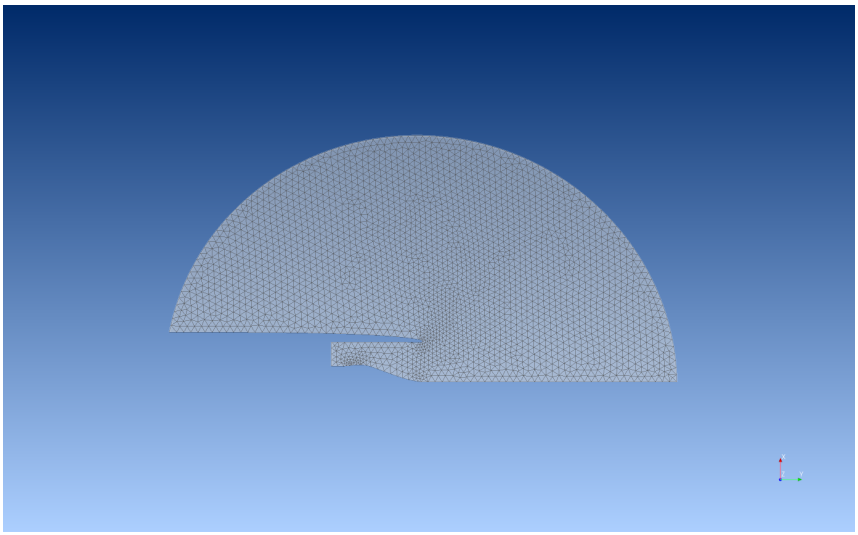

Figure 4.7: Elliptical domain

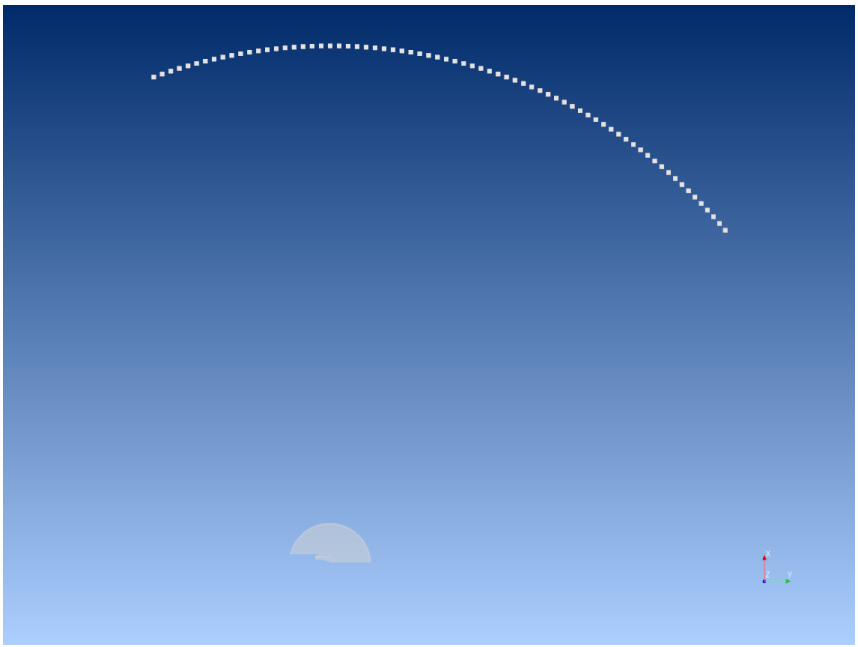

Figure 4.8: Microphones distribution from 40° to 110° respect to the y-axis

well in a series of different frequencies. The following frequencies, with their relative modes and amplitudes are summarized in Table 4.2.

Frequency [Hz]	**Amplitude [Pa]**	**m**	**n**
3200	30.45	4	6
4800	28.46	11	8
6400	12.43	26	1
8000	4.28	41	7

Table 4.2: Set of frequency to reduce

4.4 Liners and Physical constrains

Two main type of liners are investigated: SDoF and DDoF liners. The main parameter investigated are different for the two different type of liners.

SDoF liner

This liner is composed by an honeycomb core enclosed between two plates. The one at the bottom is a rigid back plate and the one that is in contact with the acoustic wave is a porous face sheet. The parameters that can be optimized are four:

- cell depth, h
- hole diameter, d
- porosity, σ
- face sheet thickness, τ

DDoF liner

A DDoF liner can be seen as a union of two liner SDoF. It is composed by two honeycomb cells between tree plates. Even in this case at the bottom is possible to find a rigid back plate and at the interface with the fluid a porous face sheet. In this case between the two honeycomb there is another porous plate called "septum". In this way the parameter that can be optimized are:

- total cell dept, h
- face sheet hole diameter, d_1
- septum hole diameter, d_2
- single cell dept parameter, b
- face sheet porosity, σ_1
- septum porosity, σ_2

- face sheet thickness, τ_1
- septum thickness, τ_2

The approach used in this work for the optimization of the two cell depth of a DDoF liner is based on the introduction of a "weight" b ($b \in [0, 1]$) on the total height h. The two cell depth can be computed as

$$\begin{aligned} h_1 &= bh \\ h_2 &= (1-b)h \end{aligned} \tag{4.1}$$

In this way the total depth is h and is possible to use all the available space.

As mentioned above, the impedance model used to define the impedance boundary condition is the Motsinger and Kraft model. The two equation for the SdoF liner and DDoF liner are presented in Equation 4.2 and Equation 4.4 respectively.

$$Z_n = R_n + i\left(X_n - \cot(kh)\right) \tag{4.2}$$

where

$$\begin{cases} R_n = \frac{a\mu\tau}{2\rho c\sigma C_d d^2} \\ X_n = \frac{k(\tau+\epsilon d)}{\sigma} \end{cases} \tag{4.3}$$

For the DDoF:

$$Z_n = Z_{n1} + \frac{\frac{Z_{n2}\cos(kh_1)\sin(kh_2)}{\sin(kh)} - i\cot(kh)}{1 + i\frac{Z_{n2}\sin(kh_1)\sin(kh_2)}{\sin(kh)}} \tag{4.4}$$

where

$$\begin{cases} Z_{n1} = R_{n1} + iX_{n1} \\ Z_{n2} = R_{n2} + iX_{n2} \end{cases} \tag{4.5}$$

and where

$$\begin{cases} R_{n1} = \frac{a\mu\tau_1}{2\rho c\sigma_1 C_d d_1^2} \\ X_{n1} = \frac{k(\tau_1+\epsilon_1 d_1)}{\sigma_1} \\ R_{n2} = \frac{a\mu\tau_2}{2\rho c\sigma_2 C_d d_2^2} \\ X_{n2} = \frac{k(\tau_2+\epsilon_2 d_2)}{\sigma_2} \end{cases} \tag{4.6}$$

More information about these equations and their parameters can be found on Section 2.1.

Physical constrains are imposed by the nacelle geometry. The position in which the boundary conditions, which represent an acoustic treatment, are imposed is shown in red in Figure 4.9. If one single liner, occupying all the available space, is chosen, it can extend just for a maximum of $3cm$ due to the space that narrows towards the tip. To avoid this problem, a configuration with multiple liners must be chosen. This is the approach mostly used in this study. The constrains for the liners on the configuration are the presented in Table 4.3.

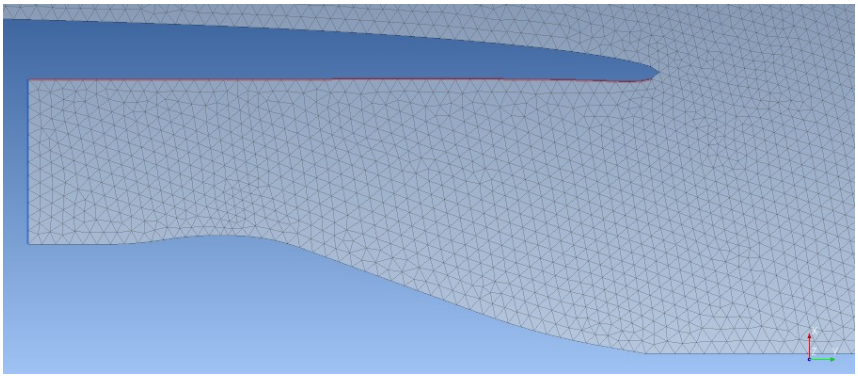

Figure 4.9: Liners position on the engine structure

Cavity depth, h	$13 - 76\ mm$
Orifice diameter, d	$1.0 - 2.4\ mm$
Porosity, σ	$5 - 13\ \%$
Plate thickness, τ	$0.5 - 1.0\ mm$

Table 4.3: Physical constrains

4.5 Noise functions to minimize

Several parameters can describe the perceived noise. The two chosen for the present work are the Overall Sound Pressure Level ($OSPL$) and the Average Sound Pressure Level ($AverageSPL$). The OSPL is an indication of the total noise over the microphones arch so, if compared to the aircraft take-off or landing phase, is the total noise that reach the specific portion of the ground. The AverageSPL is the arithmetic mean value of the Sound Pressure Level (SPL) over the set of microphones. This two parameter are functions of the pressure captured by these microphones and are described as follow

$$OSPL = 20 \log_{10} \left(\frac{p_{tot}}{p_{ref}} \right) \tag{4.7}$$

$$AverageSPL = \frac{\sum_{N_{mic}} SPL}{N_{mic}} \tag{4.8}$$

where

$$SPL = 20 \log_{10} \left(\frac{p}{p_{ref}} \right) \tag{4.9}$$

In the above equations the reference pressure represents the minimum pressure that can be perceived by an human ear. The reference pressure is $p_{ref} = 20\ \mu Pa$ and corresponds to 0 dB (32). The total pressure p_{tot} represents the sum of all the pressure that are measured on the microphones and can be expressed as

$$p_{tot} = \sqrt{\sum_{N_{mic}} p_i^2} \tag{4.10}$$

where $i = 1, ..., N_{mic}$. This is valid when only one frequency is considered. As mentioned above, the study concerning more than one frequency is about to found

one liner, or a set of liners, that can reduce the noise generated by each frequency. To do that a set of pressure value, each corresponding to a microphone, is collected for each frequency separately. Then the pressure on a single microphone is computed following the relation

$$p_i = \sqrt{\sum_{N_{freq}} p_k^2} \tag{4.11}$$

where $k = 1, ..., N_{freq}$. Now the i-th pressure can be used to compute the total pressure and then the OSPL as in Equation 4.7.

4.6 Python script

Useful for an optimization problem is the writing of a python code. One of the informatics languages used to write Actran was python so a strong connection exists between them. In this code an optimization algorithm, described above, that requires the definition of an initial point and upper and lower bounds for the optimization. Once these parameters are set, the most important part is the definition of the noise function to minimize that can be obtained using a python function. Is inside this function that the Actran code is launched and the acoustic analysis is performed. This function receives as input an array containing the parameters to optimize, for example the cell depth d and the hole diameter d. Using the above described impedance model, the impedance is computed and is directly changed in the Actran analysis. This analysis is launched directly by the python script and then is possible to extract from the results file the set of pressure on the microphones which can then be used to compute the OSPL and AverageSPL with the equations described above. Depending on what is the objective noise function of the analysis, this python function will return its value. This process will be repeated until the stopping criteria imposed by the user is satisfied.

4.6.1 Optimization algorithms

Depending on what kind of minimum value the user is looking for, different optimization algorithm can be used. Local and global are the two minimum that can be found inside a function and depending on what is the objective of our search a local or global optimization algorithm must be used. The optimization algorithm that used in the present work are part of the NLopt library. This is an open-source library that is used for nonlinear optimization. The main objective of the library is to solve the problem

$$\min_{\mathbf{x} \in \mathbb{R}^n} f(\mathbf{x}) \tag{4.12}$$

In the above equation is possible to see the objective function $f(x)$ and the vector containing the optimization parameters $\mathbf{x}$ (33). As mentioned above in the python script section 4.6, some constrains on these parameter must be defined

$$lb_i \leq x_i \leq ub_i \tag{4.13}$$

where lb_i and ub_i are the lower and upper bounds respectively.
A global optimization means finding the global minimum over the entire feasible

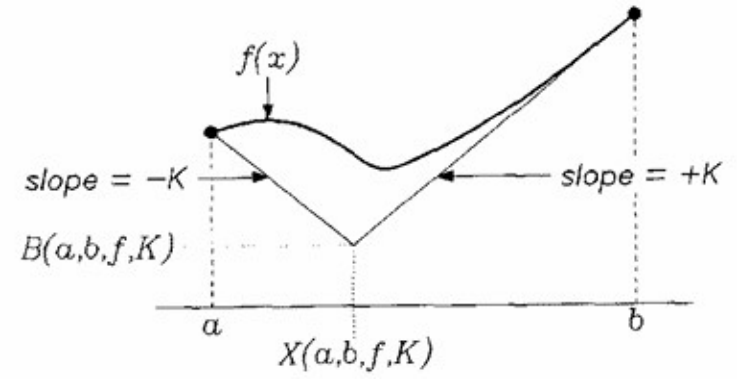

Figure 4.10: Lipschitz lower bound computation (13)

region defined by the bounds. It is very hard to find this value particularly when the number of optimizing parameter n became to large. Much simpler is the problem of finding a local minimum. These local algorithms are strongly dependent on the starting point especially in those functions that present many local minima. The condition that must be satisfied is that the function in the minimum point must be lower than the function computed in the nearby feasible point.
Both global and local optimizer are used in this study and in particular the local optimizer BOBYQA and the global optimizer DIRECT. A look to the COBYLA local optimizer will be given also.

DIviding RECTangles

Commonly called DIRECT, the DIving RECTangles algorithm is a simplification of Shubert's algorithm. This is based on two equations that comes from the Lipschitz algorithm (13). Lipschitz assumes that exists a positive constant K that satisfies the relation

$$|f(x) - f(x')| \leq K|x - x'| \tag{4.14}$$

where $f(x)$ is the objective function to minimize and it is defined in the interval $[l, u]$. The two variable x and x' are inside this interval. Equation 4.14 can be used to define the lower limit of the function in any interval $[a, b]$ substituting the lower bound a and the upper bound b of this interval to x'. In this way two inequalities are obtained

$$\begin{cases} f(x) \geq f(a) - K(x - a) \\ f(x) \geq f(b) + K(x - b) \end{cases} \tag{4.15}$$

This system establishes that the function $f(x)$ must be above the two lines described by the expressions in the right hand term. This is well represented in Figure 4.10. The intersection point of the two lines define the lower bound of the function f and represent the lowest value that the function can assume. This point is described by the two equations

$$\begin{aligned} X(a, b, f, K) &= \tfrac{a+b}{2} + \tfrac{f(a)-f(b)}{2K} \\ B(a, b, f, K) &= \tfrac{f(a)+f(b)}{2} - K(b - a) \end{aligned} \tag{4.16}$$

which are the main characters of the Shubert's algorithm. $X(a, b, f, K)$ represents the point where the function reaches its lower bound and it is inside the inter-

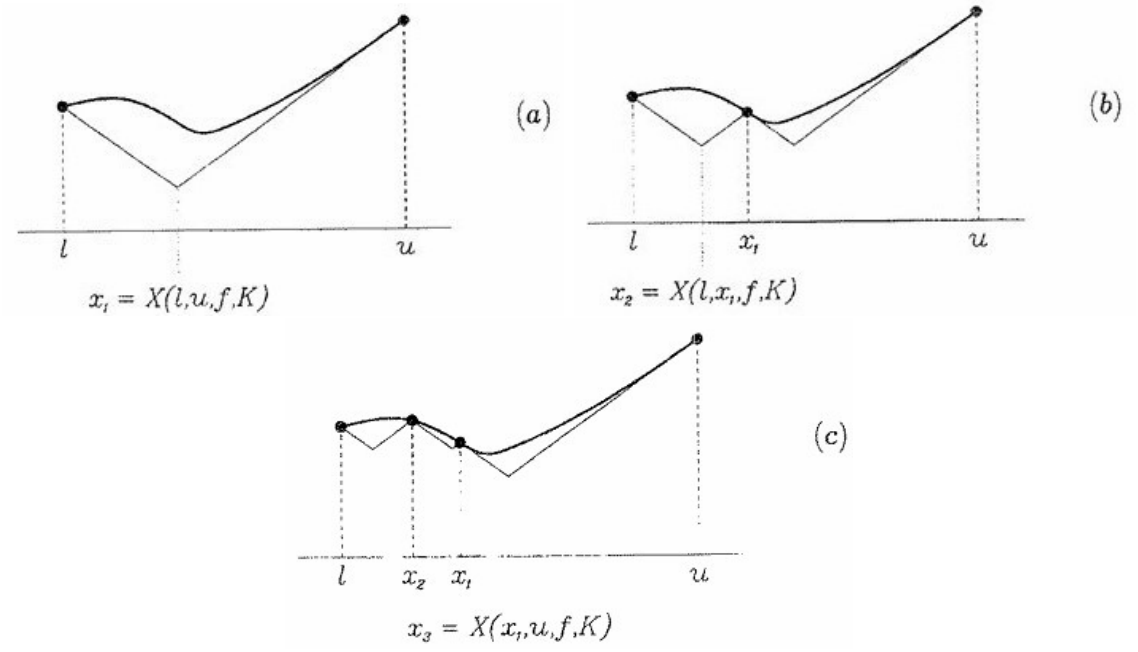

Figure 4.11: Shubert's algorithm (13)

val $[a, b]$. $B(a, b, f, K)$ is the lower bound of the function and is the value of the function in the point $X(a, b, f, K)$. Figure 4.11 may help to well understand the Shubert's algorithm. This starts evaluating the two functions shown in Equation 4.16 at the two extremes of the above mentioned interval $[l, u]$. In this way the point $x_1 = X(l, u, f, K)$ can be computed and two new intervals are created $[l, x_1]$ and $[x_1, u]$. Then evaluating the two equations in the extremes of the two intervals produce two new values of B and two new values of X. This is shown in the (b) graphic of the Figure 4.11. Then the lowest value of B is chosen (in the interval $[l, x_1]$) and this became the new separating point $x_2 = X(l, x_1, f, K)$. Now, as shown in the (c) graphic of Figure 4.11, three space are created: $[l, x_2]$, $[x_2, x_1]$ and $[x_1, u]$. Even in this case the lowest value of B is chosen and this can be found in the interval $[x_1, u]$ and becomes the new separating point. This process known as Shubert's algorithm will continue until a certain stopping criteria is reached.

DIRECT algorithm is a simplification of Shubert's algorithm. In this case the function is not evaluated in the two endpoints but in the center of the interval. This simplification comes with some changes in the original algorithm. In this case the lower bound is computed accordingly to Equation 4.18. If $[a, b]$ is the interval in which the function is defined and $c = (a + b)/2$ is the center, substituting c in Equation 4.14 is possible to obtain the following set of inequalities

$$\begin{aligned} f(x) &\geq f(c) + K(x - c), && \text{for } x \leq c \\ f(x) &\geq f(c) - K(x - c), && \text{for } x \geq c \end{aligned} \tag{4.17}$$

As mentioned previously, the right hand term of the inequalities are the two line represented in Figure 4.12.

$$\text{lower bounds} = f(c) - K\frac{a - b}{2} \tag{4.18}$$

Another change made for the DIRECT algorithm is to partition the space in several

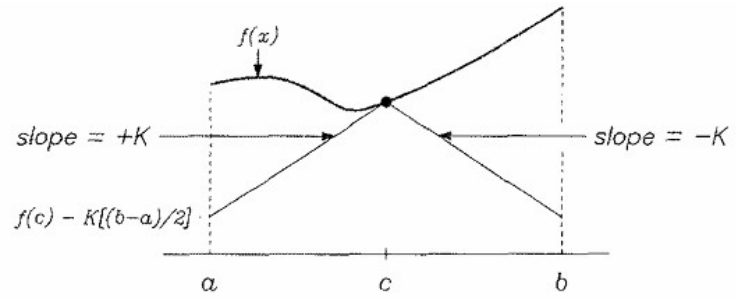

Figure 4.12: Lower bound in DIRECT algorithm (13)

intervals and evaluate their center point. The interval is divided into three portions as illustrated in Figure 4.13. The DIRECT algorithm can be divided in some steps

1. If $[a_1, b_1] = [l, u]$ and $c_1 = (a_1 + b_1)/2$ the function evaluated in the center point id $f(c_1)$ that becomes the f_{min}
2. Identify S as a set of intervals
3. select an interval $j \in S$
4. Subdividing the selected interval in three part of length $\delta = (b_j - a_j)/3$ it is possible to define $c_{m+1} = c_j - \delta$ and $c_{m+2} = c_j + \delta$ and its corresponding function $f(c_{m+1})$ and $f(c_{m+2})$. Then is possible to update the value of the f_{min}
5. The left and right sub-intervals are
   $[a_{m+1}, b_{m+1}] = [a_j, a_j + \delta]$ (c_{m+2})
   $[a_{m+2}, b_{m+2}] = [a_j + 2\delta, b_j]$ (c_{m+2})
   It is possible to modify the j interval that becomes the center sub-interval $[a_j, b_j] = [a_j + \delta, a_j + 2\delta]$ and $m = m + 2$.
6. Now is possible to remove from S the interval considered before $S = S - \{j\}$ and if $S \neq \emptyset$ the process begin again form the selection of another j interval in step 3
7. The last step is to update the iteration parameter $t = t + 1$ and if $t = T$ the algorithm stops otherwise it starts again from step 2.

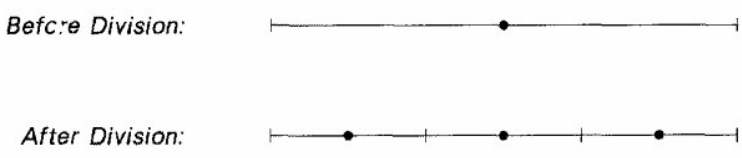

Figure 4.13: Interval division (13)

The above discussion works for DIRECT applied in one-dimension problems. In the present work the problem is defined in more than one dimensions, being the variables to optimize more than one. If the scale is normalized the space is a n-dimensional unit hyper-cube that will be portioned in hyper-rectangles. In DIRECT there is a procedure to divide rectangles shown in the following steps:

1. Identification of I, set of dimensions with the maximum side length. Once the maximum length is defined is possible to define δ as the one-third of it
2. $\mathbf{c} \pm \delta \mathbf{e}_i$ whee $i \in I$, $\mathbf{c}$ is the center of the rectangle and $\mathbf{e}_i$ is the unit vector
3. once the rectangle containing $\mathbf{c}$ is identified, it must be divided into thirds in all the dimensions $\in I$. The starting dimension is that with the lowest value of the parameter $w_i = \min\{f(\mathbf{c} + \delta \mathbf{e}_i), f(\mathbf{c} - \delta \mathbf{e}_i)\}$ and then the dimension that contains the highest value of it.

The above described w_i is the best value of the function computed inside the i dimensions. Similar to the one-dimensional case the algorithm can be summarized in some steps

1. Once the space is normalized it becomes a unit hyper-cube. Similarly to the one-dimensional case, the center point c_1 is defined and its function is calculated $f(c_1)$ and set as f_{min}. This step corresponds to $m = 1$ and $t = 0$
2. Identification of the set of potentially optimal rectangles S
3. Selection of one rectangle $j \in S$
4. Once decided how to divide the j rectangle, the value of f_{min} is updated and $m = m + \Delta m$ with Δm =number of points sampled.
5. $S = S - \{j\}$ and is S is empty the algorithm will return to step
6. The last step is the update of the iteration parameter $t = t + 1$ and if $t = T$ the algorithm stops otherwise it starts again from step 2.

A scheme of how DIRECT works is presented in Figure 4.14.

Bound Optimization BY Quadratic Approximation

Commonly called BOBYQA, this is an algorithm whose purpose is to find a local minimum of a function. The function is $F(\underline{x})$ where every element of $\underline{x} \in \mathbb{R}^n$ must be within the bound interval $[a, b]$. Let k and n be the iteration number and the number of variables. As expressed by the name, this algorithm is based on a quadratic approximation of the function that satisfies $Q(y_j) = F(y_j)$ where y_j, with $j = 1, ..., m$ are the interpolation points chosen automatically and m is the interpolation number. (34) The interpolation equation, at k-th iteration, is

$$Q_k(\underline{y}_j) = F(\underline{y}_j) \qquad j = 1, ..., m \tag{4.19}$$

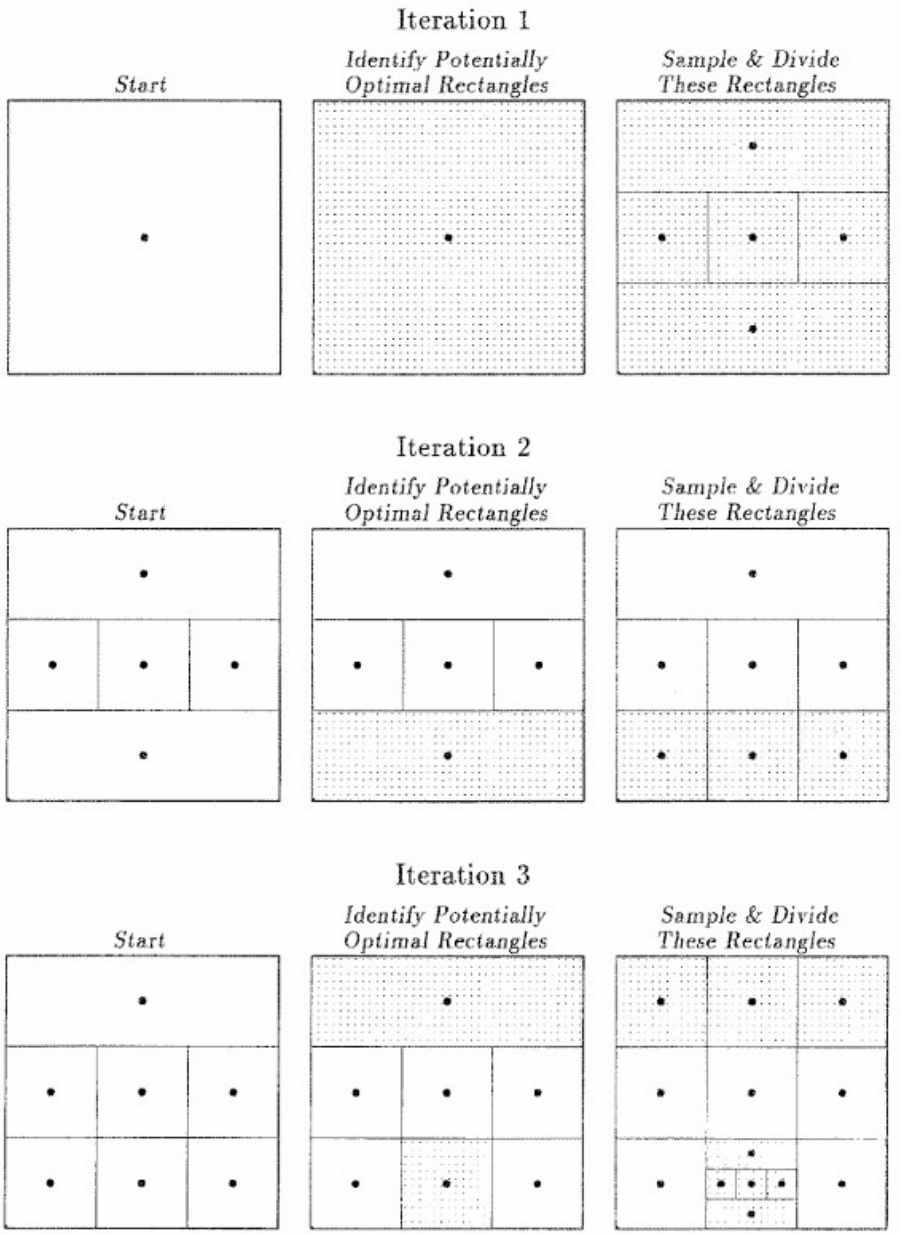

Figure 4.14: Example of the first three iteration of the DIRECT optimizer (13)

The number of interpolation conditions m is inside the interval

$$\left[n+2, \frac{1}{2}(n+1)(n+2)\right] \tag{4.20}$$

The typical value for this number is $m = 2n + 1$ but could be changed by the user. The point $\underline{x}_k$ can be defined as

$$F(\underline{x}_k) = \min\{F(\underline{y}_j) : 1, ..., m\} \tag{4.21}$$

Fundamental in this algorithm is the so called "Trust Region Radius" Δ_k. Then another variable can be introduced. $\underline{d}_k$ is a step from $\underline{x}_k$ that satisfy the condition

$||\underline{d}_k|| \leq \Delta_k$ and $\underline{x} = \underline{x}_k + \underline{d}_k$ is inside the bounds but not an interpolation point $\underline{y}_j$. The chose of small value for $\underline{d}_k$ is postponed by BOBYQA because when considering $Q_{k+1}(\underline{x}_k) = F(\underline{x}_k)$ and $Q_{k+1}(\underline{x}_k + \underline{d}_k) = F(\underline{x}_k + \underline{d}_k)$ the damage on the quadratic interpolation function Q_{k+1} tends to increases. Then the value of $F(\underline{x}_k + \underline{d}_k)$ is computed and $\underline{x}_k + \underline{d}_k$ is substituted to an interpolation point $\underline{y}_t$. The next iteration point is defined as

$$x_{k+1} = \begin{cases} \underline{x}_k, & F(\underline{x}_k + \underline{d}_k) \geq F(\underline{x}_k) \\ \underline{x}_k + \underline{d}_k, & F(\underline{x}_k + \underline{d}_k) < F(\underline{x}_k) \end{cases} \tag{4.22}$$

For the next iteration $k + 1$ they are also computed Δ_{k+1} and Q_{k+1} where the last one is computed as

$$Q_{k+1}(\underline{\hat{y}}_j) = F(\underline{\hat{y}}_j) \tag{4.23}$$

and the interpolation points are defines as

$$\underline{\hat{y}}_j = \begin{cases} \underline{y}_j, & j \neq t \\ \underline{x}_k + \underline{d}_k, & j = t \end{cases} \tag{4.24}$$

Q_{k+1} is updated using minimization of the Frobenius norm of the change to the second derivative of Q, $||\nabla^2 Q_{k+1} - \nabla^2 Q_k||_F$.

Chapter 5

Results and discussion

5.1 Discontinuous Galerkin Method (DGM) vs Direct Frequency Response (DFR)

The first analysis was made on two different resolution methods for the acoustic field: Time analysis (DGM) and Direct Frequency Response (DFR). The first method takes around 1h:12m to complete its computation while the second just 15s. As is possible to see in Figure 5.1, despite a more computation time, the curve of the SPL computed with the Discontinuous Galerkin Method is smoother than the DFR one, but the value are more or less the same. The data of SPL are collected by a series of 120 microphones extending from 120° respect to the y axis, the jet axis. Later in the analysis it was found that the source of this sharp shape in the DFR case was due to the wrong definition of the domain. Initially the domain was chosen to be rectangular as shown in Figure 4.6. This is not compatible with the ellipsoidal coordinate system defined for an infinite element (35). The coordinate system is defined by the center position of this ellipsoid (a_c, y_c, z_c) and the three principal axis (v_1, v_2, v_3). The equation for the reference ellipsoidal surface is given by

$$\frac{x^2}{a_2} + \frac{y^2}{b_2} + \frac{z^2}{c_2} = 1 \tag{5.1}$$

where a, b and c are the three semi-axes length.
The domain was changed from rectangular to elliptical and the two analyses were repeated obtaining what is shown in Figure 5.2. Since the two analyses return similar curves but the DFR analysis takes just few seconds compared to one hour of the DGM, the first was chosen for the following study.

5.2 Optimization algorithm

As discussed in the previous chapter, the selection of the right optimization algorithm was part of this study. At first, different tests were done to know how the different algorithms work and in particular GN_DIRECT, LN_BOBYA and LN_COBYLA were used. These are derivative-free algorithm so the derivative must

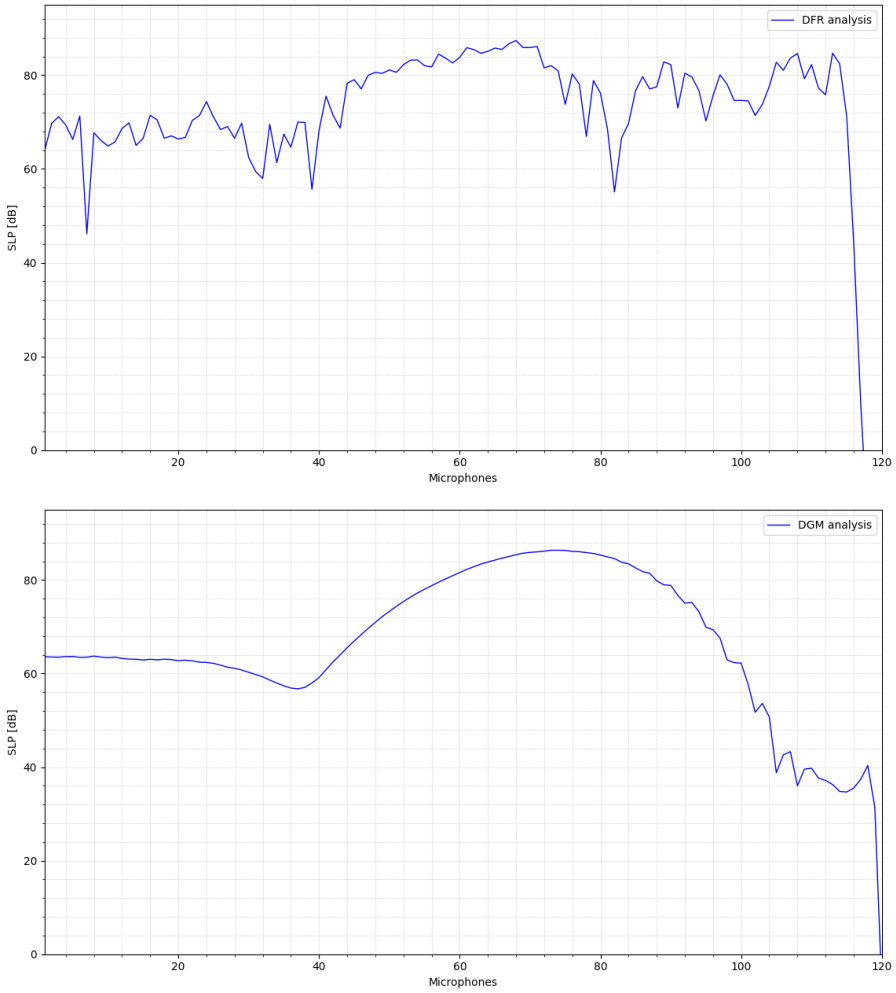

Figure 5.1: DFR and DGM analysis with rectangular domain

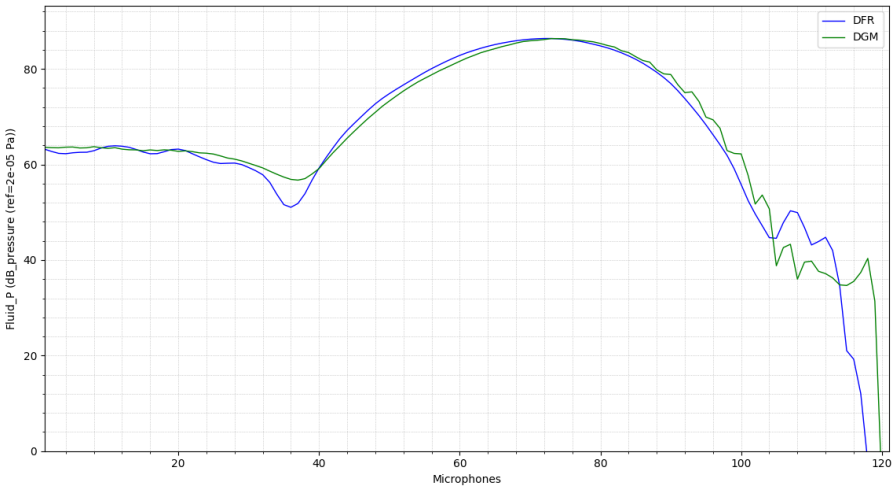

Figure 5.2: DFR and DGM analysis with elliptical domain

	No liner	1 SDoF	3 SDoF	1 DDoF	3 DDoF
COBYLA	70.26 dB	63.19 dB	62.79 dB	63.18	63.64 dB
BOBYQA	70.26 dB	63.16 dB	60.44 dB	63.19 dB	62.65 dB

Table 5.1: BOBYQA and COBYLA local optimizer with $f = 3200\ Hz$

not be computed. As discussed above, a global optimizer try to find a global minima over the space defined by the bounds, while a local optimizer search for a local minima around the starting point defined by the user, respecting the bounds. A single frequency was investigated $f = 3200\ Hz$. This is the frequency described in Tab. 4.1. At first a comparison between the two local optimizer was done. Four main configuration where considered:

- 1 SDoF
- 3 SDoF
- 1 DDoF
- 3 DDoF

What was obtained can be represented in Tab. 5.1.

In Tab. 5.1 is possible to notice that the BOBYQA local optimizer returns slightly lower values of SPL. In these analyses the studied quantity was the AverageSPL. In both cases the local optimizer return values that are lower than the case with No liner and the best configuration, as expected, is that composed by 3 SDoF liners. As discussed above, if just one liner is chosen, the maximum space that the liner can occupy is 30mm. The use of 3 SDoF allow to use more space because the second and third liner can occupy up to 76mm. From these starting analysis, is already possible to see the tendency to occupy more space. The use of a Double Degree of Freedom is not useful in this case in which just one frequency is considered. Since the BOBYQA local optimizer in some cases gave some lower values, was decided to use it for the remaining analyses.
A global optimizer was also tested. During the analyses, this kind of optimizer couldn't reach a convergence. To avoid this problem was decided to use the DIRECT global optimizer for a specific iteration number and then continue with the BOBYQA local optimizer to "refine" the search. What was obtained is shown in Figure 5.3. It is possible to notice that the result obtained from the single use of BOBYQA and the one obtained from the combined use of DIRECT and BOBYQA is not so different but the second needs more iteration and so more time. Then the single use of the BOBYQA local optimizer was chosen. In all the above analyses the starting point for the local optimizer was chosen more or less in the middle of the bounds. The starting points can be summarized as follow

- 1 SDoF: $(h, d) = [0.02, 0.0015]$
- 3 SDoF: $(h_1, d_1, h_2, d_2, h_3, d_3) = [0.02, 0.0015, 0.04, 0.0015, 0.05, 0.002]$
- 1 DDoF: $(h, d_1, d_2, b) = [0.02, 0.0015, 0.0015, 0.5]$

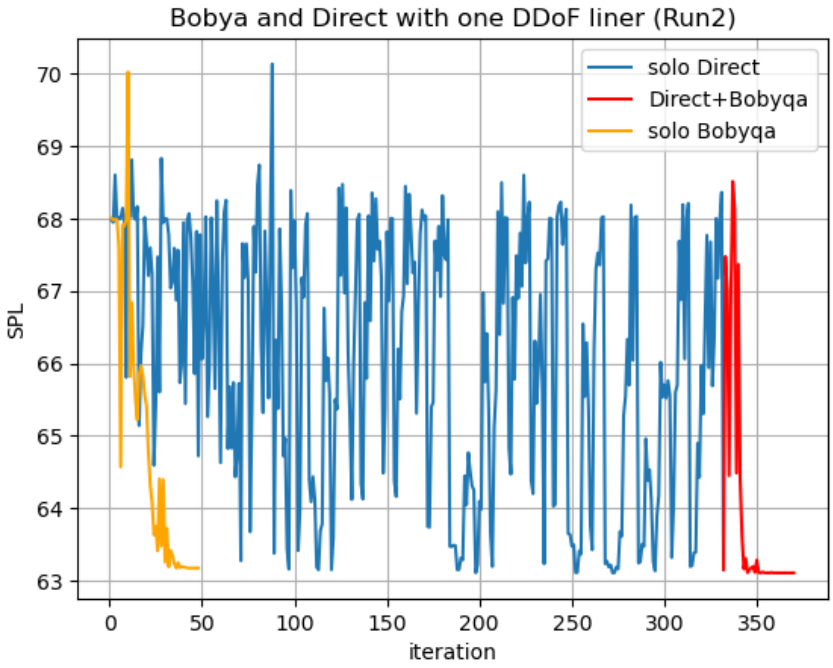

Figure 5.3: DIRECT+BOBYQA with $f = 3200\ Hz$

- 3 DDoF: $(h_1, d_{11}, d_{12}, b_1, h_2, d_{21}, d_{22}, b_2, h_3, d_{31}, d_{32}, b_3) = [0.02, 0.0015, 0.0015, 0.5, 0.04, 0.0015, 0.0015, 0.5, 0.04, 0.0015, 0.0015, 0.5]$

Two more quantities were defined above, the porosity and the plate thickness. The value assumed for these two quantities are:

- $\sigma = 5\%$
- $\tau = 1e^{-4}\ m$

Later in the analyses these values will be also analyzed and changed.
It can be represented the SPL over the microphones arch. In Figure 5.4 are represented three curves: 1) SPL with no liner, 2) SPL with 3 SDoF liners and 3) SPL with 3 DDoF liners. These two last curves were chose because they give the best results. What is possible to see is that the curves changes a lot depending on the acoustic treatment used. Even if the 3 SDoF liners return a lower AverageSPL value, in some point the SPL curve in this case is higher than the one produced using 3 DDoF liners. To see the problem to another perspective, another noise function to analyze was chosen. This function is the Overall Sound Pressure Level, describe above, that is an indication of the total sound perceived on the ground (microphones).

5.3 Overall Sound Pressure Level (OPSL) and Average Sound Pressure Level (AverageSPL)

All the analyses did in the following will be done considering the BOBYQA local optimizer. In the first section the single frequency will be discussed while in the

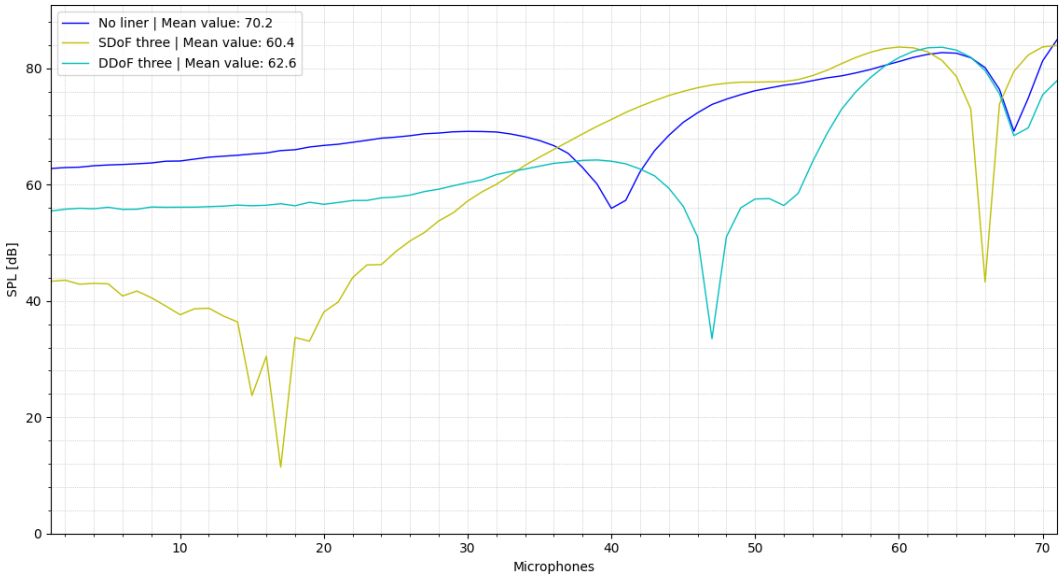

Figure 5.4: SPL curves for 3 SDoF and 3 DDoF liner with $f = 3200Hz$

	Opt. Function: AverageSPL		**Opt. Function: OSPL**	
	AverageSPL	***OSPL***	***AverageSPL***	***OSPL***
NO liner	**70.26**	**94.18**	**70.26**	**94.18**
1 SDoF	63.94	95.56	68.00	94.20
3 SDoF	59.69	94.05	55.08	86.21
1 DDoF	64.11	95.52	59.09	88.23
3 DDoF	62.58	95.46	64.31	91.35

Table 5.2: SPL [dB] for different optimized liner set-up with $f = 3200\ Hz$

second one the optimization of a liner that works well in more than one frequency will be discussed. All the useful data for the sound sources are grouped in Tab. 4.2. Another noise function was introduced and both will be discussed in the following. What was noticed during the analyses is that there is not a pure correspondence between the two functions. Finding a minimum for the OSPL doesn't mean finding a minimum in the AverageSPL due to the fact the quantities are in dB.

5.4 Single frequency $f = 3200\ Hz$

The same four configuration will be analyzed trying to find the best one. In this case the portion of the mesh dedicated to the impedance boundary condition is divided in three and when the 1 SDoF configuration is taken in analysis, the value of the impedance in Actran is set equal in the three different liner. The results obtained for the noise reduction of the single frequency can be grouped in Tab. 5.2.

In this table is possible to see, as expected, that the best value is obtained using three separated SDoF that better follow the nacelle shape. This is valid both if the objective function to minimize is the AverageSPL or the OSPL. To have an idea of

how the optimizer works is it possible to show all the values for h and d that were obtained for the liners.

Average Sound Pressure Level

- **No Liner**: SPL=70.26 dB
- **1 SDoF**: SPL=63.94 dB
  1. h=0.0199 d=0.00186
- **3 SDoF**: SPL=59,69 dB
  1. h_1=0.0196 d_1=0.00149
  2. h_2=0.0558 d_2=0.00154
  3. h_3=0.0474 d_3=0.00199
- **1 DDoF**: SPL=64,11 dB
  1. h=0.0161 d_1=0.00144 d_2=0.00156 b=0.525
- **3 DDoF**: SPL=62,58 dB
  1. h_1=0.0188 d_{11}=0.00148 d_{12}=0.00148 b_1=0.5005
  2. h_2=0.0399 d_{21}=0.0011 d_{22}=0.00151 b_2=0.5008
  3. h_3=0.0399 d_{31}=0.00149 d_{32}=0.0015 b_3=0.501

Overall Sound Pressure Level

- **No Liner**: OSPL=94.18 dB
- **1 SDoF**: OSPL=94.20 dB
  1. h=0.03 d=0.0024
- **3 SDoF**: 86,21 dB
  1. h_1=0.0235 d_1=0.00179
  2. h_2=0.0558 d_2=0.00159
  3. h_3=0.0404 d_3=0.00203
- **1 DDoF**: OSPL=88,23 dB
  1. h=0.0237 d_1=0.00145 d_2=0.00159 b=0.491
- **3 DDoF**: OSPL=91,35 dB
  1. h_1=0.0196 d_{11}=0.00149 d_{12}=0.00149 b_1=0.627
  2. h_2=0.0383 d_{21}=0.00164 d_{22}=0.00148 b_2=0.496
  3. h_3=0.0391 d_{31}=0.00208 d_{32}=0.00149 b_3=0.502

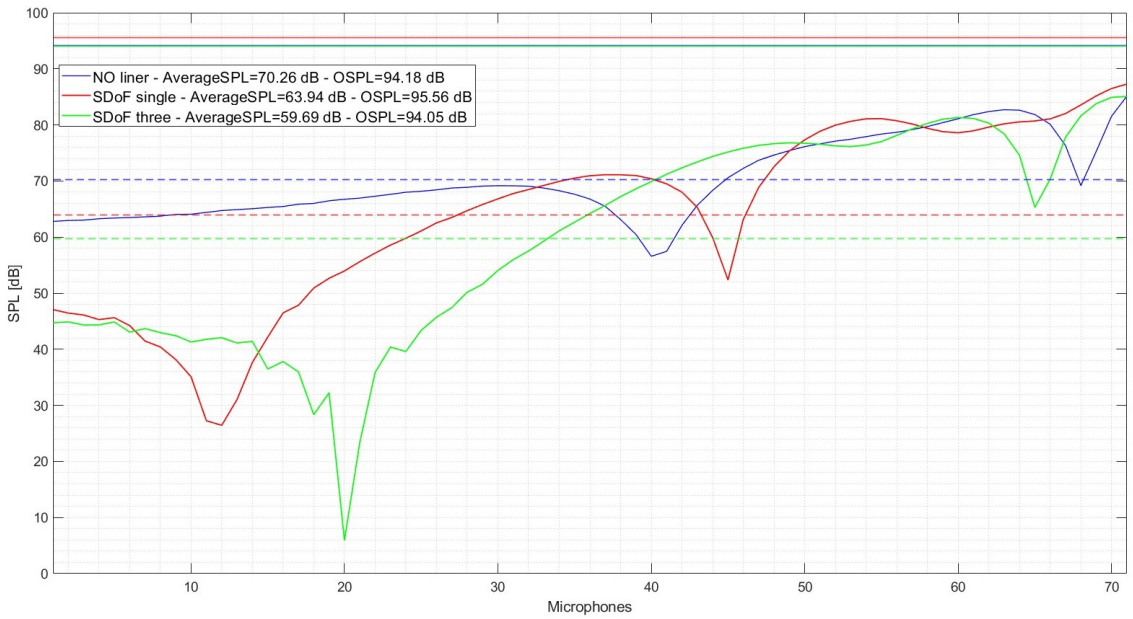

(a) Comparison between 1 SDoF and 3 SDoF with objective function: AverageSPL

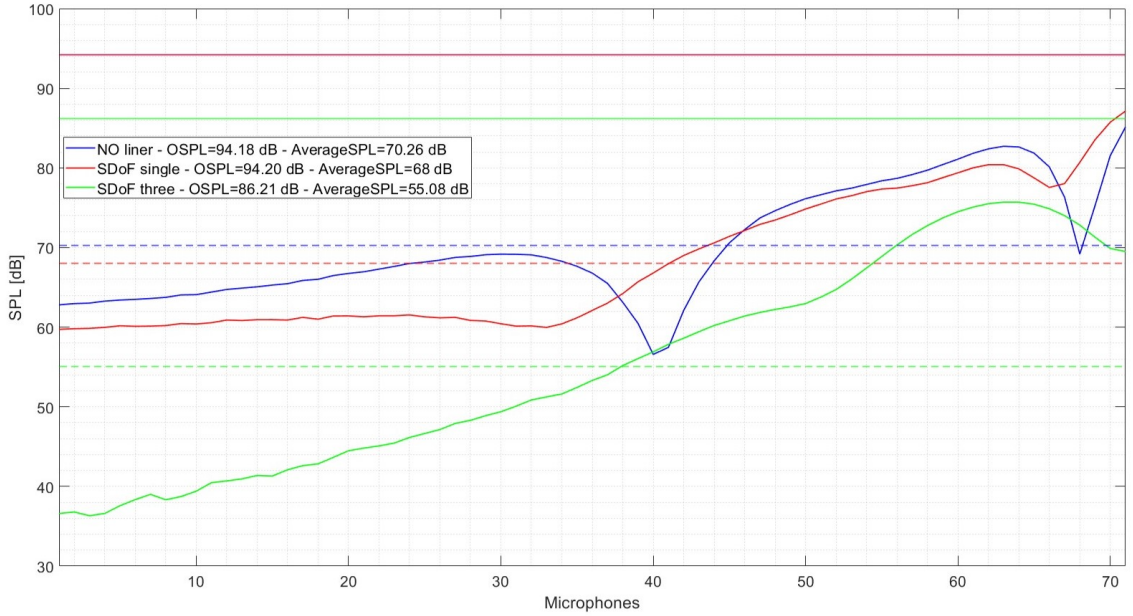

(b) Comparison between 1 SDoF and 3 SDoF with objective function: OSPL

Figure 5.5: AverageSPL and OSPL with $f = 3200\ Hz$

Figure 5.5a shows the comparison between the SPL curves obtained when No liner, 1 SDoF and a set of 3 SDoF are applied. In this case the objective function minimized is the AverageSPL. The same can be shown in Figure 5.5b where the minimized noise function is the OSPL. Figure 5.5 in useful to understand how a liner reduce the curve and the noise in general. The minimizing objective function that seems to return better values is the Overall Sound Pressure Level. In fact, this curve is "smoother" and do not present sharp changes in the SPL value. In this case a reduction in the OSPL (solid line) of 7.91 dB and a reduction in the mean value (dashed line) of 15.18 dB can be seen.

5.5 Multi-frequency liner

A liner capable to reduce more than one frequency is studied. The main idea is to find the main parameters of a liner that is supposed to work in a range of frequencies and modes injected separately. Tab. 4.2 group all the frequencies and modes of the following analyses. The process is similar to what discussed above whit a code change due to the fact that the Actran analysis must be done for each frequency. The results of these single analyses are saved and at the end used to the computation of the noise functions following the equation discussed in Section 4.5. Even in this case, the configurations that were compared are:

- 1 SDoF
- 3 SDoF
- 1 DDoF
- 3 DDoF

and the main parameter to optimize are the cell depth h and hole diameter d. What was obtained could be summarized in Tab. 5.3. As done for the single frequency

	Opt. Function: AverageSPL		**Opt. Function: OSPL**	
	AverageSPL	***OSPL***	***AverageSPL***	***OSPL***
NO liner	**74.31**	**98.94**	**74.31**	**98.94**
1 SDoF	72.28	99.15	74.49	99.06
3 SDoF	72.43	99.32	74.34	98.13
1 DDoF	71.85	98.71	74.33	98.43
3 DDoF	<u>71.05</u>	98.83	73.39	<u>97.06</u>

Table 5.3: SPL [dB] for different optimized liners set-up used to reduce the set of frequency [3200 Hz, 4800 Hz, 6400 Hz, 8000 Hz]

case, it is possible to summarize the optimized parameters that minimize the noise function.

Average Sound Pressure Level

- **No Liner**: SPL=74.31 dB
- **1 SDoF**: SPL=72.28 dB
    1. h=0.0229 d=0.00214
- **3 SDoF**: SPL=72.43 dB
    1. h_1=0.0198 d_1=0.00147
    2. h_2=0.0524 d_2=0.00145
    3. h_3=0.0514 d_3=0.00204
- **1 DDoF**: SPL=71.85 dB
    1. h=0.0247 d_1=0.00154 d_2=0.00167 b=0.499
- **3 DDoF**: SPL=71.05 dB
    1. h_1=0.0247 d_{11}=0.00152 d_{12}=0.00143 b_1=0.507
    2. h_2=0.0413 d_{21}=0.00145 d_{22}=0.00149 b_2=0.582
    3. h_3=0.0401 d_{31}=0.00149 d_{32}=0.00154 b_3=0.481

Overall Sound Pressure Level

- **No Liner**: OSPL=98.94 dB
- **1 SDoF**: OSPL=99.06 dB
    1. h=0.0265 d=0.0024
- **3 SDoF**: OSPL=98.13 dB
    1. h_1=0.0205 d_1=0.00187
    2. h_2=0.0408 d_2=0.00149
    3. h_3=0.0512 d_3=0.00199
- **1 DDoF**:OSPL=98.43 dB
    1. h=0.0264 d_1=0.00158 d_2=0.00169 b=0.443
- **3 DDoF**: OSPL=97.06 dB
    1. h_1=0.0195 d_{11}=0.00154 d_{12}=0.00147 b_1=0.508
    2. h_2=0.0385 d_{21}=0.00148 d_{22}=0.00149 b_2=0.486
    3. h_3=0.0396 d_{31}=0.00185 d_{32}=0.00150 b_3=0.5004

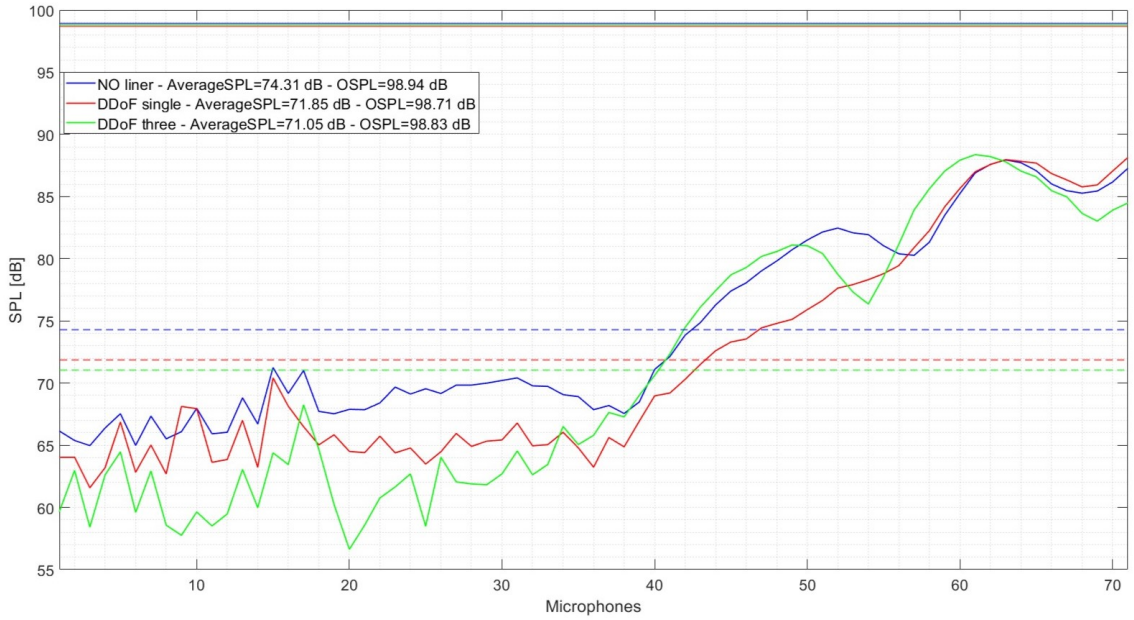

(a) Comparison between 1 SDoF and 3 DDoF with objective function: AverageSPL

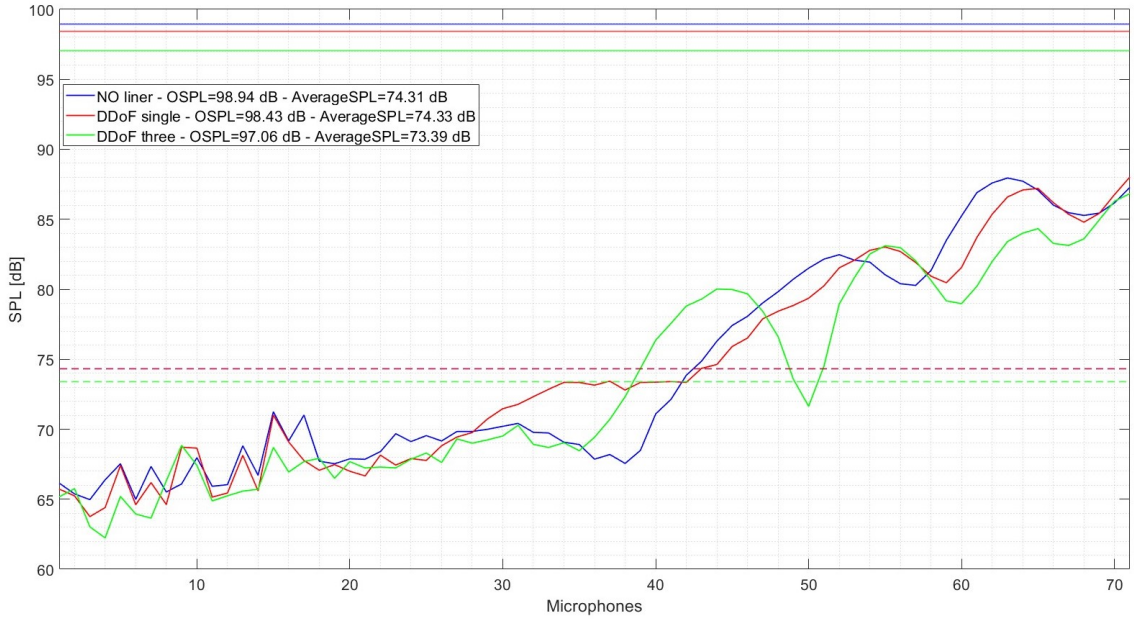

(b) Comparison between 1 SDoF and 3 DDoF with objective function: OSPL

Figure 5.6: AverageSPL and OSPL with [3200 Hz, 4800 Hz, 6400 Hz, 8000 Hz]

In Figure 5.6a and Figure 5.6b is possible to notice the comparison between the effect of one or tree DDoF liners. As expected, the DDoF is the best solution to reduce more than one frequency due its double layer. In particular, in this case the best results is reached when considering a set of three DDoF. It is passible to notice from Tab. 5.3 that the noise reduction is not so important, 3.26 dB if considering the AverageSPL as the function to minimize and 1.88 dB if considering the OSPL.

5.6 Multi-frequency liner in single frequency

To better understand in which frequency the set of liner doesn't work well other analyses on the specific frequency must be done. The idea is to use the most effective liner, obtained above, in each single frequency and compute the noise reduction. Even in this case a distinction between the minimization of the AverageSPL and the OSPL is done. In each of these analyses is used the impedance computed from the parameters obtained from the minimization of the corresponding noise function. For example, if the parameter that has been considering is the OSPL, the h and d values of the best DDoF liner obtained from the minimization of the OSPL are used. What was obtained could be summarized in Tab. 5.4.

NO liner				
	f=3200 HZ	**f=4800 Hz**	**f=6400 Hz**	**f=8000 Hz**
OSPL	94.19	96.98	80.58	79.99
AverageSPL	70.27	67.44	57.63	59.15
3 DDoF - Objective function: OSPL				
OSPL	91.38	95.44	80.93	79.31
AverageSPL	66.06	70.17	55.97	58.36
3 DDoF - Objective function: AverageSPL				
OSPL	94.88	96.31	82.47	80.12
AverageSPL	64.16	61.80	57.49	58.27

Table 5.4: SPL [dB] for a set of 3 DDoF liner obtained from the multi-frequency case used in each single frequency

In Tab 5.4 is possible to notice that, for both the minimization function, the noise produced by higher frequencies is more difficult to reduce. Other strategies must be considered to overcome this problem.

5.7 Specialized liner for single frequency

The general idea is to change the partition of the initial liner dividing it in a set of four smaller liners. This number corresponds to the number of frequency part of the analysis. The idea is to assign one of the four liner, the task to minimize the noise generated with a specific frequency and mode. Figure 5.7 represents the division made for this kind of analysis. Is presented a set of 4 liners with the same extension and their relative numeration. The idea is to optimize one at a time when just one

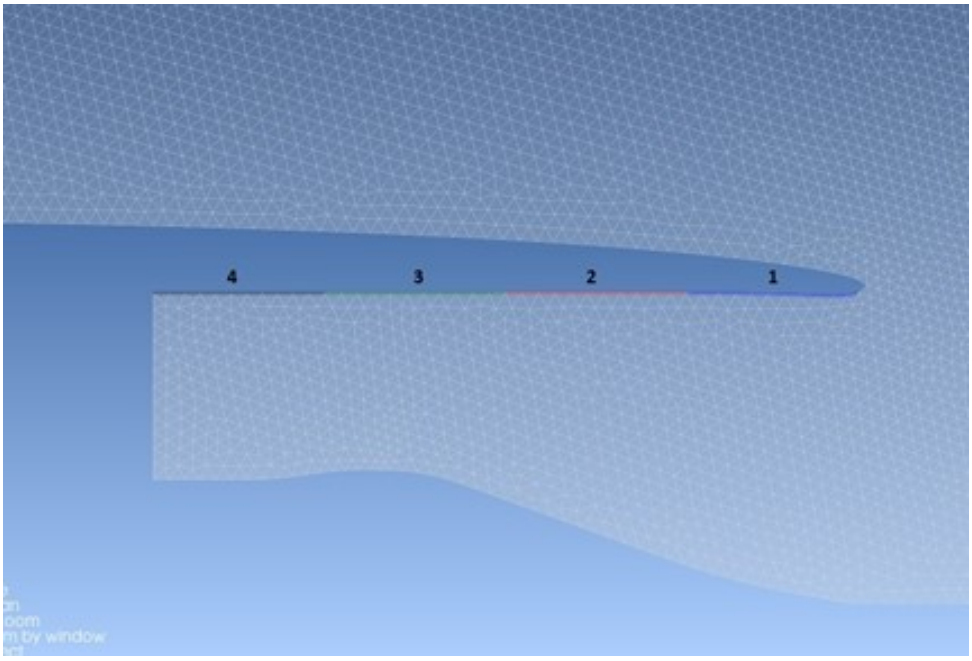

Figure 5.7: Liner division

frequency is present. Starting from the tip the optimization of the higher frequency is assigned so the division is:

- $f = 8000\ Hz \rightarrow$ liner 1
- $f = 6400\ Hz \rightarrow$ liner 2
- $f = 4800\ Hz \rightarrow$ liner 3
- $f = 3200\ Hz \rightarrow$ liner 4

The procedure could be summarized in the following steps. Once the first frequency to investigate is chosen, initial h and d values and its relative impedance value (depending on the frequency) are assigned. The remaining liners are "deleted" and a non reflecting boundary condition is imposed. Once the noise pressure is computed on the microphones, the process is repeated for the second frequency. The corresponding assigned liner is optimized to reduce the noise and once the minimum in this value is reached, the next frequency is investigated. This process is repeated for all the remaining frequencies. At the end of this analysis, a set of parameters is obtained for each single liner. Both the noise functions are investigated and what was obtained is shown in Tab. 5.5. The types of liners used in the following are those described above, SDoF and DDoF.

Tab. 5.6 shows a comparison between the 2 type of liners used. In both cases no reduction is obtained if considering the Overall Sound Pressure Level. This can be explained investigating the results obtained considering the single frequency shown in Tab. 5.5. Considering the OSPL as objective function both for a SDoF and a DDoF the reduction for higher frequency is irrelevant. In particular, the reduction of the noise generated with $f = 4800\ Hz$ is just around 1 dB. Dealing

NO liner				
	f=3200 Hz	**f=4800 Hz**	**f=6400 Hz**	**f=8000 Hz**
OSPL	94.19	96.98	80.58	79.99
AverageSPL	70.27	67.44	57.63	59.15
SDOF - Objective function: OSPL				
OSPL	92.18	96.21	80.57	78.55
AverageSPL	65.68	68.17	57.53	56.99
SDOF - Objective function: AverageSPL				
OSPL	92.73	97.02	80.74	78.82
AverageSPL	64.02	67.10	56.88	57.16
DDOF - Objective function: OSPL				
OSPL	92.17	95.83	80.56	78.41
AverageSPL	65.68	69.53	57.44	57.16
DDOF - Objective function: AverageSPL				
OSPL	92.73	97.02	83.29	80.33
AverageSPL	64.01	67.10	56.63	59.06

Table 5.5: SPL [dB] from the optimization of specialized liner in the corresponding frequency

Objective function: OSPL			
	NO liner	**4 SDoF**	**4 DDoF**
OSPL	98.94	98.83	98.28
AverageSPL	74.31	74.39	74.21
Objective function: AverageSPL			
	NO liner	**4 SDoF**	**4 DDoF**
OSPL	98.94	99.24	100.03
AverageSPL	74.31	72.18	73.03

Table 5.6: SPL [dB] given by the union of the 4 specialized liner with the set of frequency [3200 Hz, 4800 Hz, 6400 Hz, 8000 Hz]

with dB operations, and giving the highest contribution, this is the most important frequency to reduce. If considering the mean value of the SPL curve, represented by the Average Sound Pressure Level, a small reduction (around 2 dB) is shown when considering all the frequency as shown in Tab. 5.6. In this case the use of a SDoF returns better results. This better reduction can be justified referring to Tab. 5.5. Considering the AverageSPL is possible to notice that the reduction for the first frequency is quite good with a reduction of around 6 dB. This results is worsened by the small, or almost inexistent, reduction in the higher SPL given by $f = 4800$ Hz and affect the overall performance.

5.7.1 Optimization of the combined liner

The idea of this analysis is to use what obtained from the local optimization of each single liner in the assigned frequency, as a starting point for another local optimization. The configuration to analyze is given by the union of the 4 liner optimized and its goal is to reduce the usual set of frequencies. The process is similar to what was done in Section 5.5 with 3 liners. In that case, the starting point for h and d (or h, d_1, d_2 and b in case of DDoF) was defined by the user. Now the starting vector (set of parameters for the 4 liner) is composed by those parameters that, in the corresponding frequency, return the minimum of the noise function analyzed.

Objective function: OSPL					
	NO liner	**4 SDOf**	**Opt. 4 SDoF**	**4 DDOf**	**Opt. 4 DDoF**
OSPL	98.94	98.83	**97.40**	98.28	**96.99**
AverageSPL	74.31	74.39	73.27	74.21	74.28
Objective function: AverageSPL					
	NO liner	**4 SDOf**	**Opt. 4 SDoF**	**4 DDOf**	**Opt. 4 DDoF**
OSPL	98.94	99.24	99.18	100.03	100.18
AverageSPL	74.31	72.18	**71.02**	73.03	**70.50**

Table 5.7: SPL [dB] obtained with the non optimized and optimized combined liners

Slightly better results were obtained with this optimization and are presented in Tab. 5.7. In this case the best results for both the noise functions is obtained using three optimized Double Degree of Freedom. In conclusion a comparison can be done with the results obtained optimizing three liners. The optimal configuration obtained in Section 5.5 is given by a set of 3 DDoF liners and the minimum SPL values obtained are shown in Tab. 5.3. Those values are similar to what was obtained in the present section and shown in Tab. 5.7. So is possible to come to the conclusion that the use of 4 liner, at first optimized separately and then combined, doesn't bring to better results respect to directly optimize 3 liners. This is also represented in Figure 5.8. This figure shows the SPL curves obtained with No liner, 3 DDoF optimized liners and 4 DDoF optimized liners for both the noise function.

Since the noise reduction is not so important other tests were made to find the right configuration for the liners. Different position where tried for the single liners but no important changes where noticed in the SPL. Another test was performed

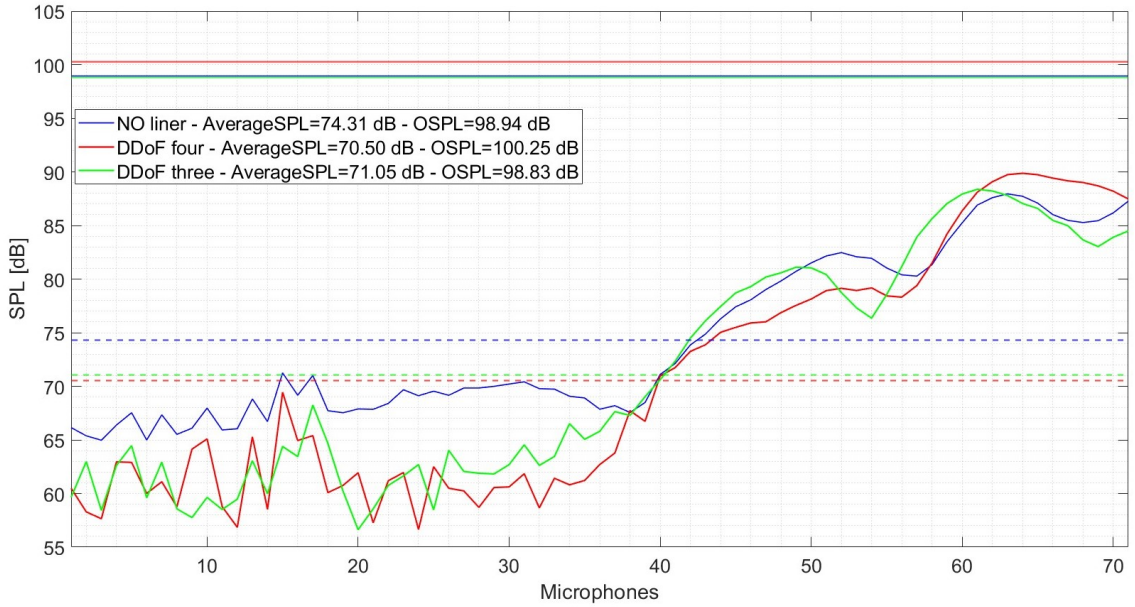

(a) Comparison between 3 directly optimized liner and 4 combined liner, Objective function=AverageSPL

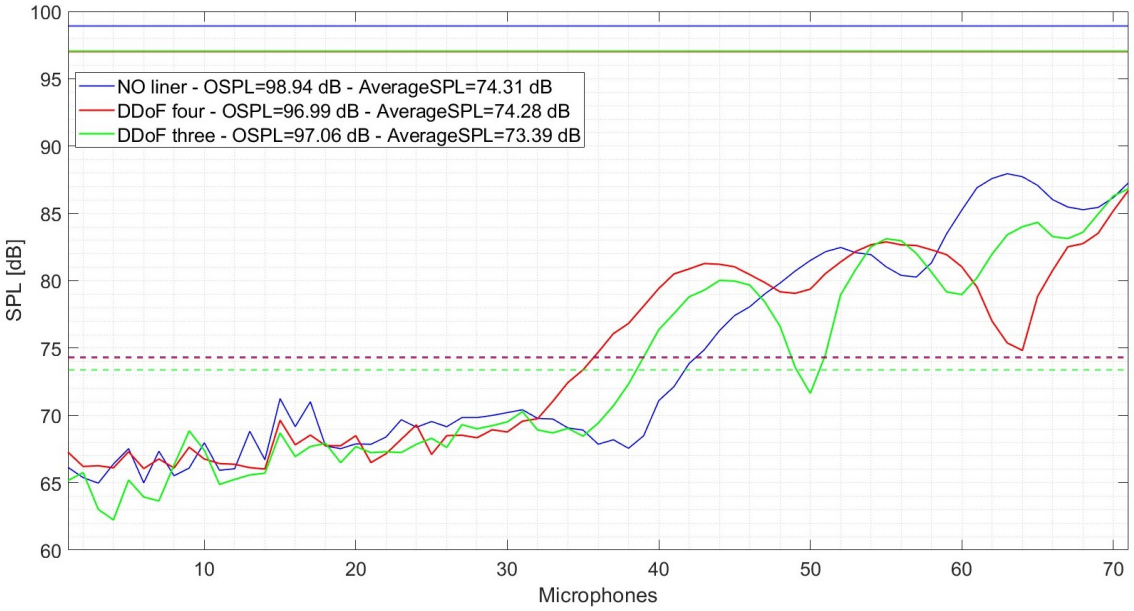

(b) Comparison between 3 directly optimized liner and 4 combined liner, Objective function=OSPL

Figure 5.8: Comparison between 3 directly optimized liner and 4 combined liner

changing the extension of the liners trying to give more space to reduction of higher frequency, more difficult to treat. Even in this case no significant change were registered in the Sound Pressure Level.

Change in σ and τ
Some analyses where made on the other parameters that can be studied σ and τ. It was found that they have not a strong influence on the noise reduction if considering the ranges presented in Tab. 4.3. In the following analyses a change in the quantities σ and τ will be done to conform with the choice made with the starting point of h and d. For this last two parameters the starting point for the optimization is a point around the middle value of the corresponding interval. Also for the first parameters mentioned a similar approach is followed and in the following analysis those will became

- $\sigma = 9\%$
- $\tau = 0.75 \cdot 10^{-3}\ m$

5.8 Liner distribution with a quadratic function

The main idea of this analysis is to find quadratic functions that, given a normalized length along the nacelle, returns the h and d values of a Single Degree of Freedom liner. The goal of the chosen optimizer is to find the right combination of the three parameters that characterize a quadratic function. Two function are needed and so 6 parameters must be optimized

$$\begin{cases} h = ax^2 + bx + c \\ d = dx^2 + ex + f \end{cases} \tag{5.2}$$

The variable x refers to an axis with the center positioned on the tip of the nacelle and directed towards the core of the engine. The parameter x is a normalized length so is inside the range $[0, 1]$. Three main analyses will be done

- 8 liners
- 16 liners
- 44 liners

Depending on this number, some change in the mesh must be done. The space on the nacelle dedicated to the liner has to be divided in as many space as the number of liners. This is done in order to allocate the right number of impedance boundary condition. The 44 value was chosen due to mesh limit and represent the maximum number in which the portion dedicated to the impedance boundary condition can be divided. The python script is done to be adaptable to these three analysis and the user must just define the number of boundary conditions (liners) and the name of the corresponding Actran Analysis. The optimizer used in these analyses is the local optimized BOBYQA defined above. The starting point is chosen to give to the

Objective function: AverageSPL					
	NO liner	**8 SDoF**	**16 SDoF**	**44 SDoF**	**3 SDoF**
OSPL	98.94	97.74	98.43	98.54	99.31
AverageSPL	74.31	**70.92**	71.44	71.59	72.43
	NO liner	**8 SDoF**	**16 SDoF**	**44 SDoF**	**3 SDoF**
OSPL	98.94	97.63	**96.38**	97.78	98.13
AverageSPL	74.31	72.99	72.18	75.53	74.34

Table 5.8: SPL [dB] depending on number of liners

functions a parabolic behavior that starts from the value of the minimum and reach the maximum of the corresponding intervals. For the three analyses the starting point can be defined as follow:

- (a,b,c)=$[-0.022, 0.085, 0.013]$
- (d,e,f)=$[0.8 \cdot 10^{-3}, 0.6 \cdot 10^{-3}, 1 \cdot 10^{-3}]$

and the upper and lower bounds given to the optimizer are:

- $a, b, c \in [-0.1, 0.1]$
- $d, e, f \in [-0.01, 0.01]$

Both Average Sound Pressure Level and Overall Sound Pressure Level were analyzed. Thinking about the h function, the structure will became a "step function" as will shown in Figure 5.12. Choosing one of the 8 points (16 or 44) it is possible to compute the value of $h(x_0)$ that remain constant until the next point where it assumes the value of the function in that point $h(x_1)$. An optimization of the 2 function with different number of liners was done and the results are shown in Figure 5.9. Two results were obtained considering the AverageSPL or the OSPL as the function to minimize. Figure 5.9a shows that the best value of the AverageSPL is reached when 8 liners are used. Figure 5.9b shows that the lowest value for the OSPL is reached when considering 16 liners. In these figures is possible to do a comparison with what was obtained considering a direct optimization of just 3 liners, shown in Section 5.5. It is possible to notice that this new approach returns better values respect to what was done before. The values obtained are summarized in Tab. 5.8.

Figure 5.10 shows how the optimizer works. The blue function represent the initial function, defined by the user with the starting vector, while the orange function represent the optimized one. In both cases is possible to see that the optimizer reduces the space occupied by the liner. As said above the initial function is defined as the quadratic function that comes from the lowest point of the interval to the highest.

Is it also possible to notice that the difference between the value of AverageSPL considering 8 and 16 liners is not so important as is shown in Figure 5.9a. It was decided to chose the configuration with 16 liners to have a continuity with the two noise function. The resulting function from these analyses are

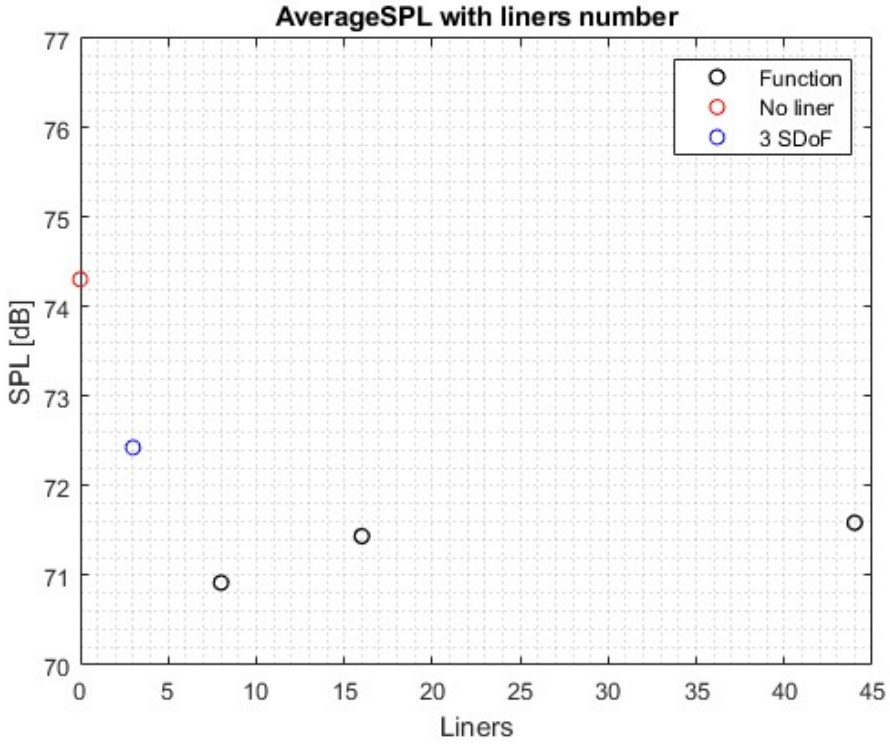

(a) Minimization function: AverageSPL

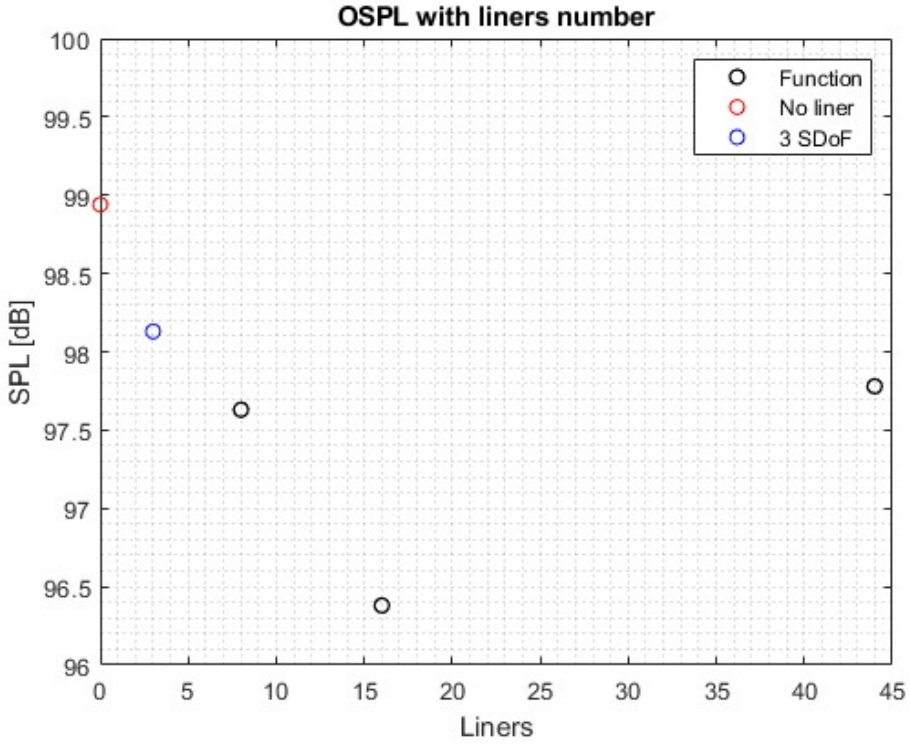

(b) Minimization function: OSPL

Figure 5.9: SPL [dB] depending on the number of liners

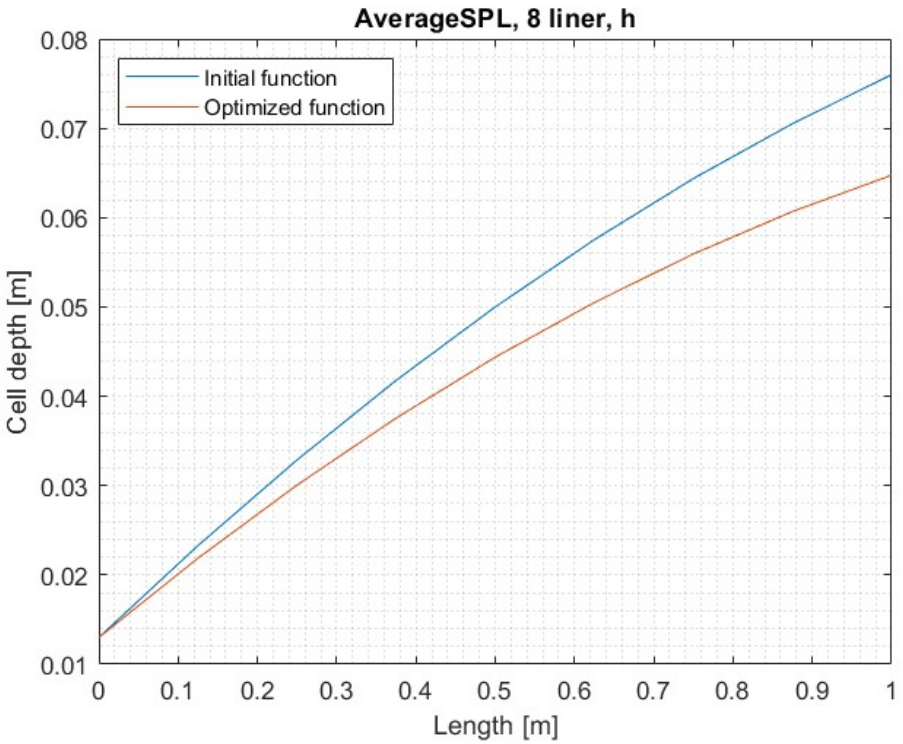

(a) "h" function with 8 liners and minimization function: AverageSPL

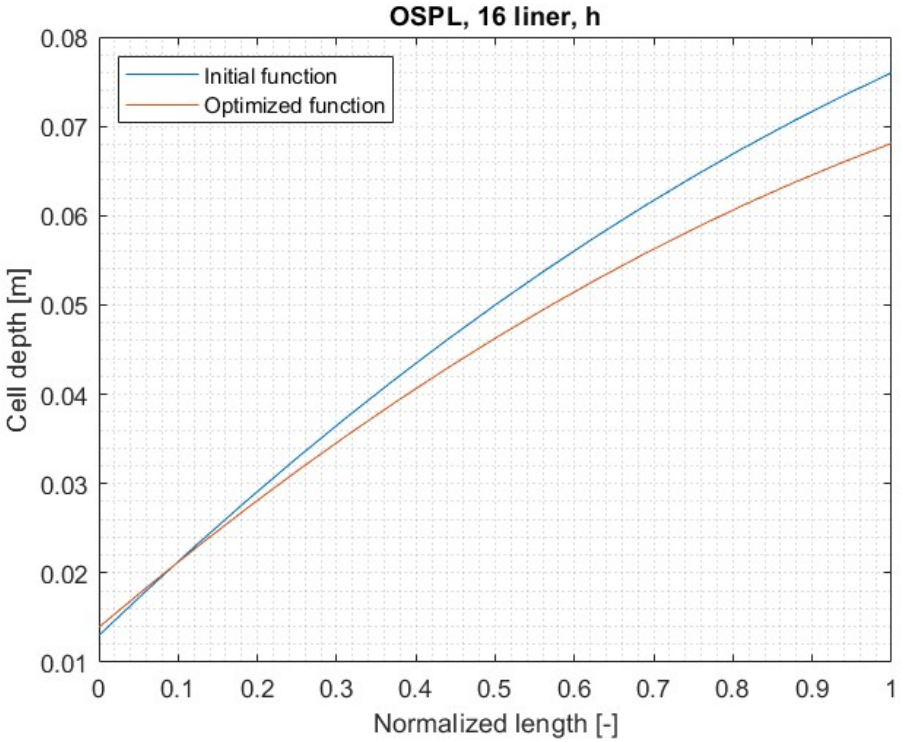

(b) "h" function with 16 liners and minimization function: OSPL

Figure 5.10: "h" function with 8 and 16 liner

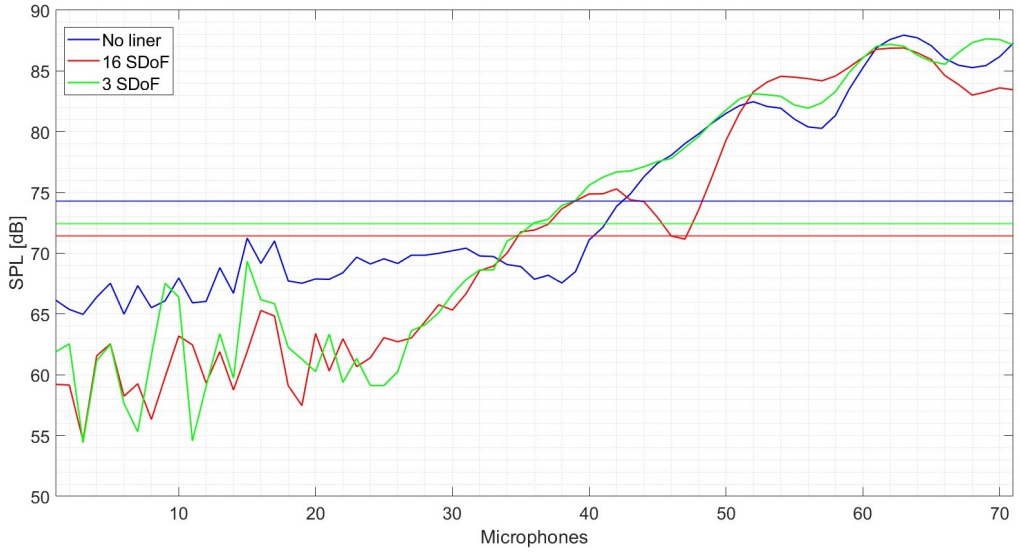

(a) Comparison between the SPL with 16 and 3 liners, Minimization function: AverageSPL

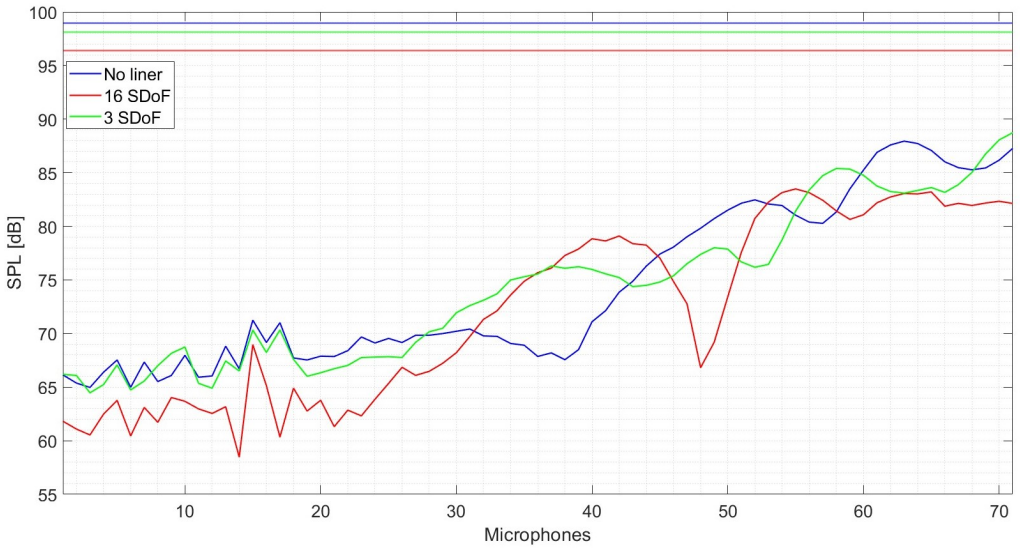

(b) Comparison between the SPL with 16 and 3 liners, Minimization function: OSPL

Figure 5.11: Comparison between the SPL with 16 and 3 liners

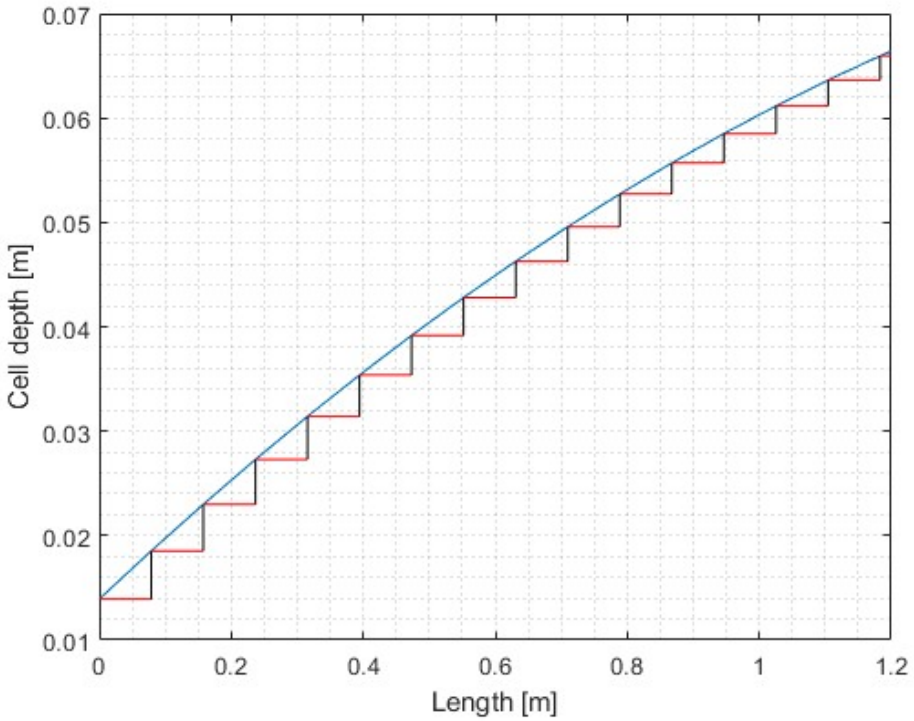

Figure 5.12: Representation of a "step function"

AverageSPL

- h function: $h = -0.022x^2 + 0.085x + 0.013$
- d function: $d = 0.0008x^2 + 0.0006x + 0.001$

OSPL

- h function: $h = 0.0211x^2 + 0.0753x + 0.0139$
- d function: $d = 0.000577x^2 + 0.000812x + 0.001133$

A comparison could be done between the SPL curve obtained considering this optimization with 16 liners and the SPL curve obtained from the optimization of just 3 liner. These figures are presented in Figure 5.11.

Pressure map

For some final considerations the configuration composed by 16 liners is used. One of the Actran's output is a map containing all the pressure (or SPL) values in the space of interest. Every value is computed solving the equation for the particular analysis as described above. These pressure map are shown in Figure 5.13. What is shown in this figure comes from the analysis with the frequency $f = 3200\ Hz$. The approach is similar to what done above in which the liner configuration obtained from the optimization of the given set of frequencies, is used in a single frequency to better understand how is its reduction. Figure 5.13 is composed by three window.

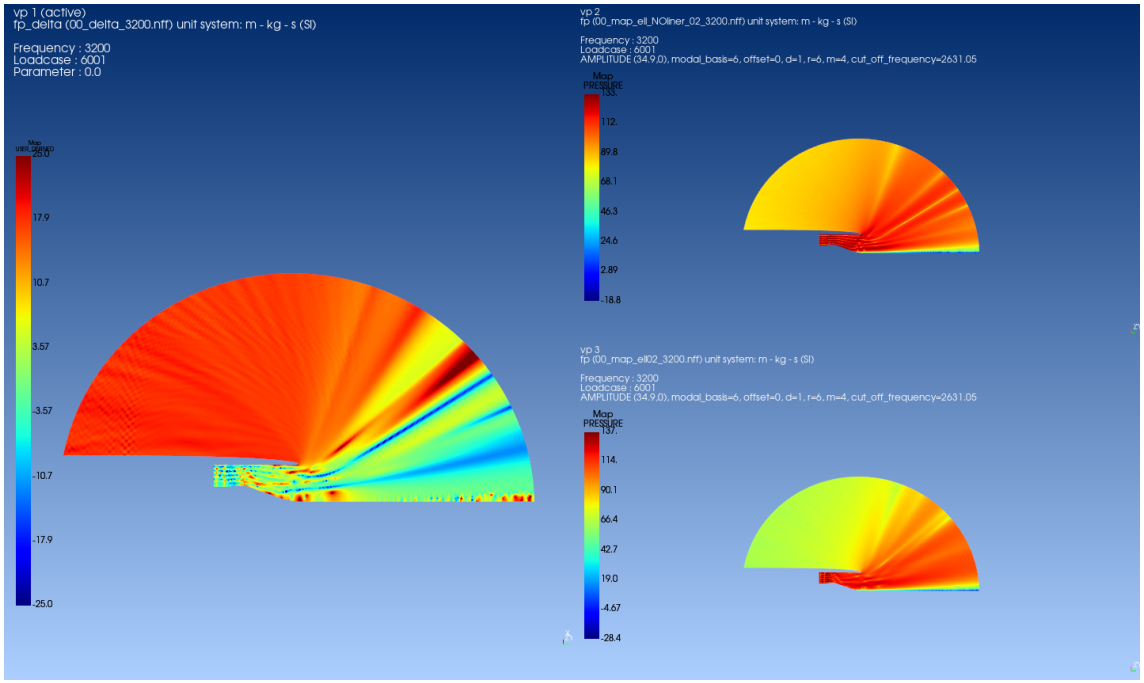

Figure 5.13: Pressure delta for $f = 3200\ Hz$ with a 16-liner configuration

On the top right is represented the pressure map obtained without any acoustic treatment and generated with a frequency of $f = 3200\ Hz$. In the bottom right, the pressure map is given using an acoustic treatment composed by 16 liners and described above. On the left is possible to see the delta between these two scenarios and in particular is described with the following expression.

$$\Delta p = p_{\text{No liner}} - p_{\textbf{liner}} \tag{5.3}$$

This is a useful tool to have a better view on the noise reduction and in particular of the acoustic pressure attenuation. The range was modified to have more reasonable values but it must be noticed that higher, and not justifiable, values of the delta are registered in proximity of the interface between the infinite and acoustic element. This lead to the conclusion that these values could be a product of computational errors.

5.8.1 Different starting point

Some consideration on the influence of different starting point are done in this section. Two more analyses are done considering the "line of minimum" and "line of maximum" as starting points for the h function. In the first analysis the starting point is a horizontal line in $h = 0.013$ that represents the lower bound of the interval. In the second the starting point is a ramp going from $h = 0.03$ (upper bound for the first liner) to $h = 0.076$ (upper bound for the remaining liners). Also a function in the middle of these two was used as a starting point. This is represented in Figure 5.14 and Figure 5.15.

Especially when the line of minimum is used as a starting point, the tendency is to occupy more space to reduce the sound. In both figures, the optimal function

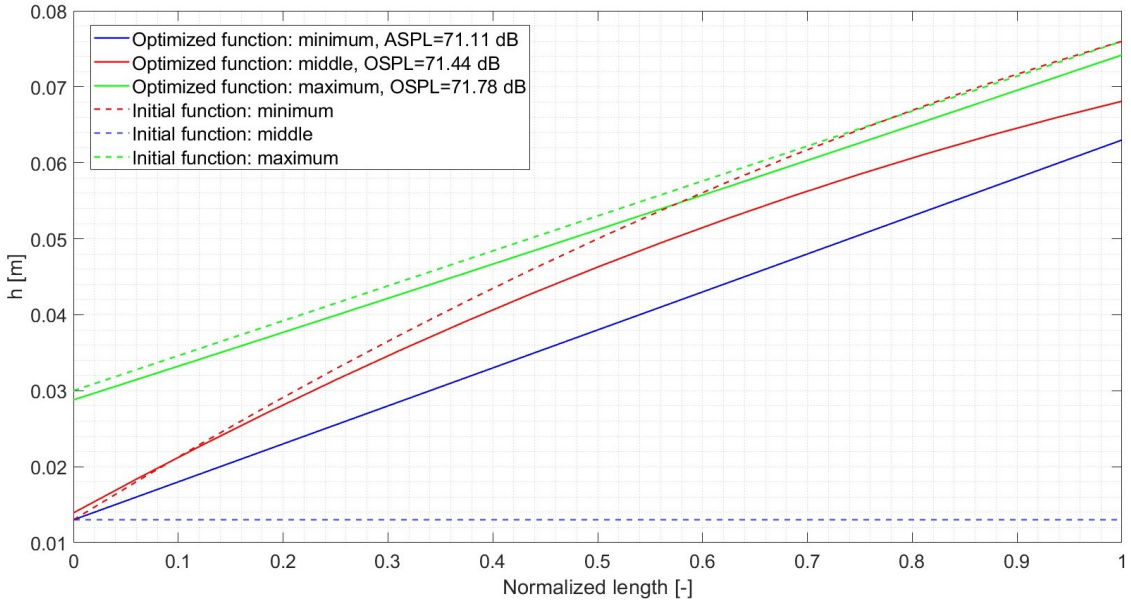

Figure 5.14: Optimization with different starting point, Minimizing function: AverageSPL

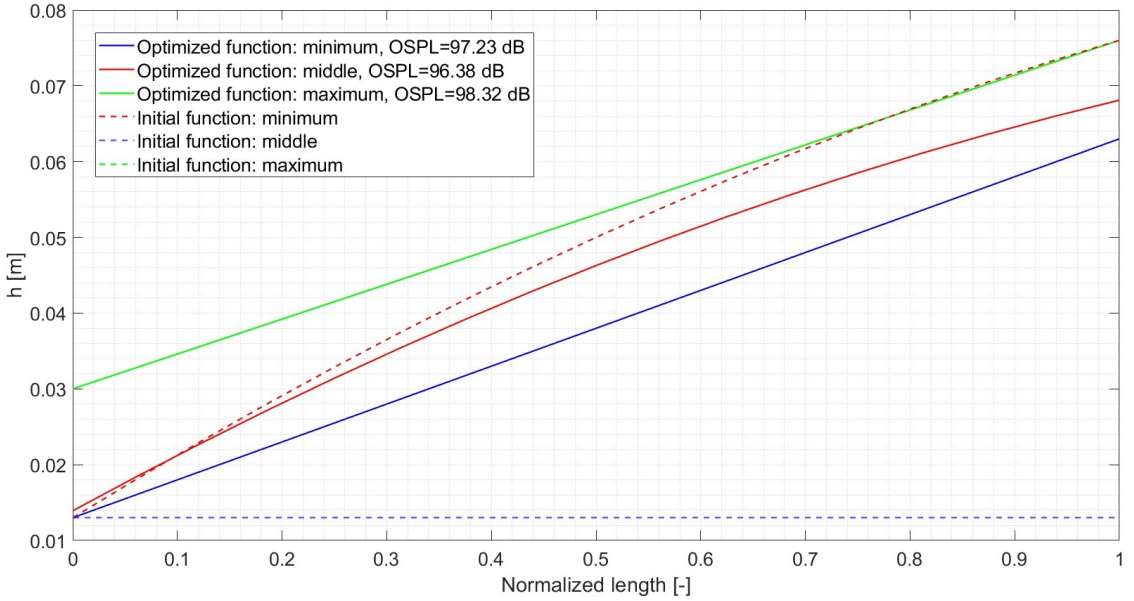

Figure 5.15: Optimization with different starting point, Minimizing function: OSPL

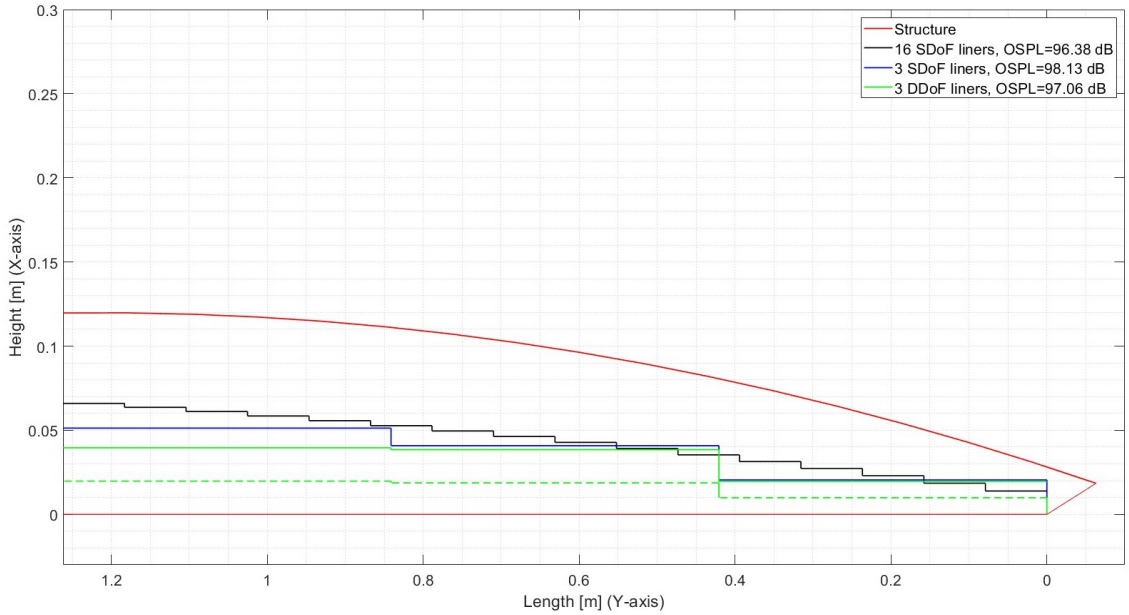

Figure 5.16: Liner integration in the engine structure

seems to be located in the middle due to the fact that both if the space is to much or to low, the curves during the optimization move to the center.

5.8.2 Final configuration

Figure 5.16 shows the integration of the different liners obtained in the above analyses. This is represented in the real engine measures. Is it possible to notice the difference between the usual set of 3 optimized liner and the set of 16 liners computed in these last analyses. The tendency is always the same occupying more space. In fact is possible to notice that considering 16 liners, being divided in more portions, the space occupied by the liner is greater. Figure 5.16 represent well the respect of the physical constrains.

Chapter 6

Conclusion

A final configuration for the set of liners that seems to reduce the noise generated by an aircraft is found. The model used to compute the impedance is the Motsinger and Kraft model. This could be used to compute both the impedance for a SDoF or a DDoF liners. After some tests, the Actran Analysis that was found to be the fastest and with enough precision is the Direct Frequency Response. Two main analyses were done: single frequency and multi-frequency noise reduction. Two noise function were investigated: Average Sound Pressure Level and Overall Sound Pressure Level. For the first analysis the noise generated with $f = 3200\ Hz$ was analyzed. If considering the AverageSPL a reduction of 10.57 dB was registered while if the function to minimize is the OSPL the reduction is of around 7.97 dB. The configuration that allow to obtain this result is composed by 3 Single Degree of Freedom liners. The main goal of the multi-frequency analysis is to find a liner configuration that reduce the noise for a set of frequencies. The set is composed by the following frequencies $[3200, 4800, 6400, 8000]\ Hz$. In this case the best results were obtained using a configuration composed by 16 liners. If considering the AverageSPL the best reduction was of around 3.39 dB while if considering the OSPL the reduction was of about 2.56 dB. This low reduction was found to be due to the not enough reduction for the higher frequencies. Future analyses must be done on these frequencies using different configuration or different optimizer. During these analyses different Global optimizer were tested like the GN_DIRECT or the GN_ESCH but in some cases the optimizer never reached a convergence. Further analyses could be done on global optimizer to be sure that all the feasible space is investigated. Future investigation could be done investigating other type of liners that works well with higher frequencies. In the present work, the effect of an external flow was not considered but future analyses can consider this aspect also.

Chapter 7

Annex A

```
1
2  #================ DO NOT SUPRESS OR EDIT THIS LINE AND THE LINES
                                    BELOW ==================
3  #
4  #  Actran 2023.1 Session file
5  #
6  #  Hostname  : DESKTOP-P2BCD1J - Windows 6.2.9200.0.0 (workstation
                                    x64)
7  #  Processor : 8x 11th Gen Intel(R) Core(TM) i7-1165G7 @ 2.80GHz
8  #  Memory    : 8153MB [ 50% of 16183MB available ]
9  #============================ DO NOT EDIT THE ABOVE LINES
                                    ================================
10
11 import numpy as np
12 from numpy import * #cos  importo tutte le funzioni, classi e
                                    oggetti definiti nel modulo numpy
13 from pyfemtown.Command import Optimizer
14 import nlopt
15
16 def impedenza_SDoF(h,d,f):
17
18     sigma=0.09 #valore medio nell'intervallo
19     tau=0.75e-3 #valore medio nell'intervallo
20     Cd=0.76
21     rho=1.225
22     c=340
23     mu=1.8e-5
24     lunghezza_onda=c/f
25     k=2*np.pi/lunghezza_onda
26     a=64
27     epsilon=0.85*(1-0.7*np.sqrt(sigma))
28
29     R_norm_SDoF=a*mu*tau/(2*rho*c*sigma*Cd*d**2)
30     X_norm_SDoF=k*(tau+epsilon*d)/sigma
31
32     Z_norm_SDoF=R_norm_SDoF+1j*(X_norm_SDoF-1/np.tan(k*h))
33
34     return Z_norm_SDoF
35
36 def impedenza_DDoF(h,d1,d2,b,f):
```

```
37
38      h_1=b*h
39      h_2=(1-b)*h
40      sigma=0.09 #valore medio nell'intervallo
41      tau=0.75e-3 #valore medio nell'intervallo
42      Cd=0.76
43      rho=1.225
44      c=340
45      mu=1.8e-5
46      lunghezza_onda=c/f
47      k=2*np.pi/lunghezza_onda
48      a=64
49      epsilon=0.85*(1-0.7*np.sqrt(sigma))
50
51      R1_norm=a*mu*tau/(2*rho*c*sigma*Cd*d1**2)
52      X1_norm=k*(tau+epsilon*d1)/sigma
53
54      R2_norm=a*mu*tau/(2*rho*c*sigma*Cd*d2**2)
55      X2_norm=k*(tau+epsilon*d2)/sigma
56
57
58      Z1_norm=R1_norm+1j*X1_norm
59      Z2_norm=R2_norm+1j*X2_norm
60
61      Z_norm_DDoF=Z1_norm+(Z2_norm*np.cos(k*h_1)*...
62          *np.sin(k*h_2)/np.sin(k*h)-1j/np.tan(k*h))/...
63          /(1+1j*Z2_norm*np.sin(k*h_1)*np.sin(k*h_2)/np.sin(k*h))
64
65      return Z_norm_DDoF
66
67  def myfunc(x,grad): # x rappresenta l'input dei differenti valori
                                    dei parametri. Grad    il
                                    gradiente della fz obiettivo
                                    rispetto ai parametri di input
                                    che non verra' usato nella
                                    seguente trattazione
68
69
70      #possiamo avere un accesso rapido a questi object
71      ge=optimizer.global_environment
72      actran=optimizer.actran
73      actranplt=optimizer.actranplt
74
75      #importiamo l'analisi Actran che abbiamo precedentemente
                                    settato
76      dfr_analysis =actran.read_analysis(file="C:\\Users\\Giuseppe\\
77      Desktop\\Politecnico di Torino\\Tesi\\AnalisiTesi\\
78      10_incontro13_01_2025_prove\\test_ell02_fourtyfour_liner.edat",
79      type='ACTRAN', load_topology=True, force_modal_components=None)
80
81
82      #Parametri h e d: oggetto dell'ottimizzazione
83
84      point_number=17
85      microphone_number=71
86
```

```
    l=np.linspace(0,1,point_number)
    h=x[0]*l**2+x[1]*l+x[2]
    d=x[3]*l**2+x[4]*l+x[5]

    t=point_number-1 #variabile di appoggio

    if h[0]>=0.013 and h[0]<=0.03 and np.all(h[1:t]>=0.013) and np.
                                all(h[1:t]<=0.076) and np.all(d[0
                                :t]>=0.001) and np.all(d[0:t]<=0.
                                0024):

        f1=3200
        f2=4800
        f3=6400
        f4=8000

        rho=1.225
        c=340
        Z0=rho*c

        #FREQUENZA 1: 3200

        ge.report_file2.write('SPL '+str(ge.iteration)+' \n') #
                                scrivo il file report con tutte
                                le informazioni che mi servono
        ge.report_file2.write('frequency=3200'+'\n')
        ge.report_file2.flush()

        #Usiamo il modello di impedenza scelto per il calcolo di
                                resistenza    reattanza che nel
                                nostro caso    quello di
                                Motsinger and Kraft

        Z_norm_SDoF=impedenza_SDoF(h,d,f1)
        Z_SDoF=Z_norm_SDoF*Z0
        A_SDoF=1/Z_SDoF


        for i in range(t):
            actran.set_prop( actran.get_bc( dfr_analysis , type='
                                Normalized Impedance', id=i+1 ),
                                field=Z_norm_SDoF[i])


        actran.set_prop( actran.get_frequency( analysis=
                                dfr_analysis, index=0, subtype="
                                freq"), freqs_list=[f1] )
        actran.set_prop( dfr_analysis, axi_order=[[4]])
        actran.set_prop( actran.get_propagating_mode( duct=actran.
                                get_component( dfr_analysis ,
                                type='Modal Duct' ), index=0 ),
                                order1= 6)
        actran.set_prop( actran.get_propagating_mode( duct=actran.
                                get_component( dfr_analysis, type
                                ='Modal Duct' ), index=0 ),
                                format='Amplitude' )
```

```
125         actran.set_prop( actran.get_propagating_mode( duct=actran.
                                 get_component( dfr_analysis ,
                                 type='Modal Duct' ), index=0 ),
                                 value= 34.92)
126         actran.set_prop( actran.get_propagating_mode( duct=actran.
                                 get_component( dfr_analysis ,
                                 type='Modal Duct' ), index=1 ),
                                 order1= 6)
127         actran.set_prop( actran.get_output_frf(dfr_analysis),
                                 filename='res.plt')
128
129         actran.run(analysis=dfr_analysis, arguments='--mem=2000')
130
131         set_1=actranplt.import_file(file=r'res.plt', ftype='plt')
132
133
134         SPL_1_amplitude=np.linspace(0,microphone_number-1,
                                 microphone_number)
135
136         for i in range(microphone_number):
137             SPL=set_1["POINT_1", str(i+1), "fp"]
138             SPL_1_amplitude[i]=np.abs(SPL)
139
140         SPL_1_dB=20*np.log10(SPL_1_amplitude/(2e-5))
141
142         ge.report_file2.write(str(SPL_1_dB)+'\n' + 'frequency=4800'
                                 +'\n')
143         ge.report_file2.flush()
144
145
146         #FREQUENZA 2: 4800
147
148
149         Z_norm_SDoF=impedenza_SDoF(h,d,f2)
150         Z_SDoF=Z_norm_SDoF*Z0
151         A_SDoF=1/Z_SDoF
152
153         for i in range(t):
154             actran.set_prop( actran.get_bc( dfr_analysis , type='
                                 Normalized Impedance', id=i+1 ),
                                 field=Z_norm_SDoF[i])
155
156         actran.set_prop( actran.get_frequency( analysis=
                                 dfr_analysis, index=0, subtype="
                                 freq"), freqs_list=[f2] )
157         actran.set_prop( dfr_analysis, axi_order=[[11]])
158         actran.set_prop( actran.get_propagating_mode( duct=actran.
                                 get_component( dfr_analysis ,
                                 type='Modal Duct' ), index=0 ),
                                 order1= 8)
159         actran.set_prop( actran.get_propagating_mode( duct=actran.
                                 get_component( dfr_analysis, type
                                 ='Modal Duct' ), index=0 ),
                                 format='Amplitude' )
160         actran.set_prop( actran.get_propagating_mode( duct=actran.
                                 get_component( dfr_analysis ,
```

```
                                type='Modal Duct' ), index=0 ),
                                value= 28.46)
161         actran.set_prop( actran.get_propagating_mode( duct=actran.
                                get_component( dfr_analysis ,
                                type='Modal Duct' ), index=1 ),
                                order1= 8)
162         actran.set_prop( actran.get_output_frf(dfr_analysis),
                                filename='res.plt')
163
164         actran.run(analysis=dfr_analysis, arguments='--mem=2000')
165
166         set_1=actranplt.import_file(file=r'res.plt', ftype='plt')
167
168
169         SPL_2_amplitude=np.linspace(0,microphone_number-1,
                                microphone_number)
170
171         for i in range(microphone_number):
172             SPL=set_1["POINT_1", str(i+1), "fp"]
173             SPL_2_amplitude[i]=np.abs(SPL)
174
175         SPL_2_dB=20*np.log10(SPL_2_amplitude/(2e-5))
176
177         ge.report_file2.write(str(SPL_2_dB)+'\n' + 'frequency=6400'
                                +'\n')
178         ge.report_file2.flush()
179
180         #FREQUENZA 2: 6400
181
182
183         Z_norm_SDoF=impedenza_SDoF(h,d,f3)
184         Z_SDoF=Z_norm_SDoF*Z0
185         A_SDoF=1/Z_SDoF
186
187         for i in range(t):
188             actran.set_prop( actran.get_bc( dfr_analysis , type='
                                Normalized Impedance', id=i+1 ),
                                field=Z_norm_SDoF[i])
189
190         actran.set_prop( actran.get_frequency( analysis=
                                dfr_analysis, index=0, subtype="
                                freq"), freqs_list=[f3] )
191         actran.set_prop( dfr_analysis, axi_order=[[26]])
192         actran.set_prop( actran.get_propagating_mode( duct=actran.
                                get_component( dfr_analysis ,
                                type='Modal Duct' ), index=0 ),
                                order1= 1)
193         actran.set_prop( actran.get_propagating_mode( duct=actran.
                                get_component( dfr_analysis, type
                                ='Modal Duct' ), index=0 ),
                                format='Amplitude' )
194         actran.set_prop( actran.get_propagating_mode( duct=actran.
                                get_component( dfr_analysis ,
                                type='Modal Duct' ), index=0 ),
                                value= 12.43)
```

```
195         actran.set_prop( actran.get_propagating_mode( duct=actran.
                                 get_component( dfr_analysis ,
                                 type='Modal Duct' ), index=1 ),
                                 order1= 1)
196         actran.set_prop( actran.get_output_frf(dfr_analysis),
                                 filename='res.plt')
197
198         actran.run(analysis=dfr_analysis, arguments='--mem=2000')
199
200         set_1=actranplt.import_file(file=r'res.plt', ftype='plt')
201
202
203         SPL_3_amplitude=np.linspace(0,microphone_number-1,
                                 microphone_number)
204
205         for i in range(microphone_number):
206             SPL=set_1["POINT_1", str(i+1), "fp"]
207             SPL_3_amplitude[i]=np.abs(SPL)
208
209         SPL_3_dB=20*np.log10(SPL_3_amplitude/(2e-5))
210
211         ge.report_file2.write(str(SPL_3_dB)+'\n' + 'frequency=8000'
                                 +'\n')
212         ge.report_file2.flush()
213
214         #FREQUENZA 2: 8000
215
216
217         Z_norm_SDoF=impedenza_SDoF(h,d,f4)
218         Z_SDoF=Z_norm_SDoF*Z0
219         A_SDoF=1/Z_SDoF
220
221
222         for i in range(t):
223             actran.set_prop( actran.get_bc( dfr_analysis , type='
                                 Normalized Impedance', id=i+1 ),
                                 field=Z_norm_SDoF[i])
224
225         actran.set_prop( actran.get_frequency( analysis=
                                 dfr_analysis, index=0, subtype="
                                 freq"), freqs_list=[f4] )
226         actran.set_prop( dfr_analysis, axi_order=[[41]])
227         actran.set_prop( actran.get_propagating_mode( duct=actran.
                                 get_component( dfr_analysis ,
                                 type='Modal Duct' ), index=0 ),
                                 order1= 7)
228         actran.set_prop( actran.get_propagating_mode( duct=actran.
                                 get_component( dfr_analysis, type
                                 ='Modal Duct' ), index=0 ),
                                 format='Amplitude' )
229         actran.set_prop( actran.get_propagating_mode( duct=actran.
                                 get_component( dfr_analysis ,
                                 type='Modal Duct' ), index=0 ),
                                 value= 4.27)
230         actran.set_prop( actran.get_propagating_mode( duct=actran.
                                 get_component( dfr_analysis ,
```

```
                                type='Modal Duct' ), index=1 ),
                                order1= 7)
231         actran.set_prop( actran.get_output_frf(dfr_analysis),
                                filename='res.plt')
232
233         actran.run(analysis=dfr_analysis, arguments='--mem=2000')
234
235         set_1=actranplt.import_file(file=r'res.plt', ftype='plt')
236
237
238         SPL_4_amplitude=np.linspace(0,microphone_number-1,
                                microphone_number)
239
240         for i in range(microphone_number):
241             SPL=set_1["POINT_1", str(i+1), "fp"]
242             SPL_4_amplitude[i]=np.abs(SPL)
243
244         SPL_4_dB=20*np.log10(SPL_4_amplitude/(2e-5))
245
246         ge.report_file2.write(str(SPL_4_dB)+'\n')
247         ge.report_file2.flush()
248
249         # SOMMA DI TUTTE LE PRESSIONI SUI SINGOLI MICROFONI
250
251         SPL_amplitude_tot=np.sqrt(SPL_1_amplitude**2+
                                SPL_2_amplitude**2+
                                SPL_3_amplitude**2+
                                SPL_4_amplitude**2)
252
253         OSPL_pressure=0
254         for i in range(microphone_number):
255             OSPL_pressure=OSPL_pressure+SPL_amplitude_tot[i]**2 #
                                OSPL visto come la radice
                                quadrata della somma delle
                                pressioni al quadrato sull'arco
                                di microfoni
256
257         OSPL=np.sqrt(OSPL_pressure)
258         OSPL_dB=20*np.log10(OSPL/(2e-5))
259
260         SPL_dB=20*np.log10(SPL_amplitude_tot/(2e-5)) #logaritmo di
                                un vettore contenente le
                                pressioni su tutti i microfoni
261         print(SPL_dB)
262
263         ge.report_file2.write('SPL for all the frequency: '+'\n'+
                                str(SPL_dB)+'\n'+'\n')
264         ge.report_file2.flush()
265
266         print(OSPL_dB)
267
268         ge.report_file2.write('Overall Sound Pressure Level: '+str(
                                OSPL_dB)+' '+'dB'+'\n'+'\n')
269         ge.report_file2.flush()
270
271         mean_value=np.mean(SPL_dB)
```

```
272         ge.report_file2.write('Average Sound Pressure Level: '+str(
                                    mean_value)+' '+'dB'+'\n'+'\n')
273         ge.report_file2.flush()
274 
275 
276         obj_func=mean_value
277 
278         ge.report_file.write('['+str(ge.iteration)+']'+' '+
279                              'h='+str(h[0:point_number-1])+'\n'+
280                              'd='+str(d[0:point_number-1])+'\n'+
281                              'a_h='+str(x[0])+' ' +'b_h='+str(x[1])+
                                    ' '+'c_h='+str(x[2])+' \n'+
282                              'a_d='+str(x[3])+' ' +'b_d='+str(x[4])+
                                    ' '+'c_d='+str(x[5])+' \n'+
283                              'SPL='+' '+str(obj_func)+' \n') #scrivo
                                     il file report con tutte le
                                    informazioni che mi servono
284         ge.report_file.flush() #questo comando permette di
                                    cancellare i dati che sono
                                    momentanemanete memorizzati in un
                                     buffer prima di essere scritti
                                    sul disco.
285 
286         ge.report_file4.write('['+str(ge.iteration)+']'+' '+str(
                                    obj_func)+'\n')
287         ge.report_file4.flush()
288 
289         optimizer.global_environment.report_file3=optimizer.
                                    openfile('last_val.dat','w')
290         ge.report_file3.write(str(obj_func))
291         ge.report_file3.flush()
292 
293         ge.iteration +=1
294         optimizer.clear_all() #Il comando clear permette di pulire
                                    l'analisi Actran in modo tale da
                                    essere preparata per l'iterazione
                                     successiva
295     else:
296         with open('last_val.dat', 'r') as file:
297             val = file.read()
298         obj_func=float(val)
299         ge.report_file.write('['+str(ge.iteration)+']'+' '+str(
                                    obj_func)+' \n')
300         ge.report_file.flush()
301         ge.report_file4.write('['+str(ge.iteration)+']'+' '+str(
                                    obj_func)+'\n')
302         ge.report_file4.flush()
303         ge.iteration +=1
304 
305     return obj_func
306 
307 def main() :
308     #inizializzazione dell'ottimizzatore
309     opt=optimizer.optimizer(nlopt.LN_BOBYQA,6) #E-1 SE CON GLOBALE
310 
311     optimizer.global_environment.iteration=0
```

```
312     optimizer.global_environment.report_file=optimizer.openfile('
                                    output.dat','w')
313     optimizer.global_environment.report_file2=optimizer.openfile('
                                    output_SPL.dat','w')
314     optimizer.global_environment.report_file4=optimizer.openfile('
                                    SPL_list.dat','w')
315
316     #Otimizer configuration
317     opt.set_min_objective(myfunc)
318     opt.set_lower_bounds([-0.1, -0.1 , -0.1 , -0.01 , -0.01 , -0.01
                                    ])
319     opt.set_upper_bounds([0.1 , 0.1, 0.1, 0.01, 0.01, 0.01])
320
321
322     opt.set_xtol_rel(1e-2)
323     #opt.set_maxeval(1)
324     #opt.set_ftol_rel(1e-3)
325     #Start optimization loop
326     x=opt.optimize([-0.022,0.085,0.013,0.8e-3,0.6e-3,0.001])  #a,b,
                                    c for h and d,e,f for d
327     ##
328     minf=opt.last_optimum_value() #questo    l'ultimo valore di
                                    ottimo
329     optimizer.message("Total number of iteration: %d"%(optimizer.
                                    global_environment.iteration-1))
                                    #numero totale di iterazioni
330     optimizer.message("Optimum at %s" %str(x)) #valore del vettore
                                    x ottimizzato
331     optimizer.message("Minimum value= %g" %minf) #valore di minimo
                                    della funzione da minimizzare
332     optimizer.message("Result code = %g" %opt.last_optimize_result
                                    ())
333
334 optimizer=Optimizer()
335 main()
```

Bibliography

[1] M. Jones, W. Watson, D. Nark, B. Howerton, and M. Brown, *A Review of Acoustic Liner Experimental Characterization at NASA Langley.*

[2] Aero-acoustic response of an acoustic liner | TU delft repository. [Online]. Available: https://repository.tudelft.nl/record/uuid:d0b525a2-ca09-4bfc-a8e3-7917d8099fc0

[3] R. Sugimoto, P. Murray, and R. Astley, *Folded Cavity Liners for Turbofan Engine Intakes*, journal Abbreviation: 18th AIAA/CEAS Aeroacoustics Conference (33rd AIAA Aeroacoustics Conference) Publication Title: 18th AIAA/CEAS Aeroacoustics Conference (33rd AIAA Aeroacoustics Conference).

[4] M. Jones and T. Parrott, "Assessment of bulk absorber properties for multi-layer perforates in porous honeycomb liners," in *12th AIAA/CEAS Aeroacoustics Conference (27th AIAA Aeroacoustics Conference)*. American Institute of Aeronautics and Astronautics. [Online]. Available: https://arc.aiaa.org/doi/10.2514/6.2006-2403

[5] M. Long, "6 - wave acoustics," in *Architectural Acoustics (Second Edition)*, M. Long, Ed. Academic Press, pp. 221–258. [Online]. Available: https://www.sciencedirect.com/science/article/pii/B9780123982582000064

[6] R.e. motsinger and r.e. kraft. design and performance of duct acoustic treatment. in NASA. lan gley research center, aeroacoustics of flight vehicles: Theory and practice, volume 2, august 1991. [Online]. Available: https://www.bing.com/search?pglt=41&q=R.E.+Motsinger+and+R.E.+Kraft.+Design+and+performance+of+duct+acoustic+treatment.+In+NASA.+Lan+gley+Research+Center%2C+Aeroacoustics+of+Flight+Vehicles%3A+Theory+and+Practice%2C+volume+2%2C+August+1991.&cvid=50863b7de91e4c00a22166e524075fb6&gs_lcrp=EgZjaHJvbWUyBggAEEUYOdIBCDI4NTJqMGoxqAIIsAIB&FORM=ANNTA1&PC=ASTS

[7] W. e. zorumski and t. l. parrott. non-linear acoustic theory for rigid porous materials. NASA TN d-6196, 1971. [Online]. Available: https://www.bing.com/search?pglt=41&q=W.+E.+Zorumski+and+T.+L.+Parrott.+Non-linear+Acoustic+Theory+for+Rigid+Porous+Materials.+NASA+TN+D-6196%2C+1971.&cvid=e897497536094137a9bd0aeb2afd9f1a&gs_lcrp=EgZjaHJvbWUyBggAEEUYOdIBBzg1NGowajGoAgCwAgA&FORM=ANNTA1&PC=ASTS

[8] Hexagon, "Introduction to actran DGM."

[9] ——, "Non convected DGM simulations."

[10] ——, "ACTRAN DGM 2023.1 user's guide."

[11] A. Snakowska, "Waves in ducts described by means of potentials," vol. 32, pp. 13–28.

[12] S. Proskurov, M. Lummer, J. W. Delfs, R. Ewert, J. Kirz, M. Plohr, and R. Jaron, "Installed fan noise simulation of a supersonic business aircraft," vol. 10, no. 9, p. 773, number: 9 Publisher: Multidisciplinary Digital Publishing Institute. [Online]. Available: https://www.mdpi.com/2226-4310/10/9/773

[13] D. Jones, C. Perttunen, and B. Stuckman, "Lipschitzian optimisation without the lipschitz constant," vol. 79, pp. 157–181.

[14] X. Liu, D. Zhao, D. Guan, S. Becker, D. Sun, and X. Sun, "Development and progress in aeroacoustic noise reduction on turbofan aeroengines," *Progress in Aerospace Sciences*, vol. 130, p. 100796, 2022. [Online]. Available: https://www.sciencedirect.com/science/article/pii/S037604212100097X

[15] K. Habibi and L. Mongeau, "Prediction of sound absorption by a circular orifice termination in a turbulent pipe flow using the lattice-boltzmann method," vol. 87, pp. 153–161. [Online]. Available: https://www.sciencedirect.com/science/article/pii/S0003682X14001947

[16] J. Winkler, J. M. Mendoza, C. A. Reimann, K. Homma, and J. S. Alonso, "High fidelity modeling tools for engine liner design and screening of advanced concepts," vol. 20, no. 5, pp. 530–560, publisher: SAGE Publications. [Online]. Available: https://doi.org/10.1177/1475472X211023884

[17] C. K. W. Tam, H. Ju, and B. E. Walker, "Numerical simulation of a slit resonator in a grazing flow under acoustic excitation," vol. 313, no. 3, pp. 449–471. [Online]. Available: https://www.sciencedirect.com/science/article/pii/S0022460X07009716

[18] "The theory of the helmholtz resonator," vol. 92, no. 638, pp. 265–275. [Online]. Available: https://royalsocietypublishing.org/doi/10.1098/rspa.1916.0012

[19] U. Ingard, "On the theory and design of acoustic resonators," vol. 25, p. 1037, ADS Bibcode: 1953ASAJ...25.1037I. [Online]. Available: https://ui.adsabs.harvard.edu/abs/1953ASAJ...25.1037I

[20] W. Zorumski and B. Tester, "Prediction of the acoustic impedance of duct liners," vol. -1.

[21] M. Delany and E. Bazley, "Acoustical properties of fibrous absorbent materials," vol. 3, no. 2, pp. 105–116. [Online]. Available: https://linkinghub.elsevier.com/retrieve/pii/0003682X70900319

[22] L. J. Heidelberg, E. J. Rice, and L. Homyak, "Experimental evaluation of a spinning-mode acoustic-treatment design concept for aircraft inlets," NTRS Author Affiliations: NASA Lewis Research Center NTRS Report/Patent Number: NASA-TP-1613 NTRS Document ID: 19800012838 NTRS Research Center: Legacy CDMS (CDMS). [Online]. Available: https://ntrs.nasa.gov/citations/19800012838

[23] E. J. Rice, "A model for the acoustic impedance of a perforated plate liner with multiple frequency excitation," NTRS Author Affiliations: NASA Lewis Research Center NTRS Meeting Information: Acoustical Soc. of Am.; 1971-10-19 to 1971-10-22; undefined NTRS Document ID: 19720004979 NTRS Research Center: Legacy CDMS (CDMS). [Online]. Available: https://ntrs.nasa.gov/citations/19720004979

[24] P. Murray and R. Astley, *Development of a single degree of freedom perforate impedance model under grazing flow and high SPL*, journal Abbreviation: 18th AIAA/CEAS Aeroacoustics Conference (33rd AIAA Aeroacoustics Conference) Publication Title: 18th AIAA/CEAS Aeroacoustics Conference (33rd AIAA Aeroacoustics Conference).

[25] M. D. Dahl, "Assessment of NASA's aircraft noise prediction capability," NTRS Author Affiliations: NASA Glenn Research Center NTRS Report/Patent Number: NASA/TP-2012-215653 NTRS Document ID: 20120012957 NTRS Research Center: Glenn Research Center (GRC). [Online]. Available: https://ntrs.nasa.gov/citations/20120012957

[26] Hexagon, "Introduction to actran TM."

[27] Actran DGM | acustica actran. [Online]. Available: https://hexagon.com/it/products/actran-dgm

[28] C.-L. Navier, "Navier stokes equation." [Online]. Available: http://games-cn.org/wp-content/uploads/2020/04/Navier_Stokes_equations.pdf

[29] M. J. Lighthill, "On sound generated aerodynamically. i. general theory," vol. 211, no. 1107, pp. 564–587, place: London Publisher: The Royal Society.

[30] F. Farassat and M. Myers, "A study of wave propagation in a duct and mode radiation," in *Aeroacoustics Conference*. American Institute of Aeronautics and Astronautics. [Online]. Available: https://arc.aiaa.org/doi/10.2514/6.1996-1677

[31] Hexagon, "Introduction to actran TM."

[32] Livello di pressione sonora SPL. Running Time: 71. [Online]. Available: https://svantek.com/it/accademia/livello-di-pressione-sonora-spl/

[33] Introduction - NLopt documentation. [Online]. Available: https://nlopt.readthedocs.io/en/latest/NLopt_Introduction/

[34] M. J. D. Powell, "The BOBYQA algorithm for bound constrained optimization without derivatives."

[35] "ACTRAN 2023110 1 user's guide - volume 1 : Installation, operations, theory and utilities."